A Contribution to Numerically Efficient Modelling of Thermodynamic Systems

Von der Fakultät für Maschinenbau
der Technischen Universität Carolo-Wilhelmina zu Braunschweig

zur Erlangung der Würde

eines Doktor–Ingenieurs (Dr.–Ing.)

genehmigte Dissertation

von: Christian Wilhelm Schulze
aus: Göttingen

eingereicht am: 29.05.2013
mündliche Prüfung am: 16.12.2013

Gutachter: Prof. Dr.–Ing. Jürgen Köhler
Prof. Dr.–Ing. Gerhard Schmitz

2014

Preface

This thesis was written against the backdrop of work carried out at TLK-Thermo GmbH and the Institut für Thermodynamik of the TU Braunschweig. The field of study was characterised by studies of air conditioning systems (Kaiser et al., 2012b) for refrigerant selection and control optimisation, conventional and CCS (carbon capture and storage) coal-fired power plants (Brunnemann et al., 2012), refrigeration (Gräber et al., 2012; Möhlenkamp et al., 2012) and power cycles (Somdalen et al., 2012) for cycle design, fuel cell system simulation, CFD simulation of ejectors (Lucas et al., 2013) and many others (Tegethoff et al., 2011). All of this work has influenced the scope of this thesis and the results of this thesis have been applied to these topics where possible.

Acknowledgements

I want to thank Prof. Köhler for clarifying the objectives of this thesis and for supporting and supervising it throughout. My thanks also go to Prof. Schmitz for actively listening to my presentations at the DYNCAP meetings and for taking over the duties of the second supervisor.

I also want to thank Willi and Niko, who provided the work environment that enabled me to write this thesis. Additionally, Willi was always available to discuss the details of the models I have designed, the papers I have published and the content of my thesis. Thanks also to Manuel G. for joining in many discussions with Willi and for proof-reading.

I wish to thank all my colleagues at TLK-Thermo GmbH and post-graduate students at the Institut für Thermodynamik, for - more or less voluntarily - testing and giving feedback on the models and calculation methods I implemented. The numerous discussions with them about simulation failures allowed me to clarify the solving the problems of the finite volume method implemented in the TIL library.

Furthermore, I want to thank Sven F. and Ragnar for providing information about and implementations of the absorption system. The same goes for Christian K., who has supported me with models and information about the bus air conditioning system. Thanks to René for introducing me to the practical aspects of transient simulation; thanks to Norbert for not moving to another office; and thanks to Roland and Christian S. for the nice evenings and advice.

Thanks to Gabi for proof-reading the chapters on thermophysical property calculation.

And special thanks to Alex for investing a lot of his free time correcting my English, especially in the last week before I finished my thesis.

Finally I want to thank my family for supporting my work, for giving guidelines and advice, for proof reading and discussing different aspects of my thesis.

The partial financial support of the TLK-Thermo GmbH for this thesis within the project DYNCAP (BMWi Förderkennzeichen: 03ET2009D) and the project TEMO (BMBF Förderkennzeichen: 01IS08013) is highly appreciated.

Contents

Chapter 1.

Introduction

1.1. The Numerical Efficiency of Thermodynamic System Models

Transient system simulation is a valuable engineering tool for the design and optimisation of a product. Transient simulations can be used to design and evaluate a system, design a controller and to understand the dynamic behaviour of a system. Often, mathematically abstracted or black box models are applied for rapid simulation. They are a simple representation of a complex physical model or experimental data. In contrast to black box models, physical models are based on first principle equations, which are a general description of a system that does not necessarily require experimental data or more detailed models.

Some complex thermodynamic physical systems, for instance thermodynamic cycles, are characterised by their non-linear behaviour. These models can only be linearised for a small range of validity. Therefore the physical system models, instead of black box models, are often solved numerically in form of an ordinary differential equation system (ODE) or differential algebraic equation system (DAE). The solving of a physical model of such a thermodynamic system is far more complex than solving a black box model.

Real-time simulation, which is a special case of transient simulation, is an important technique when it comes to the testing of partially designed or implemented systems (Popovici and Mosterman, 2013, chapter 9). Hardware-in-the-Loop (HIL) and Rapid-Control-Prototyping (RCP) are well known techniques in industry. For example, load emulation for air conditioning and refrigeration systems can be realised by HIL. A real refrigeration cycle can be connected to a simulated cooled space. The real evaporator inlet air temperature can be controlled to match the virtual temperature of a simulated cooled space. The load conditions for the real evaporator are equal to the ones that would occur during experimental testing (Otten et al., 2010). To simulate a model

synchronous to real-time, the models must be robust and run faster than real-time in each solver step. Thus, if computation intensive physical system models are applied, they are essentially required to be numerically efficient.

Even more sophisticated are non-linear model predictive controls (NMPC). This method is used to optimise future system behaviour based on a system model. It requires system models to be many times faster than real-time to enable a prediction of the system behaviour.

Since the development period of a product is often limited, numerically efficient models used during design phase enable a more detailed product development. Especially computation intensive optimisations or simulations like CFD (computational fluid dynamics) benefit from numerically efficient system modelling. In contrast, real-time simulation and NMPC essentially require numerically efficient physical modelling.

1.2. State of the Art in the Modelling of Thermodynamic Systems

This thesis covers two aspects of the numerically efficient physical modelling of thermodynamic systems: thermophysical property calculation and a simplified finite volume method. Thermophysical property calculation is one of the main contributions to the calculation time of physical models, as will be shown in section 2.1. Since physical models refer to the properties of the involved materials, the thermophysical properties have to be provided in some way. Their calculation must not fail during simulation and has a significant impact on the DAE (differential algebraic equation) solving procedure. A simplified form of finite volume method discussed in chapter 4 enables a numerically efficient description of tubes and heat exchangers. The focus of this thesis is the calculation of thermophysical properties and system modelling (Cellier, 1991). The numerical solving procedure of the DAE-system that represents the model (Cellier and Kofman, 2006) is not the focus of this thesis.

Equations of State based Property Calculation

The term “equation of state” (EoS) is used in this thesis synonymously to the term “Zustandsgleichung” in the German-language literature. It is a general relationship between thermodynamic properties. An equation of state that relates p, ϱ and T is called a “thermische Zustandsgleichung” – thermal equation of state (See for instance Spurk et al., 2008, pp. 71-74; Johnson, 1998, section 4.2; Helrich, 2009). The definition

of the caloric variables of state, such as specific internal energy u, specific enthalpy h or specific entropy s, are denoted as "kalorische Zustandsgleichung" – caloric equation of state, if they are related to the volumetric properties. A fundamental equation of state relates the properties such that all other thermodynamic properties can be derived by differentiation.

Physical models of thermodynamic systems often require consistent thermophysical properties, because many physical equations refer to the properties of the involved materials. The relationship of thermodynamic fluid properties can be approximated by all kinds of equations of state (Gmehling et al., 2012, section 2.5). They differ in precision, calculation speed and effort to fit a new EoS. Numerically efficient system modelling should account for the range of operating conditions and provide an appropriate level of detail.

Fluids are most commonly described as incompressible liquids, ideal gases and real fluids. For example, a cooling fluid for which the properties are mainly dependent on the temperature can be conceived as an incompressible liquid. An ideal gas is composed of molecules that have no volume and do not interact. This approach can be used to describe gases such as air at atmospheric pressure. At high pressures, close to the dew point, or close to the critical point, a real fluid is an appropriate representation.

Cubic EoS or virial EoS (Poling et al., 2001, chapter 3-4; Dohrn, 1994, chapter 3-5) are often employed to calculate the thermodynamic properties of real fluids in thermodynamic processes or cycles. The properties and vapour-liquid equilibria of mixtures can also be obtained based on these EoS and mixing rules. Real fluid EoS of this kind are used in tools like ASPEN Plus (2013, 3-7), ChemCAD, HySys, Pro/II or ANSYS (see Valderrama, 2003). This group of EoS has only a few parameters that can be fitted, so only a relatively low effort is required to implement an EoS for a new fluid, or adapt parameters for better representation of the fluid in the relevant region.

Chapman et al. (1990) presented a new type of EoS based on statistical associating fluid theory: the SAFT equation of state. EoS of the SAFT-type describe the Helmholtz energy by different intermolecular forces, and it was developed for predicting phase equilibria of polymers. Today this type of EoS is employed for many different fluids and mixtures.

For some fluids, highly precise multiparameter (fundamental) EoS (Span, 2000) have been published. This type of equation is based on a selection of suitable terms and an optimisation of the coefficients. They are considered the state of the art of highly precise fluid property calculation. The equations are applied in simulation tools like TIL library (Schulze et al., 2011a; Richter, 2008; Gräber et al., 2010) and the AirConditioning Library (Tummescheit et al., 2005). Multiparameter EoS can be applied to mixtures, although this is rarely done due to the computational effort and the small number

of available equations (Gmehling et al., 2012). The choice of independent variables of an EoS has a major impact on the numerical efficiency of the governing balance equations in thermodynamic models (Tillner-Roth, 1998). The independent variables of the EoS should match the state variables of the system models; otherwise the iterative state variable transformation reduces the numerical efficiency of the simulation. The pressure p, specific enthalpy h and specific entropy s are suitable variables for description of technical processes. The thermodynamic potential $h = h(p, s)$ is rarely used as fundamental equation, since the entropy cannot be measured (Baehr, 1998; Dehli, 1975; Tillner-Roth, 1998).

Today, highly precise multiparameter fundamental EoS for the Helmholtz energy $f(\varrho, T)$ for the whole fluid region are preferred. The literature also describes fundamental EoS in the form of the Gibbs energy $g(p, T)$ or enthalpy $h(p, s)$. One special case is the EoS for the entropy $s(p, h)$ (Bender, 1970; Dehli, 1975; Thorade, 2010a): The enthalpy and pressure can be calculated from the mass and energy balance (see chapter 4), therefore a fundamental EoS with these independent variables would be suitable for transient simulation based on the first principle equations.

Fast and Highly Precise Calculation of Thermophysical Properties

The description of thermodynamic properties based on EoS is a trade-off between precision and calculation speed. The higher the precision of the EoS, the lower the calculation speed. The focus of this thesis is to investigate the provision of both highly precise and rapid calculation of thermophysical properties.

White (1964) presented a computer code that provides thermodynamic property data using two-dimensional quadratic interpolation on a rectangular grid. The resulting property surfaces and the first derivatives with respect to the independent variables are continuous. The data arrays consume a high amount of memory and are generated using the least squares fit method. Schot (1968) introduces the computer code THERMOSPLINE, which uses doubly cubic splines for the description of the thermodynamic properties of water. For real-time simulations, methods that require less data and are based on blending techniques (transfinite interpolation) have been developed. The authors also report on experiments using bilinear and bicubic spline interpolation (Hall and Mutafelija, 1975).

Klaus and Ness (1967) presented an extension to spline interpolation for the interpolation of thermodynamic data that enables the description of data that is not smooth. Herbst (1976) extended this method for two-dimensional interpolation of the fundamental EoS $g(p, T)$ with analytic derivation of the inverse function $h(s, p)$.

The IAPWS (International Association for the Properties of Water and Steam) has developed and published simple and fast methods to calculate the properties of water and steam, for instance the IFC-67 and the IF97 (Wagner et al., 2000). Additionally, an approach based on a Tabular Taylor Series Expansion (TTSE) was published by Miyagawa and Hill (2001), but this approach does not provide a continuous property surface.

Based on the algorithms proposed in the numerical recipes (Press et al., 2007), two-dimensional cubic and bicubic-spline interpolation of the properties of water were investigated by Müller (1994), who presented an algorithm for the optimisation of the grid point location. Kunick et al. (2008) describe the aims and initial results of a task group established in 2007 by the IAPWS to develop extremely fast and accurate property algorithms for CFD simulation. Biquadratic spline interpolation was proposed for property calculation and compared to TTSE and IAPWS-IF97, including analytic inversion functions for $h(p,T)$. Bonilla et al. (2012) solved chattering problems of simulation models based on IAPWS-IF97 with two-dimensional hermite bicubic spline interpolation. Drawing on the work of Kunick et al. (2008) and Gräber et al. (2012), Wang et al. (2012) present a biquadratic spline description of the p-T-surface of water. To deal with the discontinuity at the saturation line, the fluid region is separated into 32 subregions, assuming a rectangular grid.

For the thermophysical property description of fluids other than water, similar approaches have recently been investigated. The interpolated data are usually obtained from a multiparameter fundamental EoS. Andresen (2009) interpolated the Gibbs energy $g(p,T)$ and its derivatives linearly to describe CO_2 from the triple point to supercritical region based on Corberán et al. (2005) for linear interpolation and Ding et al. (2009) for fit equations. Gräber et al. (2012) use bicubic spline interpolation with a deformed rectangular grid to provide the properties of subcritical R-134a for non-linear model predictive control.

Biquadratic spline interpolation of the specific Helmholtz energy $f(\varrho,T)$ of superheated R-134a based on Kunick et al. (2008) was presented by Laughman et al. (2012). The inverse functions $v = (p,T)$ and $T(s,v)$ are derived and a two-dimensional Newton solver is proposed for $(T,v) = f(p,s)$.

In contrast to the above mentioned interpolation algorithms, Ding et al. (2009) present fit equations for subcooled refrigerants and refrigerant blends. Based on the previous work by Ding et al., Sieres et al. (2012) developed similar fit equations for more refrigerants employing version 9.0 of REFPROP (Lemmon et al., 2010).

Sözen et al. (2009) propose an artificial neural network (ANN) to calculate the thermodynamic properties of R-407C. R-407C is a zeotropic refrigerant blend of R-32, R-125 and R-134a and is used as a replacement for R-22 in air conditioning systems and heat

pumps. The blend is treated as a pseudo pure fluid, similar to the approach chosen by Lemmon (2003). Rohani et al. (2011) compared an ANN for the description of one-dimensional saturated properties to an EoS of the SAFT-type. Şencan Şahin et al. (2012) compared a two-dimensional ANN description of different refrigerants with an adaptive neuro-fuzzy interference system (ANFIS).

A comparison of different methods (linear interpolation, spline interpolation, fit equations for subregions) for application in simulation and optimisation of steam cycles in power plants is given by Schiebener (1989). In this contribution, calculation times are also presented and compared.

The approaches presented in this section all seem to be capable of describing thermophysical properties for simulation. They are accompanied by many others that have not been published and only implemented in commercial tools. One aspect that none of the above presented contributions have investigated is the interaction of modern DAE-solvers (differential algebraic equation) used for the numerical solving of thermodynamic system models, and thermophysical property calculation. The choice of a suitable interpolation method for thermophysical property calculation in transient simulations of thermodynamic systems requires taking into account a comparison of all relevant aspects.

Fast and Highly Precise Calculation of the Two-Phase Region of Mixtures

More sophisticated than the description of pure fluids for simulation is the description of mixtures. Although interpolation methods could be applied to describe the whole fluid region, this is not done due to the tremendous amount of data required. Often only the calculation of the VLE is optimised, whereas the one-phase region is still calculated using EoS. In the following, the discussion concentrates exemplarily on the well-described mixture ammonia-water.

Thorin (2001) presents a comparison of calculation methods for the mixture ammonia-water used for heat exchanger design. The difference in heat transfer areas calculated from different thermophysical property models is ca. 7%. For this reason a highly precise multiparameter EoS should be preferred over less accurate ones.

The vapour-liquid equilibrium (VLE) of a mixture is often calculated based on iterative numerical solving algorithms (Dohrn, 1994; Michelsen and Mollerup, 2007). Depending on the starting values and iteration algorithms, the VLE calculation may fail. To enable a fast and robust calculation of mixture properties, simple algorithms for particular saturated properties are required that can relate, for example, pressure, temperature and the composition of liquid and vapour.

Patek and Klomfar (1995) present simple fit equations for the VLE of the mixture ammonia-water. These equations were developed for the design of absorption systems, but can also be employed in simulations. Based on these equations Sun (1997), Conde-Petit (2006), Ganesh and Srinivas (2010) and Sadhukhan et al. (2012) present extensions for the contribution of Patek and Klomfar (1995).

Togashi et al. (2007) apply an ANN to describe selected saturated and one-phase properties, and perform an optimisation on a refrigeration cycle using ammonia-water as the refrigerant. Ma et al. (2009) present a simple simulation of an absorption cycle with transportation of low-grade thermal energy over long distances, applying the equations from Sun (1997) and Patek and Klomfar (1995).

Pratihar et al. (2010) describe a model for heat and mass transfer in absorption systems based on mass, energy and momentum balances, applying the EoS from Ziegler and Trepp (1984) and the finite difference method.

The fit equations like the ones proposed by Patek and Klomfar (1995) and their extensions sufficiently reproduce the VLE properties of the mixture ammonia-water, but an application to other mixtures requires the fitting of new coefficients. The precision and range of validity is limited. To the best knowledge of the author, to date, no general method is available to precisely describe the VLE properties of a mixture similar to those of Patek and Klomfar (1995) that does not require a new fit equation or procedure.

Numerical Efficient Modelling of Heat Exchangers using Finite Volume Method

A good overview on dynamic modelling of vapour compression refrigeration cycles is given by Rasmussen (2012). This two-part article provides in its first part a literature overview of modelling approaches based on the moving boundary method, finite volume method and lumped parameter models. The article also discusses the details of the respective solving methods, step size and real-time factor with regard to real-time simulation. In the second part of the article, modelling examples are presented and discussed.

A robust general purpose heat exchanger model on the system level that enables the description of condensation, evaporation and supercritical heat transfer, including the transient switching between these modes, is often realised by the finite volume method. Numerous balance equations, discretisation schemes and solving algorithms for this modelling approach can be found in the literature.

Concentrating on the relevant thermal behaviour of a heat exchanger, several modifi-

cations of the general finite volume method can be applied. If the momentum balance is neglected and an ideal stirring of the control volumes is assumed (UPWIND or UPSTREAM scheme) then the DAE-system (differential algebraic equation) cannot always be solved, as will be shown in chapter 4.

Model libraries such as Modelica.Fluid (Elmqvist et al., 2003) or ThermoPower (finite volume method: Casella and Leva, 2006; finite element method: Schiavo and Casella, 2007) allow to neglect the momentum balance. Rasmussen (2012) reports on more publications with neglected momentum balance.

None of the mentioned publications reports on systematic failure of the modifications of the finite volume method.

1.3. Objectives of this Thesis

The main objective of this thesis is the investigation of numerical efficiency aspects of system models and thermophysical property calculations for real-time simulations, nonlinear model predictive control and transient simulations in general. A comparison of different property calculation algorithms that accounts for the DAE-solving procedure has to date not been published. A general failsafe method for the description of the two-phase region of binary mixtures eases the calculation of vapour-liquid equilibria, but is not yet available. The singularity in the simplified finite volume method has not yet been discussed in the literature; a solution for this problem has yet to be presented.

The first part of this thesis is an investigation of numerically efficient thermophysical property calculation methods for use in transient simulations of thermodynamic systems.

- Comparison and implementation of selected table-based calculation methods for the whole fluid region of a pure or pseudo pure fluid in terms of calculation speed, thermodynamic consistency, amount of data required and influence on DAE-solving process. The approaches investigated will also be able to describe multicomponent blends with a wide temperature glide including the two-phase region as pseudo pure fluid.
- Development of a table-based approach to describe the two-phase region of a binary mixture. This approach should not dependent on a particular equation of state, and the accuracy needs to be adaptable to the requirements by automatic table creation.

The second part of this thesis is on the location and elimination of a singularity occurring

in finite volume method with a simplified momentum balance.

- Location of the singularity by analytically solving the governing balance equations
- Elimination of the singularity by a suitable modification of the finite volume method such that the models can be implemented in an object-oriented manner
- Numerically efficient combination of complex heat transfer and pressure drop correlations with the modified finite volume method

The third part of this thesis presents the application of the thermophysical property calculation methods and the simplified finite volume method on city bus alternative air conditioning systems, similar to the system evaluations of Kaiser et al. (2012a); Kossel (2011):

- Evaluation of the drop-in scenario with R-445A in a conventional R-134a air conditioning system, employing a table-based calculation method for the thermophysical properties.
- Evaluation of a transient system model for an absorption air conditioning system with ammonia-water as working pair and ammonia as refrigerant. This requires a suitable control strategy to enable transient operation.

Chapter 2.

Table-Based Calculation of Thermophysical Properties

In this chapter, bicubic spline interpolation of each property is identified as an appropriate method to interpolate the thermophysical properties of pure or pseudo pure fluids used in transient system simulation.

Interpolation or table-based methods are used to provide accurate data such as complex calculations are avoided. In the following, different approaches for table-based calculation methods are presented, details on the particular implementation are discussed and their performance is evaluated. Finally, the presented approaches are compared.

2.1. Requirements for Table-Based Methods

Fluid property calculations often dominate the calculation effort of a transient simulation of thermodynamic cycles on the system level. In figure 2.1 two exemplary profiling results of a CO_2 and an R-407C heat pump system modelled with the TIL library (Richter, 2008; Gräber et al., 2010; Schulze et al., 2011a) are shown. In software engineering, "profiling" is a form of dynamic program analysis used to trace the execution times of different parts of the source code.

The heat exchangers are modelled with a finite volume method as described in chapter 4. Additionally an efficiency-based compressor model, a Bernoulli valve model and a separator model with ideal separation between 10% and 90% filling level were used.

In both examples the property calculation of the working fluid as real fluid (VLEFluid) takes up more than 50% of the simulation time. The fluid properties are calculated using the multiparameter equation of state (EoS) implemented in the property library

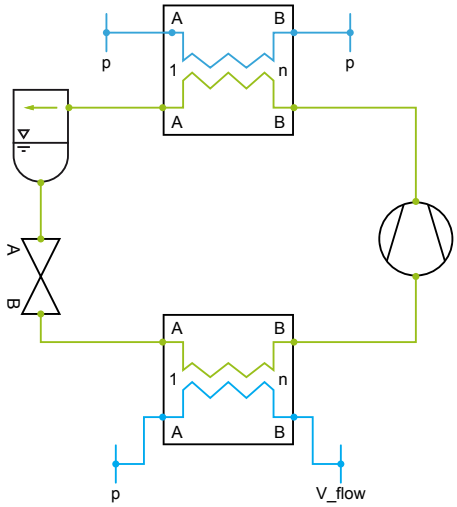

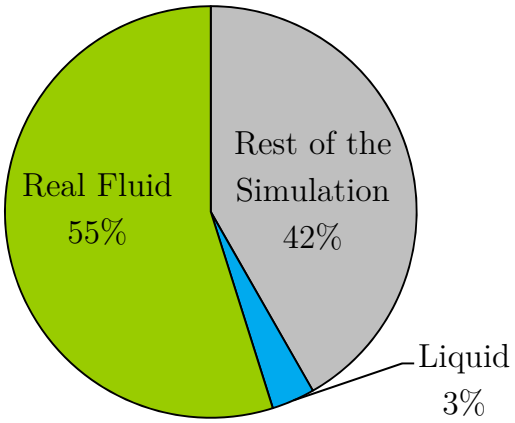

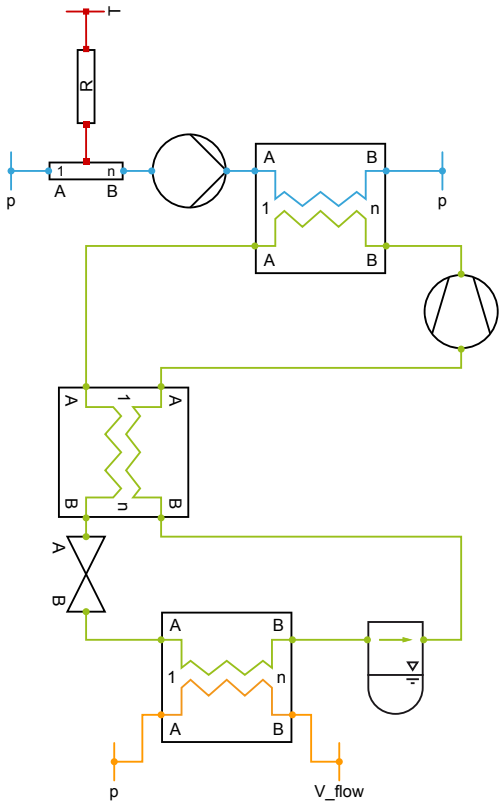

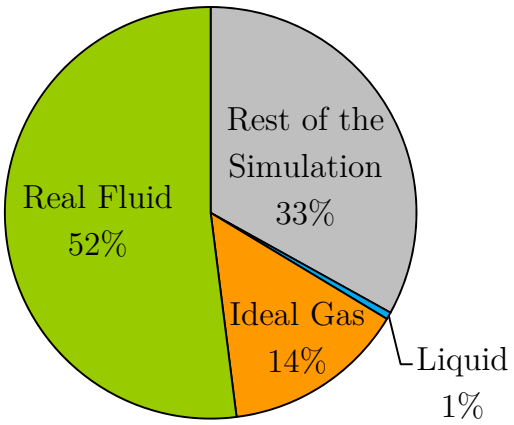

Figure 2.1.: Contributions to the execution time of an R-407C (upper diagram) and a CO_2 heat pump system simulation (lower diagram). Thermophysical property calculation dominates the simulation time, so this contribution must be investigated in terms of numerical efficiency.

TILMedia, whereas the properties at saturation are interpolated. The calculation effort for incompressible one-phase fluids (Liquid) is very low. Gas-vapour mixtures like moist air (Gas) cause a relatively high calculation effort of 14% due to the iterative solving algorithm of the heat exchanger model (thus it is a modelling issue).

Multiparameter EoS (Span, 2000) usually result in a high CPU-workload as they require many exp()-function calls. To accelerate the thermophysical property calculation of real fluids, simpler cubic EoS like the van der Vaals or the Soave-Redlich-Kwong equation could be applied (Poling et al., 2001, section 3-6). But if it is not possible or undesirable to replace the multiparameter EoS by a simpler but less accurate one, it seems reasonable to use table-based property calculation methods to replace the multiparameter EoS. Table-based calculation methods are usually faster than EoS-based calculation methods. Additionally, the independent variables of the EoS can be altered when the tables are generated.

When implementing a table-based interpolation procedure, the following aspects have to be taken into account (details further below):

- saturation properties $f(p)$ and $f(T)$ must be available, and output exactly the same as the 2D-interpolation routines: $f(p,h)$,$f(p,s)$,$f(p,T)$
- properties must be thermodynamically consistent (see Swesty, 1996):

$$\int_{t_1}^{t_2} \left(c_p \frac{dT}{dt} + \left(\frac{\partial h}{\partial p} \right)_T \frac{dp}{dT} \right) dt = \Delta h_{p=\text{const.}} \quad \text{or} \tag{2.1}$$

$$\int_{t_1}^{t_2} \left(\left(\frac{\partial \varrho}{\partial p} \right)_h \frac{dp}{dt} + \left(\frac{\partial \varrho}{\partial h} \right)_p \frac{dh}{dt} \right) dt = \Delta \varrho \tag{2.2}$$

- the amount of data that can be stored may be limited in some way
- close to the critical point, properties like c_p and β are equal to infinity and must not have poles
- the influence on the DAE-solver during simulation must be minimised

The saturation properties calculated from the 1D algorithm must be equal to the saturation properties calculated from the 2D algorithm. Usually the thermodynamic properties in the two-phase region are calculated from the saturation properties and the vapour quality. In this case, deviating properties at saturation cause discontinuities at the dew and bubble line. Since it is possible to implement algorithms and thermodynamic models that require a consistent description between 1D and 2D algorithms, the calculation methods should not implicitly narrow the range of application from the very beginning.

$$\varrho = \frac{1}{\frac{1}{\varrho_{\text{liq}}}(q-1) + \frac{1}{\varrho_{\text{vap}}}q} \tag{2.3}$$

The two-phase region should not be interpolated the same way as the one-phase region. All properties inside the two-phase region can be calculated from the saturation properties and the vapour quality q, as it is done for the density ϱ (2.3) when using an EoS. For the density close to the bubble line in particular, this procedure provides a higher precision.

The calculated properties should be as thermodynamically consistent as possible. If for example $s = f(p,h)$ and $T = f(p,h)$ are described by interpolation routines, then T calculated from the derivative $\left(\frac{\partial s}{\partial h}\right)_p = \frac{1}{T}$ does not necessarily match $T = f(p,h)$.

On the one hand, the partial derivatives of the density with respect to pressure and specific enthalpy in the one-phase region can be derived from the thermodynamic relations (2.4)-(2.5) (see appendix A on page 117 or Bejan, 2006, Bridgeman's Table, page 182). On the other hand, they can be obtained by analytical differentiation of the interpolant surface of the density $\varrho = f(p,h)$. If an interpolation method is used to calculate each thermodynamic property, then the thermodynamic relations are not necessarily fulfilled. The partial derivatives of the density required by the mass balance of the simulation model (see section 4.2) do not exactly match the density surface of the interpolation routine. Consequently, mass will appear or disappear during simulation. To eliminate this error during simulation, the mathematically correct derivative of the density surface must be used for the mass balance.

In the two-phase region, the expression is more complex (2.7)-(2.6). The derivation of these expressions can be found in appendix B on page 119. These relations are valid both for common EoS and interpolation routines.

$$\left(\frac{\partial \varrho}{\partial p}\right)_{h,\text{one-phase}} = -\frac{1}{v^2}\left(\frac{T\beta^2 v^2 - \beta v^2 - \kappa v c_p}{c_p}\right) \tag{2.4}$$

$$\left(\frac{\partial \varrho}{\partial h}\right)_{p,\text{one-phase}} = -\frac{1}{v^2}\left(\frac{\beta v}{c_p}\right) \tag{2.5}$$

$$\left(\frac{\partial \varrho}{\partial p}\right)_{h,\text{two-phase}} = -\frac{1}{v^2}\left[\left(\frac{\partial v_{\text{liq}}}{\partial p}\right)_{\text{sat}} + \left(\left(\frac{\partial v_{\text{vap}}}{\partial p}\right)_{\text{sat}} - \left(\frac{\partial v_{\text{liq}}}{\partial p}\right)_{\text{sat}}\right) \cdot q + (v_{\text{vap}} - v_{\text{liq}}) \cdot \left(\frac{\partial q}{\partial p}\right)_h\right] \tag{2.6}$$

$$\left(\frac{\partial \varrho}{\partial h}\right)_{p,\text{two-phase}} = -\frac{1}{v^2}\frac{v_{\text{vap}} - v_{\text{liq}}}{h_{\text{vap}} - h_{\text{liq}}} \tag{2.7}$$

The amount of data that can be stored to interpolate fluid properties may be limited in some way. For example, some real-time simulation environments run models in the kernel-space of Linux; thus an external file on the hard disk cannot be accessed directly. In that case all data have to be included into the source code. If the size of the executable or the memory is limited, then the amount of data is limited, too.

For some properties such as specific heat capacity c_p or the linear isobaric thermal expansion coefficient β, the interpolation quality increases significantly if the inverse value is interpolated. On the one hand, these properties are equal to infinity at the critical point of a pure fluid. On the other hand, β can be less than 0 (for example liquid water below $4°C$), which may cause a division by 0 if β is inverted. A preconditioning of the interpolated values needs to account for these aspects.

The interpolation quality influences variable step size BDF-solvers like DASSL (Petzold, 1983). Depending on the internal integration order, the solver senses discontinuities of fluid properties and their derivatives. Solvers often assume the continuity of the system up to the order of 16. In case of discontinuous or non-differentiable systems, reliable error estimation cannot be guaranteed, and the step size will be reduced (Schuler, 2008, pp. 59).

In the following, different interpolation methods to describe fluid properties with the independent variables pressure and specific enthalpy are presented and compared. These methods incorporate the aspects mentioned above. The two-phase region is dealt with differently from the one-phase region and the properties are preconditioned. The saturation properties can be accessed with a separate 1D function. The algorithms were optimised to increase the thermodynamic consistency and reduce the amount of data that needs to be stored. Finally, the results and the influence on the DAE-solving procedure are evaluated.

2.2. State of the Art Spline Interpolation Routines

This section describes the spline interpolation routines used in the following sections 2.3.2, 2.3.3 and chapter 3.

Cubic spline interpolation can be used to interpolate between a given set of function values. The benefits of spline interpolation are a relatively low amount of data needed to gain a high interpolation quality. A bicubic spline is a piecewise-defined two times continuously differentiable function. Mathematical BDF-solvers of a DAE or derivative-based optimization in particular require these qualities. For descriptions of splines see de Boor (1962, 2001); Späth (1995a,b). Spline interpolation as discussed in this section has already been published in Schulze and Köhler (2013).

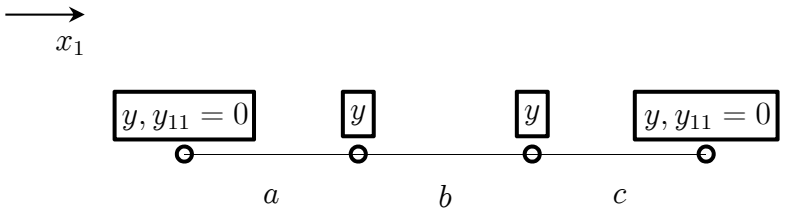

Figure 2.2.: Transition and boundary constraints of a cubic spline. The function values y at the grid points, the second derivative y_{11} (or similar information) at both ends are required.

The basic equation used for interpolation is a cubic polynomial (2.8).

$$y = \sum_{i=0}^{3} c_i \cdot x^i \tag{2.8}$$

In figure 2.2 the constraints at the transition from one interval to another are shown. y denotes a function value, y_1 the first derivative with respect to the first dimension and y_{11} the second derivative with respect to the first dimension. The values that are required by the user are framed. At the transition from an interval a to an interval b, the constraints are given by the equations (2.9) - (2.11).

$$y_a = y_b \tag{2.9}$$

$$\frac{\partial y_a}{\partial x} = \frac{\partial y_b}{\partial x} \tag{2.10}$$

$$\frac{\partial^2 y_a}{\partial x^2} = \frac{\partial^2 y_b}{\partial x^2} \tag{2.11}$$

Thus the resulting spline function must be two times continuously differentiable. Further spline boundary conditions (2.12)-(2.15) are needed (here at the end of the interval a and c). Usually the first or the second derivative can be set at both ends. A spline with the second derivative set to 0 is called a natural spline.

$$\frac{\partial y_a}{\partial x} = \ldots \quad (2.12) \qquad \text{or} \qquad \frac{\partial^2 y_a}{\partial x^2} = 0 \quad (2.14)$$

$$\frac{\partial y_c}{\partial x} = \ldots \quad (2.13) \qquad \frac{\partial^2 y_c}{\partial x^2} = 0 \quad (2.15)$$

Table 2.1.: Comparison between number of constraints and number of unknowns. n function values and two boundary conditions are needed to create a twice continuously differentiable spline

	number of constraints
function values	n
constraints eq. (2.9)–(2.11)	$3 \cdot (n-2)$
boundary condition eq. (2.12)–(2.15)	2
total	$4 \cdot (n-1)$

	number of unknowns
unknowns per interval	4
intervals	$n-1$
total	$4 \cdot (n-1)$

In table 2.1 the number of constraints and unknown variables are summarised. Easy-to-use implementations of cubic spline coefficient generation algorithms and interpolation algorithms are provided by Press et al. (2007).

Bicubic interpolation (not spline) follows the same concept as one-dimensional interpolation. Equation (2.16) is the polynomial that describes the surface between four grid points.

$$y = \sum_{i=0}^{3} \sum_{j=0}^{3} c_{ij} \cdot x_1^i \cdot x_2^j \qquad (2.16)$$

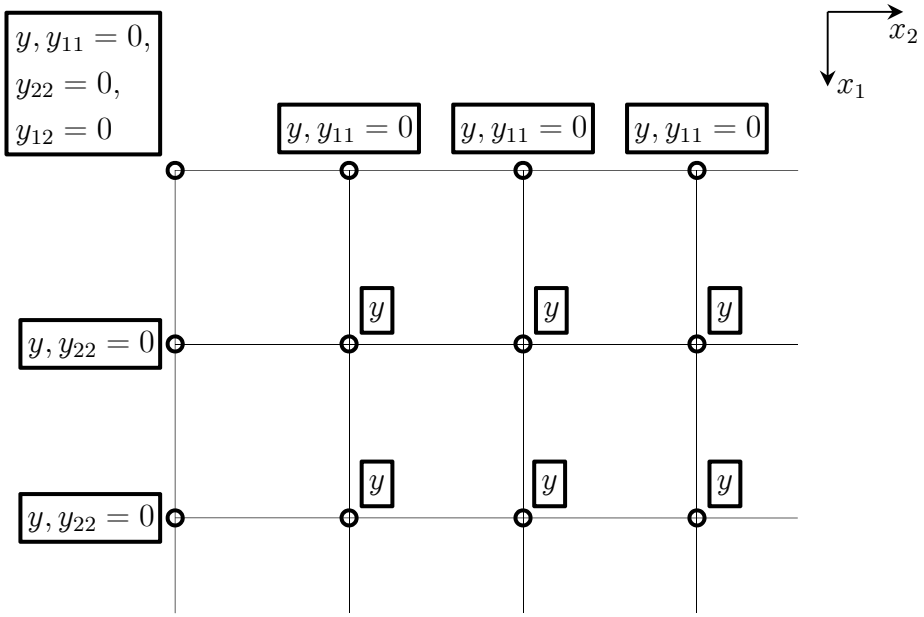

Figure 2.3.: Values that are required for bicubic spline interpolation on a two-dimensional rectangular grid. Function values y at the grid points, the derivatives y_1 respectively y_2 at the borders and a cross derivative at the edges are required.

Sixteen coefficients are used to describe equation (2.16). To calculate these coefficients the values of y, y_1, y_2 and y_{12} at each grid point can be used. So if these four values are given for $n \cdot m$ grid points, then $(m-1)(n-1)$ surfaces can be obtained from it, as they share the information at the grid points.

If y, y_1, y_2 and y_{12} are given or approximated, then it can only be guaranteed that the surface is continuous at the grid points and at the connecting line from one grid square to another. If the four values y, y_1, y_2 and y_{12} are determined globally using 1D-splines, then this approach is usually called bicubic "spline" interpolation (Press et al., 2007).

There are different ways to perform the bicubic spline interpolation. In the following the 1D-splines in the direction of x_1 are termed column-splines and the 1D-splines in the direction of x_2 are row-splines. The basic algorithm "splin2", presented in the numerical recipes (Press et al., 2007) and applied to fluid properties by Müller (1994) is:

- create row-splines for all rows
- perform 1D interpolation in direction x_1 for all rows
- create temporary column-spline through the results of the last step
- perform 1D interpolation in direction x_2

A different algorithm is implemented in the ALGLIB 3.7 library (Shearer and Wolfe, 1985), which is an open source library for data processing and numerical analysis. Similar to the approach mentioned in Press et al. (2007), 1D-splines are used to calculate y, y_1, y_2 and y_{12} at each grid point. The coefficients for equation (2.16) can then be determined and stored. No further algorithm is required, and only equation (2.16) needs to be evaluated:

- create row-splines for all rows through the function values y
- analytically differentiate the row-splines to obtain y_2 at each grid point
- create column-splines for all columns through the function values y
- analytically differentiate the columns-splines to obtain y_1 at each grid point
- create row-splines for all rows through the derivative of the function values y_1 (the results of the last step) to obtain the cross derivative y_{12} at each grid point
- calculate quantities c_{ij} for each grid square from y, y_1, y_2 and y_{12}
- perform 2D interpolation using c_{ij}

The algorithm implemented in ALGLIB 3.7 does not provide a twice continuously differentiable surface since more boundary conditions are given by the user than actually are needed. The 1D-splines that are used to describe y_1 in direction of x_2 need a boundary constraint at both ends. If only the cross derivative at the edge of the grid is given, then the cross derivatives at the first and last column of grid points can be calculated, which then can be used as boundary condition at both ends of the row-splines for the cross derivative.

Following the approach of de Boor (1962), the constraints and values to be given by the user (framed) are illustrated in figure 2.3. From these constraints the required values for y, y_1, y_2 and y_{12} can be calculated using 1D-splines. The algorithm to calculate the coefficients of a twice continuously differentiable surface (bicubic spline interpolant) applied in this work follows de Boor (1962) and is based on 1D-splines:

- create row-splines for all rows through the function values y (de Boor, 1962, eq. (11))
- analytically differentiate the row-splines to obtain y_2 at each grid point
- create column-splines for all columns through the function values y (de Boor, 1962, eq. (13))
- analytically differentiate the columns-splines to obtain y_1 at each grid point
- create 1D-splines in direction x_2 for first and last row through the derivative of the function values y_1 using the cross derivative given by the user as boundary condition (de Boor, 1962, eq. (12))

- create column-splines for the first and last row through the derivative of the function values y_2 to obtain the cross derivative y_{12} at the grid points of the first and last column
- create row-splines for all rows through the derivative of the function values y_1 to obtain the cross derivative y_{12} at the remaining grid points
- calculate quantities c_{ij} for each grid square from y, y_1, y_2 and y_{12}
- perform 2D interpolation using c_{ij}

The 1D-spline algorithms are applied in section 2.3.2 and 2.3.3 for the saturated enthalpies and the calculation of the coefficients c_{ij} of the 2D surface in section 2.3.2. The algorithms presented in chapter 3 are also based on the 1D-spline algorithm.

2.3. Investigated Interpolation Algorithms

2.3.1. Linear Interpolation of Each Property

In this section, a simple method is presented that enables the consistent description of properties at saturation and two-dimensional properties in the one-phase region using linear interpolation.

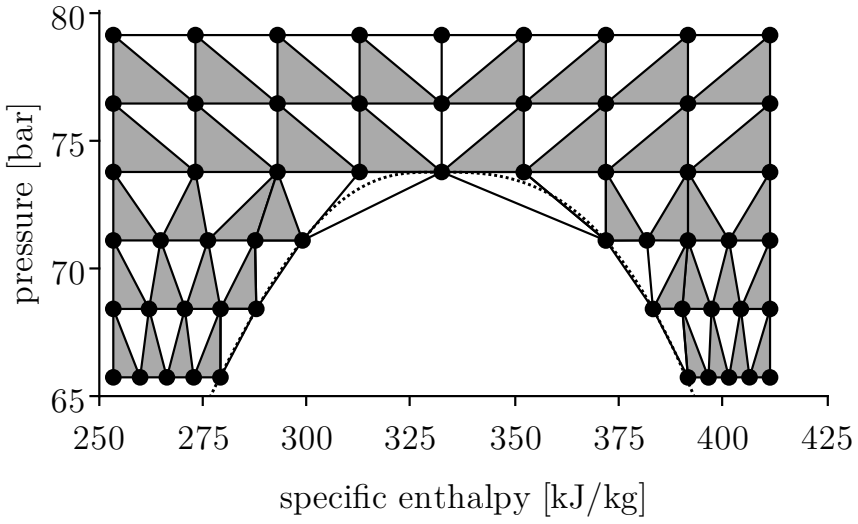

Figure 2.4.: Grid of linear interpolation algorithm in the critical region of a p-h-diagram. Grid is narrower in sub-critical region and requires a triangulation algorithm.

The step size in the direction of pressure can be set constant on a linear or a logarithmic scale. To avoid a search algorithm to find the pressure grid index i_p for a given pressure, the inverse function must be accessible $i = f_\mathrm{inverse}(p)$, assuming a logarithmic scale $f_\mathrm{inverse}(p) = \frac{log(p) - p_\mathrm{min}}{l_\mathrm{p,log}}$, whereas $l_\mathrm{p,log}$ is the logarithmic step size.

As shown in figure 2.4, the grid points are narrower in the direction of specific enthalpy on both sides of the two-phase region. This approach provides a higher precision in the sub-critical one-phase region and describes the saturation properties with a 1D interpolation at a constant enthalpy grid index i_h. The saturation properties exactly match the 2D properties. The properties in the two-phase region are calculated from the saturated liquid and vapour properties.

The following triangulation algorithm is used to select the closest three grid points for linear interpolation: For a given pressure p^* and a given specific enthalpy h^*, the upper and lower pressure index $i_\mathrm{p,upper}$, $i_\mathrm{p,lower}$ can be calculated from the given pressure p^*. Based on the step size in direction of specific enthalpy, the interpolation interval and the corresponding grid index i_h can be determined.

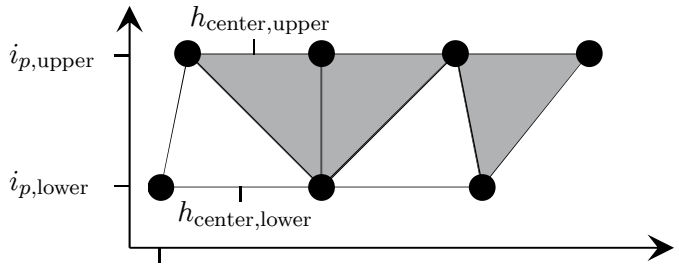

Figure 2.5.: Illustration of the triangulation algorithm. The line between two grid points at the same pressure is always connected to the grid point at the next pressure index that is closest in direction of specific enthalpy to its h_center.

To calculate the properties with other independent variables (p-T or p-s), a search algorithm or another 2D interpolation table $h = f(p, T)$ can be implemented. In this case, separate tables for $h = f(p, T)$ and $s = f(p, T)$ were implemented.

The amount of data needed by this algorithm is defined by the number of grid points and the number of interpolated properties. Tables for the temperature T, density ϱ, specific entropy s, isobaric specific heat capacity c_p, isobaric linear thermal expansion coefficient β, speed of sound w, compressibility κ, thermal conductivity λ and dynamic viscosity η were stored. Some properties are preconditioned, namely $\frac{1}{c_p}$, $\frac{1}{\beta+\beta_0}$, $\frac{1}{\varrho}$ and $\frac{1}{\kappa}$ are stored instead of the original value.

The partial derivatives of the density $\left(\frac{\partial \varrho}{\partial h}\right)_p$ and $\left(\frac{\partial \varrho}{\partial p}\right)_h$ are determined thermodynamically correct according to (2.4)-(2.7). The density surface is not continuously differentiable due to the linear interpolation, so analytical differentiation leads to a piecewise constant surface. All symbols in (2.4)-(2.7) are represented by linearly interpolated surfaces and consequently, the values calculated from them are continuous. If finite volume models as described in section 4.2 are used, then discontinuities in the partial derivatives of the density cause discontinuities in the mass flow rate and should therefore be avoided.

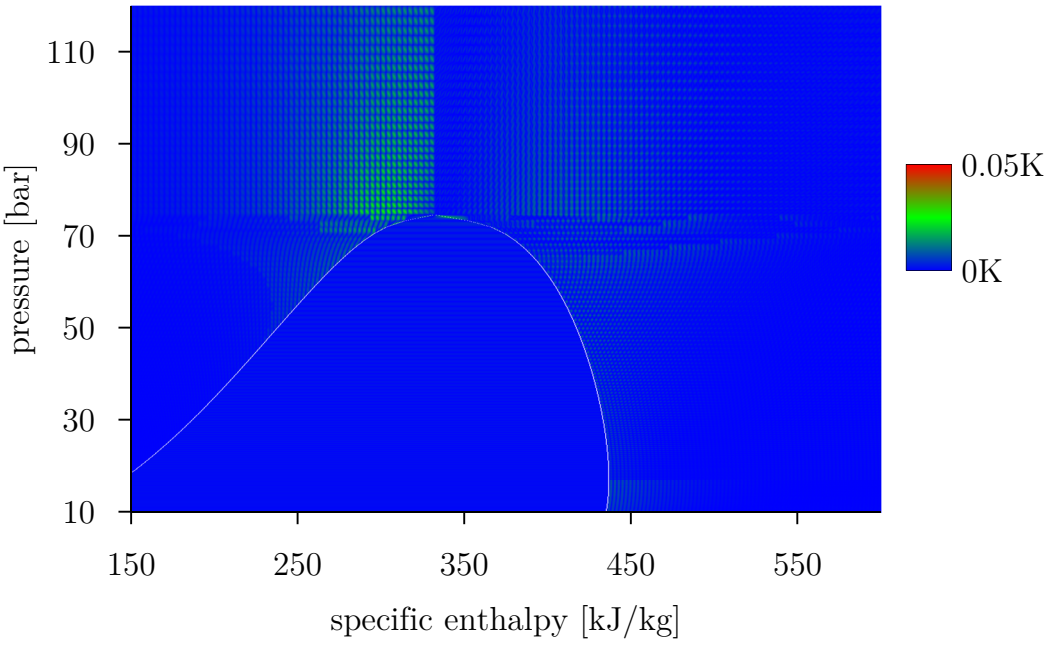

Figure 2.6.: Deviation of the temperature from the EoS for CO_2 (Span and Wagner, 1996) in a p-h-diagram, applying the linear interpolation algorithm to CO_2 with $200 \cdot 200$ grid points, with p in $[5.2bar, 200bar]$, and h in $[50\frac{kJ}{kg}, 700\frac{kJ}{kg}]$.

In figure 2.6 the deviation of the temperature from the multiparameter EoS for CO_2 (Span and Wagner, 1996) implemented in REFPROP is depicted. This EoS is a fundamental equation of state. $200 \cdot 200$ grid points were stored with p in $[5.2bar, 200bar]$ and h in $[50\frac{kJ}{kg}, 700\frac{kJ}{kg}]$. Red represents a deviation of $>= 0.05$K. The deviation is mainly caused by the interpolation quality. Above the critical pressure, a change in the orientation of the triangles left and right of the critical specific enthalpy is visible as a change in the deviation pattern.

In the one-phase region the deviation of the thermodynamic properties from the original fundamental EoS is less than in the two-phase region. As the properties in the two-

phase region are calculated from the saturation properties, a small deviation in the two-phase region implies a small deviation of the saturation properties.

Table 2.2.: Summary of linear interpolation algorithm

property tables	$T, v, s, \frac{1}{c_p}, \frac{1}{\beta+\beta_0}, \frac{1}{\kappa}, w, \quad \eta, \lambda$
size of property table	$n \cdot m$ values
additional tables	saturation enthalpy ($2 \cdot m$ values)
inverse functions	2 separate tables (p-T, p-s) of the same size
properties saturation	separate 1D interpolation for a given pressure
derivatives of density	thermodynamically consistent

2.3.2. Bicubic Spline Interpolation of Each Property

Spline interpolation of fluid properties has been proposed and successfully implemented by other authors. It was applied to the properties of steam and water and to the properties of refrigerants (see section 1.2).

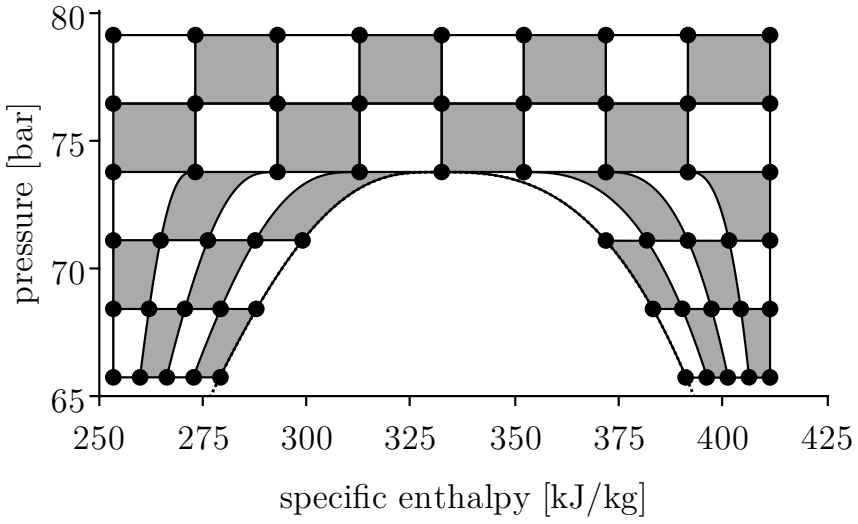

Figure 2.7.: Potentially applicable non-rectangular grid for spline interpolation algorithm in the critical region of a p-h-diagram. The grid causes steps at critical pressure and non-linear deformation in sub-critical region.

The main challenge when implementing this approach is to integrate the two-phase region into the spline surface. One interesting approach to doing so this is to offset and/or deform the one-phase region around the two-phase region (Gräber et al., 2012). The same grid point positions as for the linear interpolation algorithm presented in section 2.3.1 can be used to do so (see figure 2.7). The polynomial surface is used to describe the surface between the four grid points as if it ware a rectangular grid so that the deformation and offset can be applied to the independent variables. The fluid properties are required only at the grid points in the one-phase region. The offset applied to the independent variable is the saturated specific enthalpy.

However, the derivative of the saturated specific enthalpy with respect to pressure (2.17) goes to infinity in the limit as p approaches the critical pressure.

$$\lim_{p \to p_c} \frac{dh_{\text{dew}}}{dp} = -\infty \tag{2.17}$$

The non-linear specific enthalpy offset and the deformation below the critical point leads to a comparably poor description of properties around the critical pressure. The saturated specific enthalpy is described by a 1D-spline as a function of the pressure, so that the derivative will never go to infinity. The lesser the precision of the saturated specific enthalpy close to the critical pressure, the higher the precision of properties in the one-phase region.

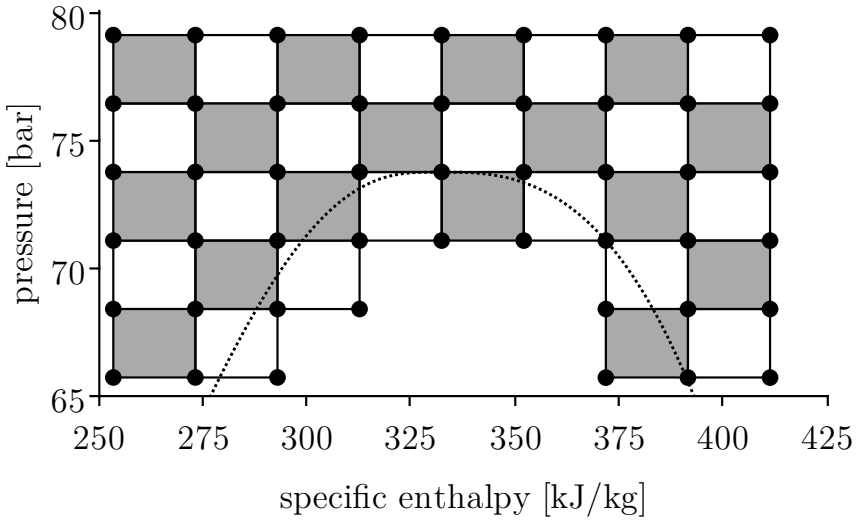

Figure 2.8.: Rectangular grid used for spline interpolation in the critical region of a *p-h*-diagram. Determination of extrapolated fluid properties in the two-phase region is required.

Another approach based on the rectangular grid is illustrated in figure 2.8. The main problem that arises from this grid is that some of the grid points are in the two-phase region.

These grid points inside the two-phase region are needed to calculate the coefficients of the surface pieces located only partially in the one-phase region. The determination of 1-3 grid points in the two-phase region is required per surface. These theoretical fluid states can on the one hand be considered metastable (Kretzschmar, 2012) states of the fluid and on the other hand as extrapolation into the two-phase region. Close to the saturation lines, the properties in the two-phase region from the EoS can be used.

Wagner and Pruß (2002, section 7.3.2, page 474) write: "In contrast to an equation of state of the so-called van der Waals type whose isotherms form only one minimum and one maximum in the two-phase region, state-of-the-art multiparameter equations of state have, sufficiently far from the critical point, several minima and maxima along an isotherm. This is also true for the IAPWS-95 formulation. Taking this into account, the "real" spinodals are only those lines that connect the outermost minima and the maxima of the isotherms. The inner minima and maxima are only of mathematical and not of physical importance."

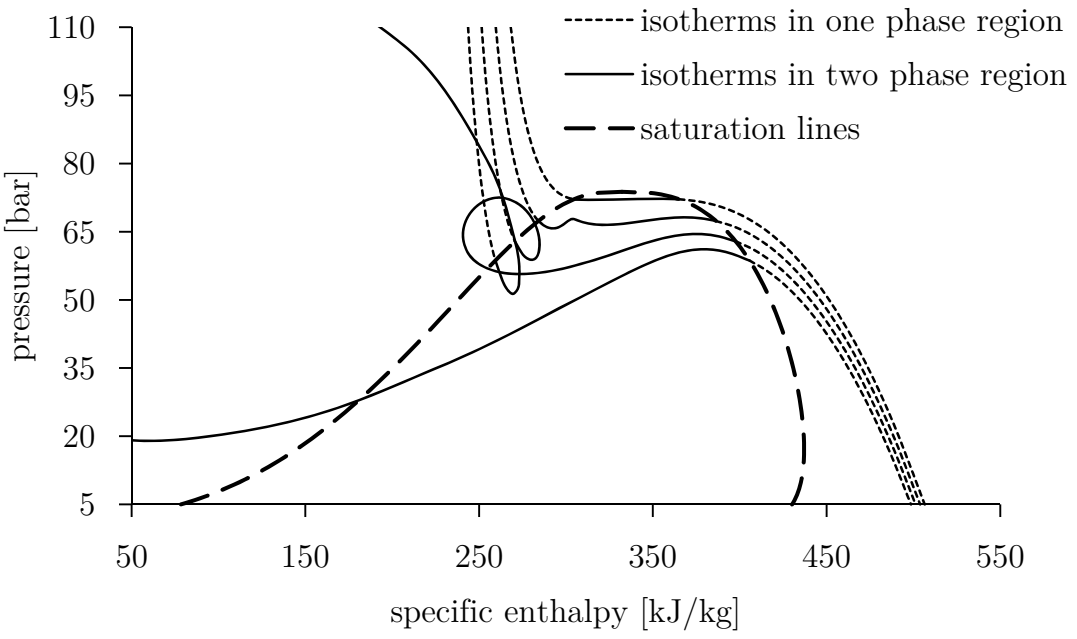

Figure 2.9.: Isotherms of CO_2 at $T = \{21°C, 24°C, 27°C, 30°C\}$ including the two-phase region, where they are physically not correct. The shape of the isotherms is highly non-linear.

In figure 2.9 isotherms of the multiparameter EoS of CO_2 (Span and Wagner, 1996) evaluated in the one and two-phase regions are depicted. The results in the two-phase region have no physical meaning. The figure illustrates the described minima and maxima of the EoS.

The numerical solving algorithm to calculate $\{\varrho, T\} = f(p, h)$ using a multiparameter EoS must not evaluate the EoS between the spinodals. If the EoS can be evaluated between the spinodals then there are many mathematically correct solutions for the inversion function $\{\varrho, T\} = f(p, h)$, the solutions are not necessarily unique. Figure 2.9 also illustrates that metastable states inside the two-phase region should be calculated very carefully from a multiparameter EoS.

The extrapolation of the thermophysical properties into the two-phase region on the other hand, is an inaccurate albeit reliable approach. If the extrapolation is based on the one-phase grid points using 1D-splines, the following issues have to be taken into account:

- The extrapolation from different directions (x_1 or x_2) will lead to different results. One value must be selected when calculating the spline coefficients.
- The integration of the two-phase region into the property surface, without affecting the differentiability, requires an adaptation of the algorithms discussed in section 2.2
- The extrapolation of properties like density ϱ or specific heat capacity c_p through the critical point need special attention

The properties at saturation are obtained from the one-phase region spline surfaces. The saturated specific enthalpies $h_{\text{sat}} = f(p)$ are stored in a 1D-spline. So for a given pressure the specific enthalpy at dew and bubble point can be calculated, which can then be used to calculate the other saturation properties. The edge of the two-phase region is connected continuously to the one-phase region, but there is no constraint that requires $T_{\text{bubble}} = T_{\text{dew}}$.

The inverse functions to calculate the specific enthalpy from temperature or specific entropy at a given pressure are based on a search algorithm. First the search algorithm identifies the indexes between which the 2D-spline surface crosses the correct output value; second the cubic spline equation at the given pressure is solved analytically for the input value using Cardano's method (Bronštejn et al., 2003, section 2.4.2.3).

The partial derivatives of the density can be calculated from the specific volume spline surface. The first and second derivative of the polynomial surface are known and continuous. The exact mathematical solution $\left(\frac{\partial \varrho}{\partial p}\right)_h$ and $\left(\frac{\partial \varrho}{\partial h}\right)_p$ are calculated from the spline surface $v = f(p, h)$ and its derivatives. This prevents an error in the mass

calculation during simulation caused by the fluid properties. The partial derivatives of the density are consistent with the $v = f(p, h)$-surface but not necessarily with the other ones, so that the thermodynamically correct equations (2.4) and (2.5) will not apply exactly.

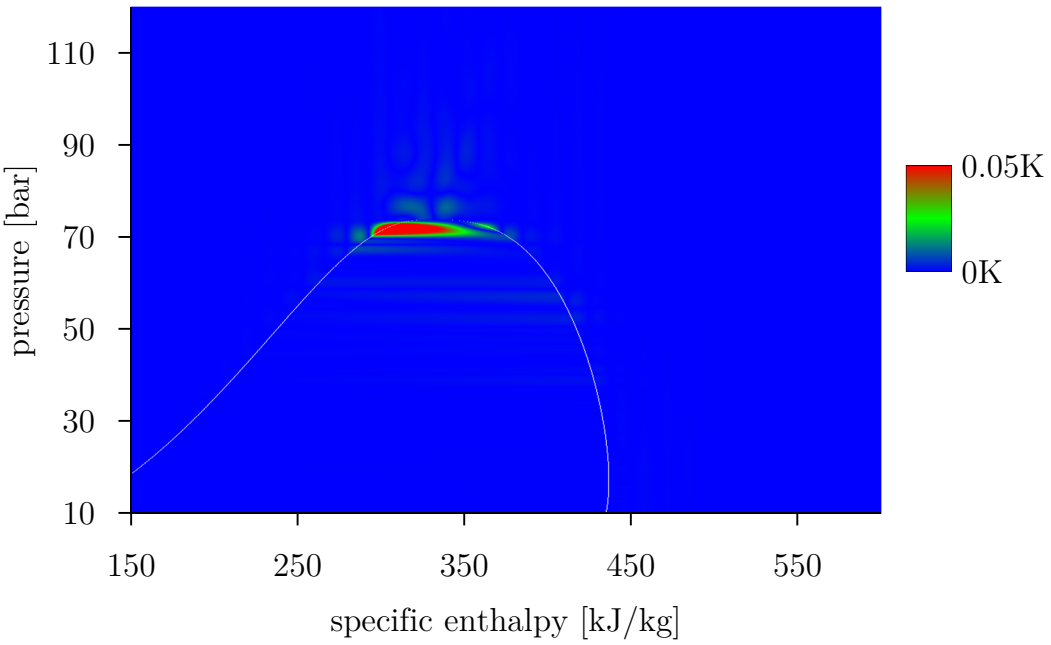

Figure 2.10.: Deviation of the temperature from the EoS for CO_2 (Span and Wagner, 1996) in a p-h-diagram, applying the bicubic spline interpolation algorithm to CO_2, with $50 \cdot 50$ grid points with p in $[5.2bar, 200bar]$, and h in $[50\frac{kJ}{kg}, 700\frac{kJ}{kg}]$. The high deviation of the temperature around the critical region is caused by the extrapolated properties in the two-phase region below the critical point.

In figure 2.10 the deviation of the temperature from the EoS for CO_2 (Span and Wagner, 1996) is shown in a p-h-diagram. The deviation is only high close to the critical region due to the inaccuracy of the extrapolation into the two-phase region.

The chosen method to was invert the functions is the exact solution (search algorithm + inversion of the cubic function $\{T, s\} = f(h)_{\text{p=const.}}$). The time needed for the search algorithm depends on the number of grid points. The more grid points that are used, the more time is needed by the search algorithm. An additional table for the inverse functions could also be implemented, but a mapping of the region boundaries p-h to p-T is difficult, assuming a rectangular grid for the inverse function.

Table 2.3.: Summary of bicubic spline interpolation algorithm

property tables	$T, v, s, \frac{1}{c_p}, \frac{1}{\beta+\beta_0}, \frac{1}{\kappa}, w, \quad \eta, \frac{1}{\lambda}$
size of property table	$n \cdot m \cdot 4$ values
additional tables	saturation enthalpy (variable size)
inverse functions	search algorithm and analytic inversion
properties at saturation	evaluation of one-phase properties
derivatives of density	mathematically correct derivative

2.3.3. Bicubic Interpolation describing a fundamental EoS

Although all thermodynamic properties can be obtained from a fundamental EoS, transport properties (viscosity, thermal conductivity) cannot. Usually an EoS has only one set of coefficients per fluid. For example, the ideal gas law requires only one coefficient, namely the gas constant. The terms in the far more complex multiparameter EoS are selected from a bank of terms based on the fluid data set. Some fluid groups were fitted simultaneously to select the terms that are optimal for the description of all fluids of the group (Span and Wagner, 2003). Besides fitting the coefficients and selecting suitable terms, it is an important and challenging task to fill the bank of terms with suitable terms.

For technical applications the relevant independent variables are often pressure and specific enthalpy (Thürmer, 1969; Baehr, 1971, 1998; Tillner-Roth, 1998; Casella, 2006). An equation that describes the specific entropy s with the independent variables pressure p and specific enthalpy h is a fundamental EoS. This has already been discussed by Bender (1970); Dehli (1975) and more recently by Thorade (2010a,b). The equations (2.18)-(2.23) can be derived from the Bridgeman's table (Bejan, 2006) and were published already by Dehli (1975). They show how the properties can be determined from the fundamental EoS $s(p, h)$.

$$T = \frac{1}{\left(\frac{\partial s}{\partial h}\right)_p} \tag{2.18}$$

$$c_p = -\frac{\left(\frac{\partial s}{\partial h}\right)_p^2}{\left(\frac{\partial^2 s}{\partial h^2}\right)_p} \tag{2.19}$$

$$\varrho = -\frac{\left(\frac{\partial s}{\partial h}\right)_p}{\left(\frac{\partial s}{\partial p}\right)_h} \tag{2.20}$$

$$\beta = \left(\frac{\partial s}{\partial h}\right)_p \left(1 - \frac{\frac{\partial^2 s}{\partial p \partial h} \cdot \left(\frac{\partial s}{\partial h}\right)_p}{\left(\frac{\partial^2 s}{\partial h^2}\right)_p \cdot \left(\frac{\partial s}{\partial p}\right)_h}\right) \tag{2.21}$$

$$\kappa = \frac{\frac{\frac{\partial^2 s}{\partial p \partial h}^2}{\left(\frac{\partial^2 s}{\partial h^2}\right)_p} - \left(\frac{\partial^2 s}{\partial p^2}\right)_h}{\left(\frac{\partial s}{\partial p}\right)_h} \tag{2.22}$$

$$w = \sqrt{-\frac{\frac{\partial s}{\partial p} \cdot \frac{\partial s}{\partial p} \cdot \frac{\partial s}{\partial h}}{2 \cdot \frac{\partial^2 s}{\partial p \partial h} \frac{\partial s}{\partial h} \frac{\partial s}{\partial p} - \frac{\partial^2 s}{\partial p^2} \frac{\partial s}{\partial h}^2 - \frac{\partial^2 s}{\partial h^2} \frac{\partial s}{\partial p}^2}} \tag{2.23}$$

If the surface $s(p, h)$ is used to describe the fundamental EoS, then the general form of the equation is of course a bicubic polynomial. The coefficients are only valid for a small region, so it is a piecewise-defined simple fundamental EoS (similar to the extension proposed by Laughman et al., 2012). Compared to the approach in section 2.3.2, to use a spline surface for each property, this approach only requires a table for specific entropy and the transport properties, which cannot be derived from an EoS.

The bicubic polynomial has to be differentiated two times to get all information needed (eq. (2.18)-(2.23)). The second derivative of a cubic polynomial is linear, so the quality of the second derivatives of the EoS is low. For instance $\left(\frac{\partial^2 s}{\partial h^2}\right)_p = f(p, h)$ depends linearly on specific enthalpy. Properties that are calculated from the second derivative, for example specific heat capacity c_p or speed of sound w, are very sensitive to the step size of the grid. The interpolation quality could be improved by using a higher order interpolation, for example biquartic (Kobza, 1995) or biquintic (Swesty, 1996) interpolation.

This approach is very sensitive to the extrapolation of the properties into the two-phase region, which cannot be avoided for the chosen grid. A small deviation of the extrapolated specific entropy inside the two-phase region, leads to significant deviation of the second derivatives, and hence to a deviation of the properties calculated from them.

The information needed to describe the bicubic interpolation surface of the specific entropy $s(p, h)$ (namely y, y_1, y_2 and y_{12} at each grid point) are calculated from T, c_p, ϱ and β using equations (2.18) - (2.21). The surface is not twice continuously differentiable as the coefficients have not been calculated using a twice continuously differentiable spline. The discontinuities of the second derivative drop with increasing number of grid points.

The temperature was calculated using equation (2.18), so the surface used to describe this property was reduced to a quadratic polynomial in direction of specific enthalpy. The deviation of the temperature from the EoS for CO_2 (Span and Wagner, 1996)

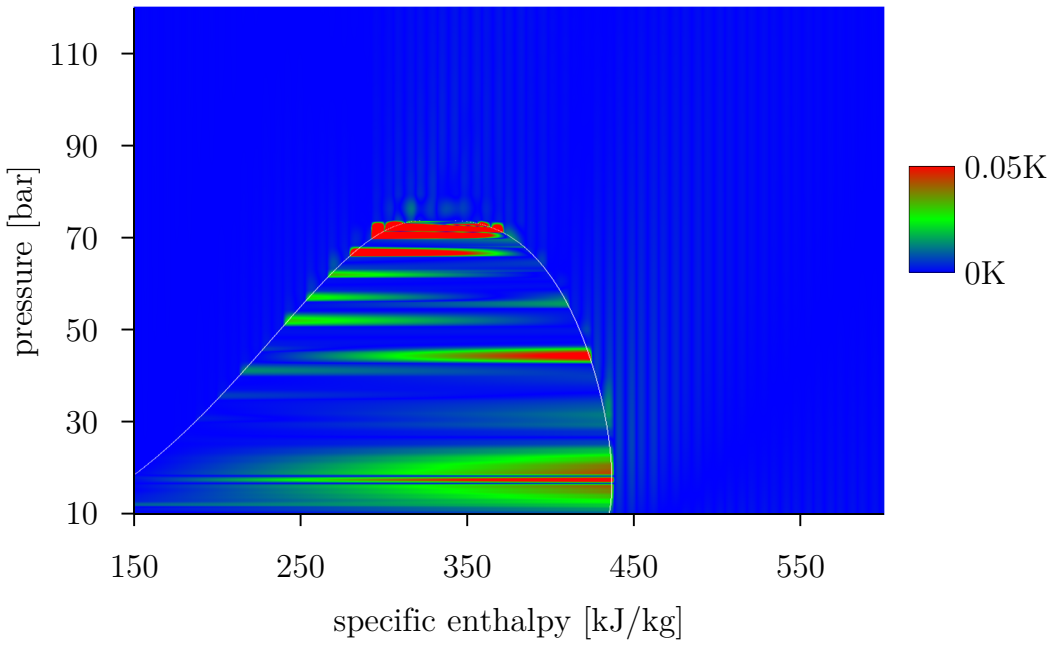

Figure 2.11.: Deviation of the temperature from the EoS for CO_2 (Span and Wagner, 1996) in a p-h-diagram, applying the bicubic interpolation of an EoS algorithm to CO_2 with $50 \cdot 50$ grid points, p in $[5.2bar, 200bar]$, and h in $[50\frac{kJ}{kg}, 700\frac{kJ}{kg}]$. The high deviation of the temperature in the two-phase region is caused by the extrapolated specific entropy. The deviation in the one-phase region is caused by reduced quality of interpolation due to differentiation.

shown in figure 2.11 is high in the two-phase region. This deviation is caused by the extrapolation into the two-phase region.

This approach provides a thermodynamic fully consistent description of the thermodynamic properties with a relatively low effort to set up the equation. The drawback of this approach is that it requires that more data be stored than conventional EoS, and fluid states in the two-phase region be estimated. A piecewise definition of a fundamental EoS $s(p,h)$ based on interpolation is an interesting alternative to a multiparameter EoS for the specific entropy, as discussed in the literature (Bender, 1970; Dehli, 1975; Baehr, 1998; Thorade, 2010a).

Table 2.4.: Summary of bicubic interpolation algorithm describing an equation of state

property tables	$s, \quad \eta, \frac{1}{\lambda}$
size of property table	$n \cdot m \cdot 4$ values
additional tables	saturation enthalpy (variable size)
inverse functions	search algorithm and analytic inversion
properties at saturation	evaluation of one-phase properties
derivatives of density	math. and therm. correct derivative

2.3.4. Set of Curves Interpolation of Selected Properties

The basic idea of this approach is to treat the independent variables pressure and specific enthalpy differently. For specific enthalpy at a constant pressure, the properties are described by a curve $f(h)_p$ fitted to the actual property curve. This is done for m pressure levels. The gaps between the curves of the set are closed via interpolation between two curves. This approach was discussed earlier in a slightly different form (Schulze et al., 2010), and it was applied to several real-time simulations (Schulze et al., 2011a) and CFD simulations of CO_2 ejectors (Lucas et al., 2013).

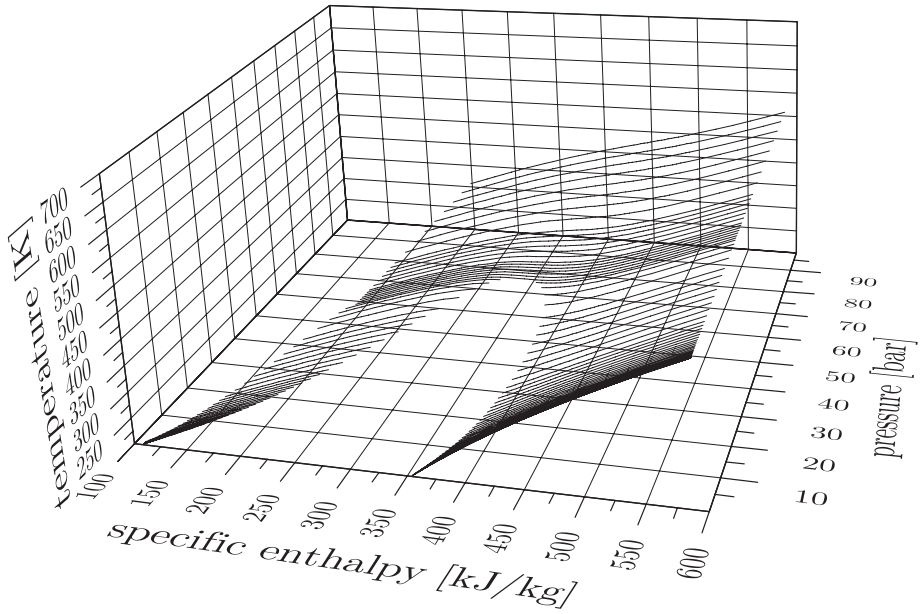

Figure 2.12.: A set of curves describes the temperature T of R-134a over pressure p and specific enthalpy h.

$$y_{p_{i=1..m}}(h) = c_0 + c_1(h+h_0) + c_2(h+h_0)^2 + c_3(h+h_0)^3 \\ c_4 \cdot arctan\,(c_5(h+h_0)) \tag{2.24}$$

$$\left(\frac{\partial y_{p_{i=1..m}}(h)}{\partial h}\right)_p = c_1 + 2c_2(h+h_0) + 3c_3(h+h_0)^2 \\ \frac{c_4 c_5}{(c_5(h+h_0))^2+1} \tag{2.25}$$

Equation (2.24) is used for the non-linear curve fitting of the thermodynamic properties. It is a polynomial of the third order plus an arctangent term. The seven unknowns of this equation are fitted subject to a set of constraints: the function values as well as the derivatives at the beginning and end of the interval have to be given. For the transport properties (viscosity and thermal conductivity) a simple polynomial instead of (2.24) is used as the basic fit function.

Linear interpolation with respect to the pressure is used to close the gaps between the curves of the set. Thus, to determine one function value on the property surface, two curves must be evaluated. If a higher order interpolation method in p direction is applied, then the number of curve function evaluations may increase and the implementation of the two-phase region may get more complicated.

The relevant fluid region is separated into n subregions on the left and on the right side

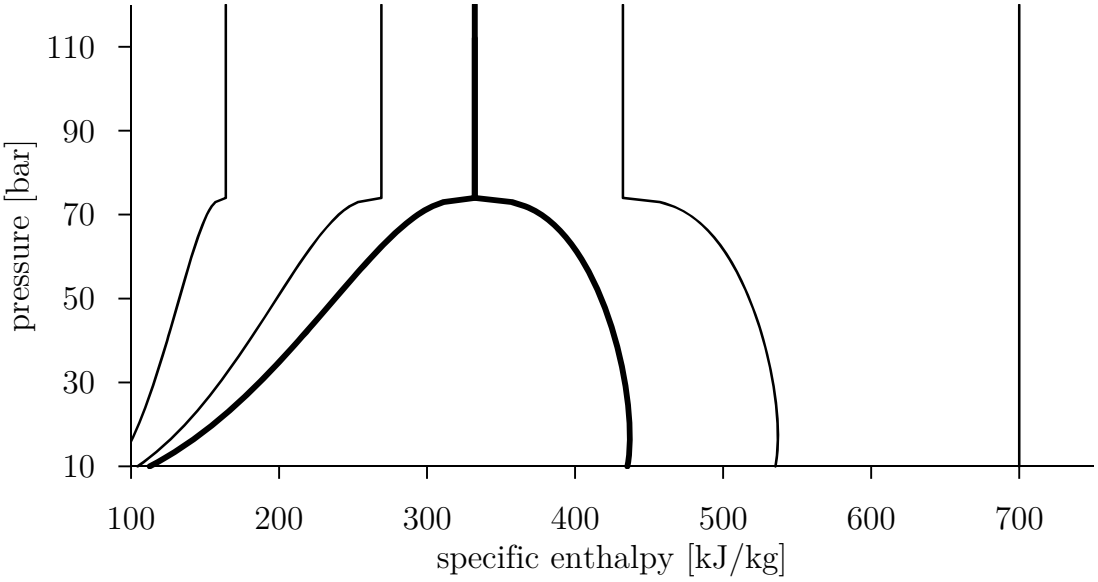

Figure 2.13.: The fluid region is separated into at least three subregions with a set of curves for each region.

of the two-phase region as shown in figure 2.13. The subregions are numbered starting from the two-phase region (e.g. first subregion on the left). The coefficients for the set of curves are stored separately for each subregion. Due to the constraint that the function value and the derivative must be equal, the connected curves of two subregions are once continuously differentiable in the direction of specific enthalpy.

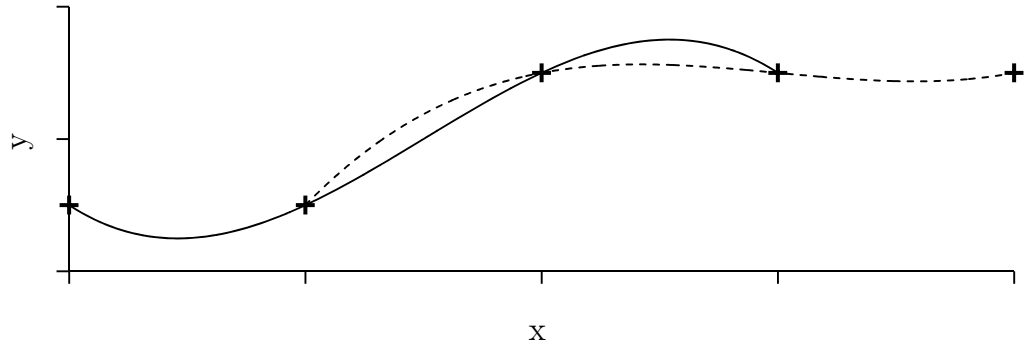

Figure 2.14.: Neville's algorithm applied to exemplary function values. The result is not continuously differentiable, if the four closest grid points are used for interpolation.

The properties at saturation are calculated from the stored properties at the beginning of the intervals next to the two-phase region. Neville's algorithm (Lyness and Moler,

1966) was chosen as interpolation method since it enables an efficient interpolation between an undefined number of given function values and does not require more data. It is used to interpolate between the four closest saturated states. The curve is not continuously differentiable as illustrated for example in figure 2.14. 1D-spline interpolation would be a better choice if a continuously differentiable curve were required and the additional amount of data can be stored. Since the properties in the one-phase region between two curves are interpolated linearly and the saturation properties are interpolated using Neville's algorithm, the property surface is not continuous at the saturation lines.

The thermodynamic consistency is improved by employing the derivative in the direction of specific enthalpy for calculation of other properties. The properties that are described by sets of curves are temperature T, specific volume v, isothermal compressibility κ and specific entropy s. The equations (2.26)-(2.28) are used to obtain the other properties from the derivatives of the interpolated properties. κ and s are stored in separate sets of curves, although it is theoretically possible to calculate them from the sets of curves of T and v. If they had been calculated from the available T and v sets of curves, then the precision of κ and s would be comparably low.

$$\frac{1}{c_p} = \left(\frac{\partial T}{\partial h}\right)_p \tag{2.26}$$

$$\beta = \frac{c_p \cdot \left(\frac{\partial v}{\partial h}\right)_p}{v} \tag{2.27}$$

$$c_v = c_p \left(1 - \frac{c_p \cdot T \left(\frac{\partial v}{\partial h}\right)_p^2}{\kappa \cdot v}\right) \tag{2.28}$$

A profiling of the calculation routines reveals that the call of the *arctan*()-function causes a comparably high share of the overall fluid property calculation time. Evaluating the basic fit function (2.24) is significantly more complex than evaluating a low order polynomial such as a spline surface. This is evident in the execution times if called in C++, as discussed in the following section. A polynomial as basic fit function does not provide good extrapolation behaviour. Thus despite the high calculation time, (2.24) is chosen.

Contrary to the other presented approaches, the set of curves algorithm requires a non-linear fitting procedure. At each pressure level the basic function is fitted to the actual property curve using the Levenberg-Marquardt algorithm (Levenberg, 1944). Although this method does not provide an automatic table generation algorithm, the method is presented here since it requires very few data points.

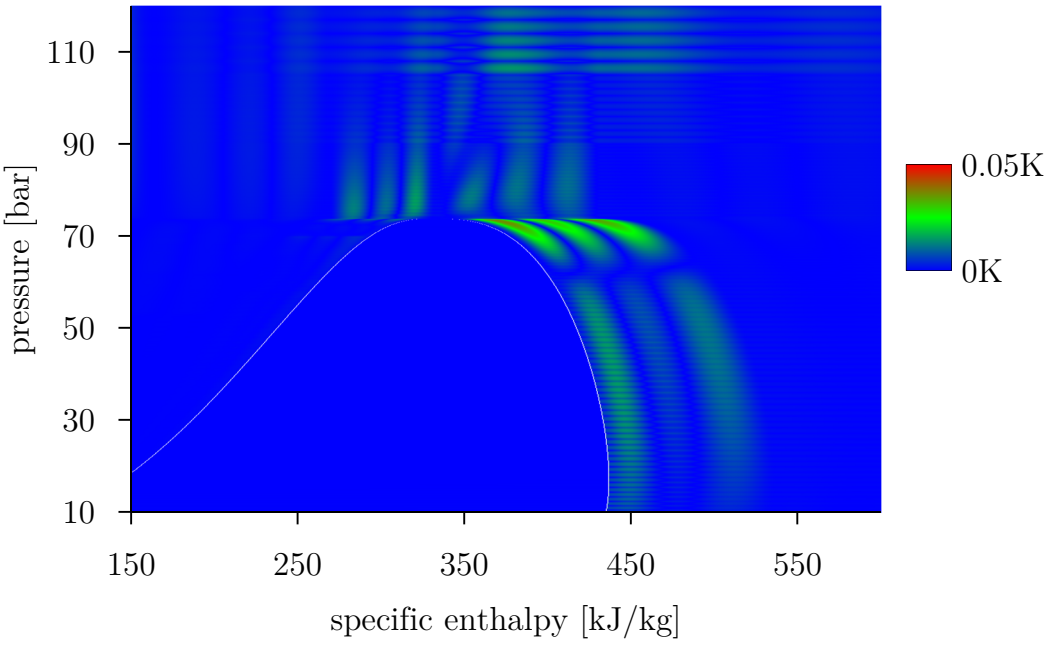

Figure 2.15.: Deviation of the temperature from the EoS for CO_2 (Span and Wagner, 1996) in a p-h-diagram, applying the set of curves interpolation algorithm to CO_2, with $m = 160$ pressure levels, and $n = 4$ subregions. The precision of the superheated gas temperature description is limited by the basic fit function.

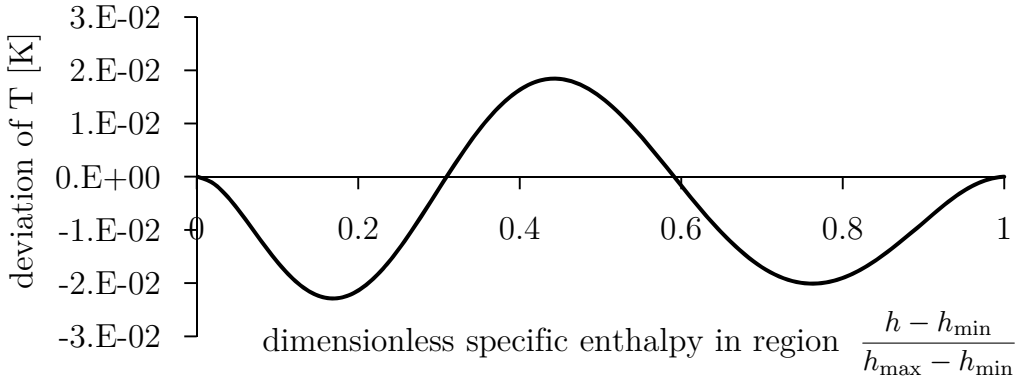

Figure 2.16.: Deviation of the temperature in first superheated region at 70.2 bar cannot be reduced any further using the basic fit function.

Figure 2.15 shows the deviation of the temperature when the approach is applied to CO_2. $m = 160$ pressure levels were fitted in $n = 4$ subregions. The deviation plot illustrates that the first region on the right side of the two-phase region seems to be most sensitive.

With the non-linear fit algorithm the square of the deviation is minimised, but the chosen basic function does not seem to be able to describe the non-linear behaviour in detail. In figure 2.16 the deviation of the temperature from the EoS for CO_2 (Span and Wagner, 1996) in the first superheated region is plotted at the pressure 70.2 bar.

Table 2.5.: Summary of the set of curves algorithm

property tables	$T, v, s, \frac{1}{\kappa}, \quad \frac{1}{\nu}, \frac{1}{\lambda}$
size of property table	$(n \cdot m \cdot 5) + (n \cdot m \cdot 6 + n \cdot m \cdot 10)$ values
additional tables	all properties at saturation (variable size)
inverse functions	newton solver
properties at saturation	separate table
derivatives of density	mathematically correct derivative

2.4. Comparison of the Investigated Interpolation Algorithms

In this section the investigated property calculation methods are evaluated on two test cases: a direct call from C++ source code and a transient simulation of a CO_2 heat pump with the TIL library (Richter, 2008; Gräber et al., 2010; Schulze et al., 2011a) using Dymola (2013).

The calculation speed of the fluid property routines can only give a hint as to whether the simulation speed of the thermodynamic system is high or not. The simulation speed in general is influenced by two aspects: the effort to numerically evaluate the model equations and the number of necessary evaluations. Thermophysical properties influence both aspects.

On the one hand, only a part of the simulation time is caused by fluid property calculation. On the other hand, the fluid properties influence the solving procedure and number of DAE-solver steps needed. Therefore the first test case - C++ integration -

will evaluate the performance in each region without interdependencies, the second test case - a CO_2 heat pump - the overall performance of a transient simulation.

The basic procedure when calculating the thermophysical properties was implemented as follows:

- calculate properties at saturation at the given input pressure
- if state point is outside the two-phase region, then apply the algorithms for the one-phase region, if not, the algorithms for the two-phase region are applied
- output all or only a part of the results

Basically, if one thermophysical property is needed, all of them are calculated in this implementation. This applies to the property calculation during simulation as well as to the property calculation called from C++.

Table 2.6 summarises the number of evaluations per second if the calculation methods are called from C++. The higher the value listed in the table, the higher the calculation speed. As the calculation of the properties at saturation above the critical pressure is not necessary/impossible, the calculation speed is evaluated for three test cases: a state point inside the two-phase region (properties at saturation), a state point above the critical pressure (one-phase properties) and a state point in the one-phase region below critical pressure (properties at saturation + properties in one-phase region).

Table 2.6.: Test case 1: evaluations per second computing all thermodynamic properties in $\left[\frac{1}{\mathrm{s}}\right]$ if called from C++ using an Intel Core i7-2620M @ 2.7GHz

	two-phase region	$p > p_c$	superheated and $p < p_c$
linear	1.630.000	2.250.000	1.130.000
bicubic spline	1.130.000	3.130.000	1.010.000
bicubic EoS	1.110.000	4.050.000	1.250.000
set of curves	830.000	1.013.000	535.000
TILMedia EoS	1.760.000	63.000	61.000
REFPROP EoS	7.500	8.600	3.180

The table illustrates that the bicubic spline interpolation algorithm is slowed by the calculation of the saturation properties. At pressures above the critical pressure, no saturation properties are calculated and that is where the bicubic spline interpolation

algorithm is three times faster than at pressures below p_c. The linear interpolation algorithm is unexpectedly slow in the one-phase region. Profiling of the source code shows that this is caused by the triangulation algorithm that selects the three grid points for interpolation. The set of curves algorithm is slowed down by the pressure level search algorithm, the arctan()-function of the basic fit function and Neville's algorithm used for saturation properties.

The multiparameter EoS implemented in TILMedia is the fastest method for calculating properties in the two-phase region. Instead of using a VLE-algorithm, in TILMedia, all saturation properties are described by 1D-splines $\{\varrho, h, s, T, c_p, \beta, \kappa, w\} = f(p)$ and the EoS is not actually evaluated. The bicubic spline interpolation is slower in the two-phase region because the algorithm evaluates the two-dimensional one-phase property surfaces to obtain the saturation properties. The TILMedia EoS saturated property calculation is even faster than the linear interpolation algorithm that was presented. The linear interpolation algorithm requires an inverse pressure curve $i_p = f(p)$, which contains a time consuming call to the log()-function.

In the one-phase region, all interpolation methods that were presented are significantly faster than the EoS implemented in TILMedia or REFPROP.

In table 2.7 the precision of the presented interpolation methods is listed. The deviation of temperature T, density ϱ and specific entropy s from the multiparameter EoS implemented in REFPROP is shown. Other properties like c_p go to ∞ when approaching the critical point, and the resulting deviation is dominated by minor deviations around this region. Additionally, the total amount of data stored in a file is shown in the last column. The amount of data required during simulation is different, as the 16 coefficients of the spline surface pieces are stored temporarily in the memory. The file only contains the four values per grid point required to calculate the 16 coefficients.

The average error of linear interpolation is higher than that of bicubic spline interpolation. The overall deviation of bicubic spline interpolation from original EoS is mainly caused by high deviation close to the two-phase region; in the one-phase region the deviation is low. The overall deviation of bicubic interpolation of an EoS is very high, at some points almost 4%. The overall deviation of the set of curves algorithm is very low compared to the other approaches.

The amount of data needed to be stored is highest for linear interpolation. For the bicubic spline interpolation algorithm far less data is required. The bicubic interpolation of an EoS algorithm requires just one property table for the thermodynamic properties and therefore less data. The set of curves algorithm requires about as much data as the bicubic spline interpolation algorithm at $50 \cdot 50$ grid points.

In the following, the simulation speed rather than the thermophysical property calcu-

Table 2.7.: Accuracy Comparison

method	temperature	density	specific entropy	total amount of data
linear				
$\sqrt{\frac{\sum \text{error}^2}{N-1}}$	2.25E−03K	4.59E−02$\frac{kg}{m^3}$	3.54E−03$\frac{kJ}{kgK}$	
$\frac{\sum \text{error}}{N}$	−4.66E−04K	−1.67E−02$\frac{kg}{m^3}$	−1.80E−04$\frac{kJ}{kgK}$	3860 KB
$\max\left\{\left\lvert\frac{\text{error}}{\text{value}}\right\rvert\right\}$	5.79E−05	5.96E−03	3.26E−05	
bicubic spline				
$\sqrt{\frac{\sum \text{error}^2}{N-1}}$	2.25E−03K	6.04E−02$\frac{kg}{m^3}$	3.44E−04$\frac{kJ}{kgK}$	
$\frac{\sum \text{error}}{N}$	1.14E−04K	2.19E−03$\frac{kg}{m^3}$	−1.05E−05$\frac{kJ}{kgK}$	728 KB
$\max\left\{\left\lvert\frac{\text{error}}{\text{value}}\right\rvert\right\}$	2.69E−04	3.14E−03	4.37E−06	
bicubic EoS				
$\sqrt{\frac{\sum \text{error}^2}{N-1}}$	1.36E−02K	3.80E−01$\frac{kg}{m^3}$	4.86E−04$\frac{kJ}{kgK}$	
$\frac{\sum \text{error}}{N}$	6.08E−04K	4.93E−03$\frac{kg}{m^3}$	−7.15E−05$\frac{kJ}{kgK}$	344 KB
$\max\left\{\left\lvert\frac{\text{error}}{\text{value}}\right\rvert\right\}$	1.97E−03	3.99E−02	1.20E−05	
set of curves				
$\sqrt{\frac{\sum \text{error}^2}{N-1}}$	2.59E−03K	1.09E−02$\frac{kg}{m^3}$	1.93E−02$\frac{kJ}{kgK}$	
$\frac{\sum \text{error}}{N}$	−6.70E−04K	−1.36E−04$\frac{kg}{m^3}$	5.96E−03$\frac{kJ}{kgK}$	674 KB
$\max\left\{\left\lvert\frac{\text{error}}{\text{value}}\right\rvert\right\}$	8.25E−05	3.65E−04	8.99E−05	

lation speed is evaluated. The CO_2 heat pump shown in figure 2.17 is modelled with the TIL library using heat exchangers that are based on the finite volume method as presented in section 4.2. Zero pressure drop and a constant heat transfer coefficient are assumed. A steady state model compressor with an isentropic, volumetric and effective isentropic efficiency is used as well as a dynamic ideal separator model (ideal phase separation between 10% and 90% filling level) assuming thermodynamic equilibrium.

The heat pump system starts in steady state, and as the expansion valve is opened following a ramp function, the steady state solution changes from state A to state B. The transient behaviour of the system is simulated for 10 minutes after the ramp starts. The relative and absolute tolerance of the solver (DASSL modified by Dynasim) is set to 1E-08.

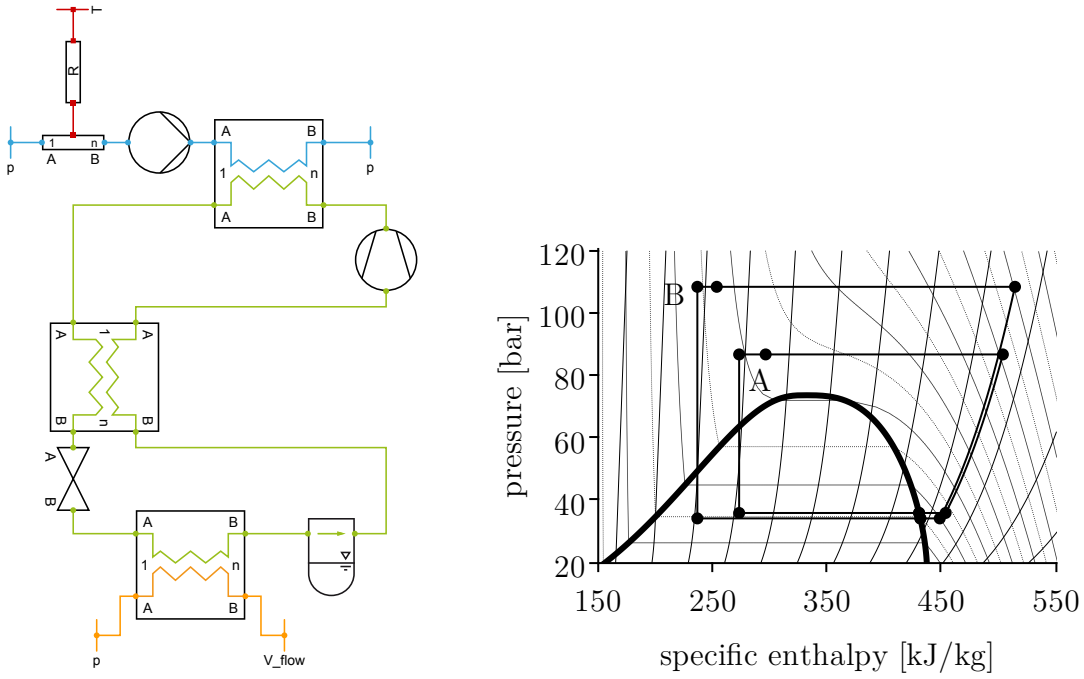

Figure 2.17.: Test case 2: A CO_2 heat pump moves from system state A to state B as the expansion valve is opened following a ramp function.

The results of a batch simulation comparing the presented approaches are shown in figure 2.18. Each mark represents a simulation of the system using interpolated fluid properties with a different number of grid points. The number of steps in each direction ($m = n$, abscissa) is equal to the square root of the total number of grid points. The lines represent those approaches that are based on coefficients that cannot be generated automatically (curve array, reference EoS).

The plots illustrate that linear interpolation and the reference EoS implemented in REFPROP require about twice as many successful solver steps. First there is an increase and above 800 a slight decrease with the increasing number of grid points for the linear interpolation. The number of solver steps using the set of curves and the bicubic interpolation of an EoS are slightly higher than the reference EoS of TILMedia. This plot illustrates the influence of the interpolation quality on the DAE-solver.

The number of F-evaluations is decreases on a constantly high level using linear interpolation but is almost constant when using the other approaches. The overall simulation time is dominated by the F-evaluation curve shape but also accounts for the calculation times and the successful solver steps. The bicubic spline interpolation leads to the lowest simulation times.

If the EoS implementation in TILMedia is used, the simulation time is significantly

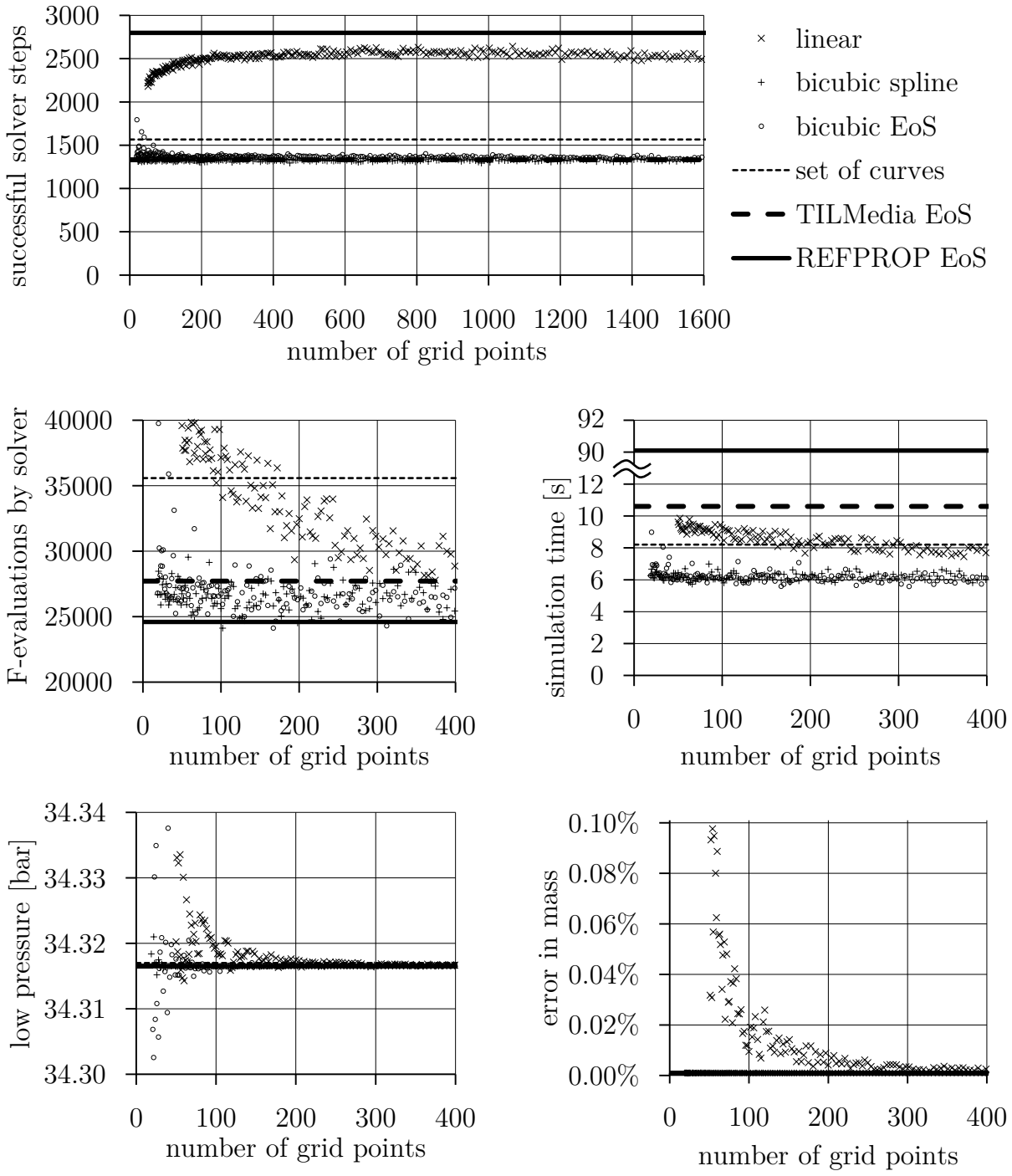

Figure 2.18.: Solver statistics, simulation times and results. Each mark represents a transient simulation of the CO_2 heat pump system with another grid step size ($m = n$). Linearly interpolated fluid properties increase the number of successful solver steps, F-evaluations reduce with increasing number of grid points. Spline interpolation is faster despite the higher calculation effort.

higher but in the same order of magnitude as if the interpolation methods were used. The fluid property calculation causes about 40% of the overall simulation time if TILMedia EoS is used. Thus, based on the simulation time comparison, it can be concluded that using the bicubic spline interpolation algorithm requires 40% less simulation time than using the reference EoS of TILMedia.

If an implementation of the reference EoS is used that calculates the saturation properties iteratively with a VLE-algorithm, then the simulation time of the system is much higher (in this case it is 90.1 seconds using REFPROP). This is caused by small deviations in the VLE algorithm and leads to a significant increase of successful solver steps and an increase in F-evaluations.

The quality of the results can be estimated by the steady state low pressure level. With an increasing number of grid steps, the deviation decreases and all methods lead to the same result. The results using spline interpolation converge faster with increasing number of grid steps than linear interpolation, but the amount of data needed (16 coefficients per surface piece, which can be calculated from four values per grid point) is much higher.

The bicubic interpolation of an EoS is accurate enough for a transient simulation using simple models. The first derivatives of the specific entropy, giving temperature and density, are most important for the simulation of heat and mass transfer. The second derivatives giving thermal expansion coefficient β, compressibility κ and speed of sound are less accurate, and if used, lead to a higher sensitivity to the number of grid points.

2.5. Extension to the Bicubic Spline Interpolation – Multicomponent Blends with a wide Temperature Glide

To provide the thermophysical properties of a multicomponent blend with a wide temperature glide, the composition can be assumed to be constant. The fluid states for the interpolation algorithm are calculated at the given bulk mixture composition and thus, the blend is described similar to pseudo pure fluids. This approach is similar to the one chosen by Lemmon (2003), who presents multiparameter EoS for R-410A, R-404A, R-507A and R-407C. He uses one EoS for each blend.

A blend can be considered a pseudo pure fluid because in the steady state of a thermodynamic cycle, the composition of the mixture entering and leaving all components of the system must be equal. If this composition of the mixture is equal to the one

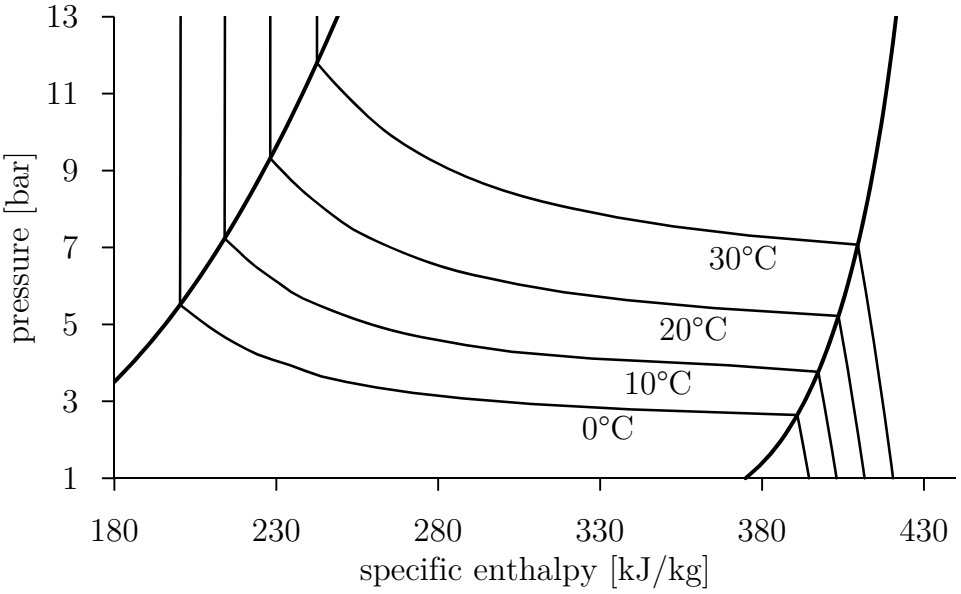

Figure 2.19.: Isotherms of R-445A in a p-h-diagram. The temperature glide of R-445A is high and has a large influence on the system behaviour.

of the blend, then the simulation results will be equal to those of the pseudo pure fluid. The outlet mixture composition of phase separating components, a receiver for instance, must also be identical to the blend composition. This is only possible if the total mixture composition in this kind of component differs. Thus in the case that a receiver at high pressure level is used to separate the condenser from the subcooler, the liquid composition leaving the receiver is the same as the blend composition. The total composition in the receiver can be calculated from pressure, temperature, liquid composition and filling level. The total mass balance in the receiver is fulfilled, but the mass balances for the mixture components are not.

Inside the two-phase region, the temperature curve differs significantly from a linear interpolation between the properties at saturation. Figure 2.19 shows the shape of the isotherms in the two-phase region of R-445A. The non-linear behaviour has a high impact on the temperature curve over the heat exchanger length and should therefore not be simplified.

An extension of the approach presented in section 2.3.2 is necessary to describe the properties within the two-phase region correctly. A new set of surfaces has to be stored and interpolated. The chosen basic approach is represented in (2.29) - (2.32). The vapour quality q is assumed to be different for each interpolated saturated property and is described by an additional 2D-spline surface: $q_T(p, q_h)$, $q_v(p, q_h)$. This is a purely mathematical approach to reproduce the properties correctly.

$$
\begin{aligned}
h &= h_{\mathrm{bubble}}(p) + q_{\mathrm{h}} \cdot (h_{\mathrm{dew}}(p) - h_{\mathrm{bubble}}(p)) && (2.29)\\
T &= T_{\mathrm{bubble}}(p) + q_{\mathrm{T}} \cdot (T_{\mathrm{dew}}(p) - T_{\mathrm{bubble}}(p)) && (2.30)\\
v &= v_{\mathrm{bubble}}(p) + q_{\mathrm{v}} \cdot (v_{\mathrm{dew}}(p) - v_{\mathrm{bubble}}(p)) && (2.31)\\
q_{\mathrm{T}}(p, q_{\mathrm{h}}) &\neq q_{\mathrm{v}}(p, q_{\mathrm{h}}) \neq q_{\mathrm{h}}(p, h) && (2.32)
\end{aligned}
$$

The partial derivatives of the density $\left(\frac{\partial \varrho}{\partial p}\right)_h$ and $\left(\frac{\partial \varrho}{\partial h}\right)_p$ can be calculated from the two partial derivatives of the vapour quality of the specific volume $\left(\frac{\partial q_v}{\partial p}\right)_{q_h}$ and $\left(\frac{\partial q_v}{\partial q_h}\right)_p$. The equations (2.33)-(2.35) were derived from (2.31).

$$
\begin{aligned}
-\frac{1}{\varrho^2}\left(\frac{\partial \varrho}{\partial h}\right)_p &= \left(\frac{\partial v}{\partial h}\right)_p = \left(\frac{\partial q_{\mathrm{v}}}{\partial q_{\mathrm{h}}}\right)_p \left(\frac{\partial q_{\mathrm{h}}}{\partial h}\right)_p (v_{\mathrm{dew}} - v_{\mathrm{bubble}}) && (2.33)\\
-\frac{1}{\varrho^2}\left(\frac{\partial \varrho}{\partial p}\right)_h &= \left(\frac{\partial v}{\partial p}\right)_h = \left(\frac{\partial v_{\mathrm{bubble}}}{\partial p}\right)_h + \left(\frac{\partial q_{\mathrm{v}}}{\partial p}\right)_h (v_{\mathrm{dew}} - v_{\mathrm{bubble}})\\
&\quad + q_{\mathrm{v}}\left(\left(\frac{\partial v_{\mathrm{dew}}}{\partial p}\right)_h - \left(\frac{\partial v_{\mathrm{bubble}}}{\partial p}\right)_h\right) && (2.34)\\
\left(\frac{\partial q_{\mathrm{v}}}{\partial p}\right)_h &= \left(\frac{\partial q_{\mathrm{v}}}{\partial p}\right)_{q_{\mathrm{h}}} + \left(\frac{\partial q_{\mathrm{h}}}{\partial p}\right)_h \left(\frac{\partial q_{\mathrm{v}}}{\partial q_{\mathrm{h}}}\right)_p && (2.35)
\end{aligned}
$$

Similarly to this extension, the other three interpolation algorithms can also be adapted to blends with a high temperature glide.

2.6. Conclusion and Summary

In this chapter, basic problems caused by table-based fluid property calculation were discussed and four methods of table-based thermophysical property calculation for transient simulation were presented: linear interpolation, bicubic spline interpolation, bicubic interpolation of an EoS, and set of curves interpolation.

The calculation routines need to describe a continuous property surface in the one-phase region, and the one-dimensional properties at saturation need to be consistent to this property surface, as they should be used to calculate the properties in the two-phase region. The properties should be described as thermodynamically consistent as possible, require as few data as possible, account for the range of valid values and should not

influence the DAE-solver of the simulation. Additionally, the calculation of the partial derivatives of the density was discussed.

These aspects were discussed for each method and finally evaluated on two test cases: A direct calculation routine call from C++ and a heat pump simulation using Dymola.

The calculation speed and interpolation quality suggest the bicubic spline interpolation for transient simulation. The integration of the two-phase region requires special attention. Using bicubic interpolation to describe a fundamental EoS $s(p, h)$ is a promising option, but this approach is more sensitive to the integration of the two-phase region, and the precision of the thermodynamic properties derived from the second derivative of the EoS is low.

Chapter 3.

Table Based Calculation of the Two-Phase Region of Binary Mixtures

In this chapter it is shown how solving problems and numerical inaccuracies in the vapour-liquid equilibrium of binary mixtures can be avoided using interpolation and thus making fast and robust transient simulations based on multiparameter EoS for binary mixtures possible.

Spline interpolation can be applied to describe the two-phase region of mixtures. The algorithms presented in this chapter replace conventional vapour-liquid equilibrium algorithms during simulation. Interpolation data can be generated automatically for any binary mixture with the same type of two-phase region shape.

3.1. Requirements for Transient Simulation

Empirical multiparameter Equations of State (EoS) are today considered the scientific standard for describing precisely the thermodynamic properties of a real fluid (Span, 2000). EoS for the Helmholtz energy were published for many fluids and were implemented in the REFPROP library (Lemmon et al., 2010). The thermodynamic properties of a mixture can be calculated based on these equations and general mixing rules, or specific mixing equations.

Often, when EoS are implemented, the VLE of a pure fluid or a mixture is calculated using an iterative VLE algorithm. These algorithms assume a thermal, mechanical and chemical equilibrium between vapour and liquid and vary the independent variables to determine the VLE. If the starting values for the independent variables are inadequate, the solver will fail. This particularly applies to multiparameter EoS due to their non-physical behaviour in the two-phase region (see figure 2.9 on page 24).

If fluid property libraries that calculate the VLE properties with an iterative algorithm are used, the solving procedure of transient simulations is influenced by small discontinuities in the VLE due to numerical inaccuracy. This influence increases if the properties of a mixture are calculated.

To simulate a model transiently, the differential algebraic equation (DAE) system of the system model is integrated numerically. The errors occurring during simulation are cumulated. In other words, if the calculation of the partial derivatives of the density fails once, it causes an error in the calculation of mass at a specific point in time during simulation that will influence the results of the whole simulation after that point in time. A miscalculated temperature causes a miscalculated heat transfer and therefore influences the further simulation. So to enable the reliable generation of simulation results, the calculation of fluid properties should never fail and should at best be deterministic.

For the reliable transient simulation of systems operating with mixtures, the following requirements for the VLE-calculation can be formulated:

- Fail-safe calculation (the calculation must not fail)
- Reduction of numerical inaccuracy (to reduce the influence on the DAE-solving procedure)
- Provision of partial derivatives of the density (as needed for the models presented in section 4.2)
- Independence of a particular EoS (to preserve flexibility)

The requirements can be fulfilled if spline interpolation is used to describe the two-phase region. Spline interpolation algorithms are deterministic and provide the derivatives along the saturation surface.

An approach to describe the two-phase region of a binary mixture is shown in this chapter (an earlier version of this approach was published in Schulze and Köhler, 2013). It is also shown how this approach could be integrated thermodynamically consistently into the one-phase property calculation using multiparameter EoS. The two-phase flash algorithm and the dew and bubble temperature algorithm are replaced entirely by spline interpolation.

There exist many publications about the thermophysical properties of the working pair ammonia-water. Patek and Klomfar (1995) is a well-reputed contribution, giving simple explicit functions for the rapid calculation of selected properties. For example, the bubble temperature (3.1) is described by the independent variables pressure and

liquid mole fraction:

$$T_{\mathrm{liq}}(p,x) = T_0 \sum_i a_i (1-x)^{m_i} \left[\ln\left(\frac{p_0}{p}\right)\right]^{n_i} \tag{3.1}$$

These purely empirical equations are based on a non-linear fit. Contributions like Conde-Petit (2006), Ganesh and Srinivas (2010) and Sadhukhan et al. (2012) have developed more fit functions or computer code based on Patek and Klomfar (1995) to enable a faster computation of the properties of ammonia-water, particularly at saturation.

The approach presented in this chapter is different from the ones discussed before. Here the two-phase region is calculated based on interpolation, so no fitting procedure or coefficients are given. The required data can be generated automatically for every binary mixture, which has a shape of the two-phase region similar to ammonia-water. Thus this is a general method to describe the two-phase region, and it is discussed in this chapter for the mixture ammonia-water. To generate the data set, it is still necessary to implement an iterative VLE algorithm or to use a tool that provides one.

3.2. Calculating VLE iteratively using Equations of State

In this section two algorithms for VLE calculation are presented (similar algorithms can be found in Orbey and Sandler, 1998; Poling et al., 2001): A bubble point algorithm and a p-T-flash algorithm (Dohrn, 1994). The bubble point algorithm (3.3) is used to locate the two-phase region: The bubble temperature T_{liq} and saturated densities $\{\varrho_{\mathrm{liq}}, \varrho_{\mathrm{vap}}\}$ are calculated from a given pressure and liquid mole fraction. This algorithm is presented here since the pressure, specific enthalpy and composition are known from the models presented in chapter 4. The p-T-flash algorithm (3.2) is used to obtain state points inside the two-phase region: the saturated mole fractions $\{x, y\}$ and densities $\{\varrho_{\mathrm{liq}}, \varrho_{\mathrm{vap}}\}$ for a given pressure and temperature are calculated.

$$\{x, y, \varrho_{\mathrm{liq}}, \varrho_{\mathrm{vap}}\} = f(p^*, T^*, z^*) \tag{3.2}$$

$$\{T_{\mathrm{bubble}}, \varrho_{\mathrm{liq}}, \varrho_{\mathrm{vap}}\} = f(p^*_{\mathrm{bubble}}, x^*) \tag{3.3}$$

In figure 3.1 an isobaric isothermal flash algorithm is shown. This algorithm can be interpreted as follows: in a vessel with known pressure, temperature and total composition in the system, mass of the same composition is added or removed correcting

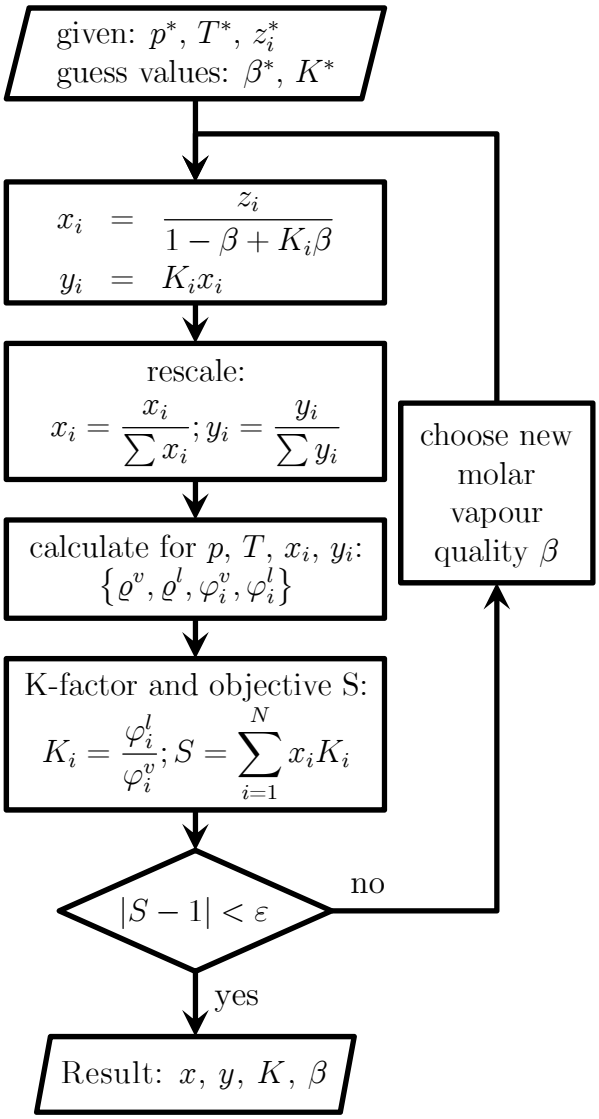

Figure 3.1.: Isobaric isothermal flash algorithm, the values given by the user are denoted by an asterisk (taken from Schulze and Köhler, 2013)

p	pressure
T	temperature
z_i	total mole fraction of comp. i
x_i	liquid mole fraction of comp. i
y_i	vapour mole fraction of comp. i
β	vapour quality (mole basis)
K_i	K-factor of comp. i
φ_i	fugacity factor of comp. i
S	objective function
*	values required by the user

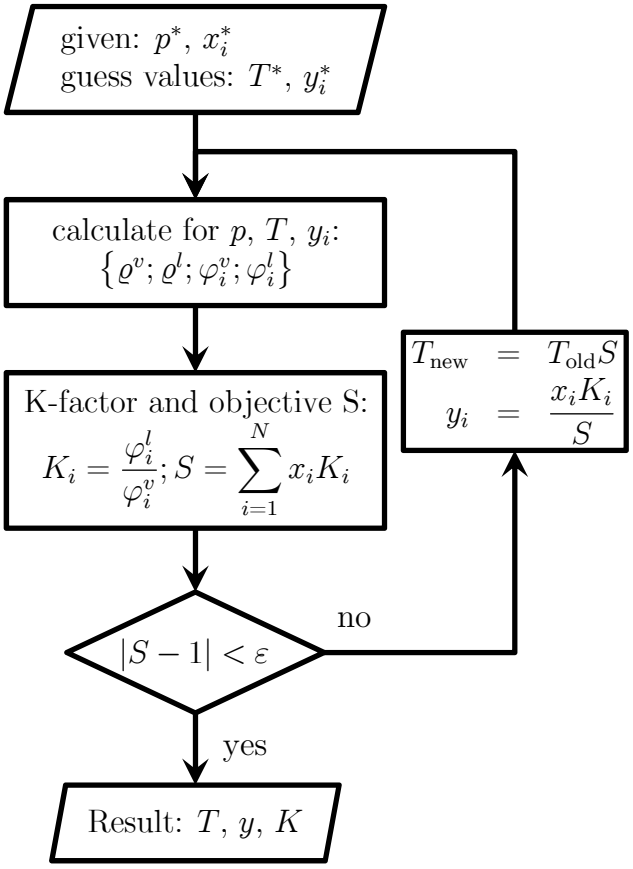

Figure 3.2.: Iterative bubble point temperature algorithm

the vapour quality until the VLE is stable. At first the mole fraction vector in liquid phase x and gas phase y are calculated from the given pressure p, temperature T and the total mole fraction vector z. Then the fugacity factors, the ratios of mole fractions (K-factors) and the objective function S are calculated. From the derivative $\frac{dS}{d\beta}$ a new β can be chosen using Newton's method as proposed by Dohrn (1994). In each step of the iteration loop the vapour quality is corrected, until the objective function S is equal to 1 within ϵ.

In figure 3.2 an algorithm to calculate the bubble point temperature is shown. This algorithm can be interpreted as follows: a liquid of known composition is heated at a given pressure until a stable vapour phase has formed. Pressure p^*, composition in liquid phase x_i^* and starting values for temperature T^* and gas phase composition y_i^* must be set before the iteration loop starts. The fugacity coefficient φ_i^l of the liquid and φ_i^v of the vapour are calculated to determine the K-factors and objective function S. The objective function is the sum of the K-factors weighted with the liquid mole composition. In each step of the iteration loop, the bubble temperature and the gas composition are corrected until the objective function S is equal to 1 within ϵ. A dew temperature algorithm follows the same pattern.

The calculation of the derivative $\frac{dS}{d\beta}$ is more complicated. The mole fraction vectors of liquid and vapour phase depend on the vapour quality β; the liquid and vapour density is calculated from these mole fraction vectors and the K-factors from the fugacity coefficients that were calculated from the densities ($\beta \rightarrow \varrho_{\mathrm{l,v}} \rightarrow \varphi_{\mathrm{l,v}} \rightarrow K_i \rightarrow S$). An analytic derivation of this chain requires a derivation of the mixture EoS with respect to mole fraction. This can be avoided simply by using another solving method that does not require a derivative of the objective function $R = S - 1$.

The VLE calculation using multiparameter EoS is more complicated than using cubic equations of state. The presented algorithms do not verify if the state is in the two-phase region when iteratively determining the density of a phase from pressure, temperature and composition. So in practice the EoS will be evaluated inside the two-phase region. Taking the shape of the isotherms in figure 2.9 on page 24 into account, the density has to be calculated carefully to avoid non-physical results. Cubic EoS describe only two extrema inside the two-phase region and therefore their behaviour can be predicted.

The presented algorithms need to evaluate the EoS very often. The subordinate determination of the liquid and vapour density $\varrho_{\mathrm{sat}} = f(p)$ requires several evaluations and the superordinate flash or saturation point algorithm also requires many steps. The calculation time of a VLE using these algorithms is high. VLE algorithms influence the solving process of a transient simulation due to their inherent numerical inaccuracy. So in addition to the high calculation time for the fluid properties itself, the numerical inaccuracy of the properties of liquid and vapour phase will lead to a reduction of the step size of the DAE-solver and, hence, higher simulation times.

The literature describes many variations of algorithms to calculate the VLE. Michelsen and Mollerup (2007) give many useful hints and methods to ease the iterative calculation of a VLE. See also Somdalen (2011); Somdalen et al. (2012). These algorithms can only calculate specific VLE state points - points on the saturation surfaces. The shape of the two-phase region and the derivatives along the saturation surfaces cannot be drawn from them, so they do not allow for the calculation of the partial derivatives of the density with respect to pressure, specific enthalpy and mass fraction inside the two-phase region, which are required by models like the ones presented in section 4.2.

3.3. Describing VLE using Spline Interpolation

To overcome the above mentioned drawbacks of VLE calculation based on EoS, in this section a method is presented to deterministically calculate VLE as well as selected properties at saturation using 1D cubic spline interpolation (see section 2.2). The functions shown in equations (3.4) - (3.6) have to be implemented

$$\{T_{\text{bubble}}, \varrho_{\text{liq}}, \varrho_{\text{vap}}\} = f(p^*_{\text{bubble}}, \xi^*_{\text{liq}}) \tag{3.4}$$

$$\{T_{\text{dew}}, \varrho_{\text{liq}}, \varrho_{\text{vap}}\} = f(p^*_{\text{dew}}, \xi^*_{\text{vap}}) \tag{3.5}$$

$$\{\xi_{\text{liq}}, \xi_{\text{vap}}, \varrho_{\text{liq}}, \varrho_{\text{vap}}, h_{\text{liq}}, h_{\text{vap}}, s_{\text{liq}}, s_{\text{vap}}\} = f(p^*, T^*, \xi^*). \tag{3.6}$$

ξ_i is the mass fraction of component i. The dimensionless temperature Θ^* (3.7) is the actual temperature T^* related to the minimal and maximal saturation temperature of the pure components at the current pressure p^*. It is preferred as independent variable since it enables the description of the two-phase region relative to the vapour pressure curve of the pure component.

$$\Theta^* = \frac{T^* - T_{\text{sat,min}}}{T_{\text{sat,max}} - T_{\text{sat,min}}} \tag{3.7}$$

In figure 3.3 the dew and bubble line of the mixture ammonia-water is shown at the pressures $p = 1, 10, 100$ bar in a Θ-ξ diagram. The basic shape of the two-phase region is always the same. The reason for the similarity is that the Θ-ξ-diagram only describes the transition of the saturated temperature from one component to the other; the general curve is obtained from the saturation temperatures of the pure components. As long as the interaction of the components is not strongly dependent on the temperature and the pressure, the dimensionless temperature simplifies the description of the two-phase region.

The algorithms presented in this chapter determine the dew and bubble surface in the p-T-ξ-space. Since $\{p, h, \xi\}$ are chosen as continuous time state variables of the

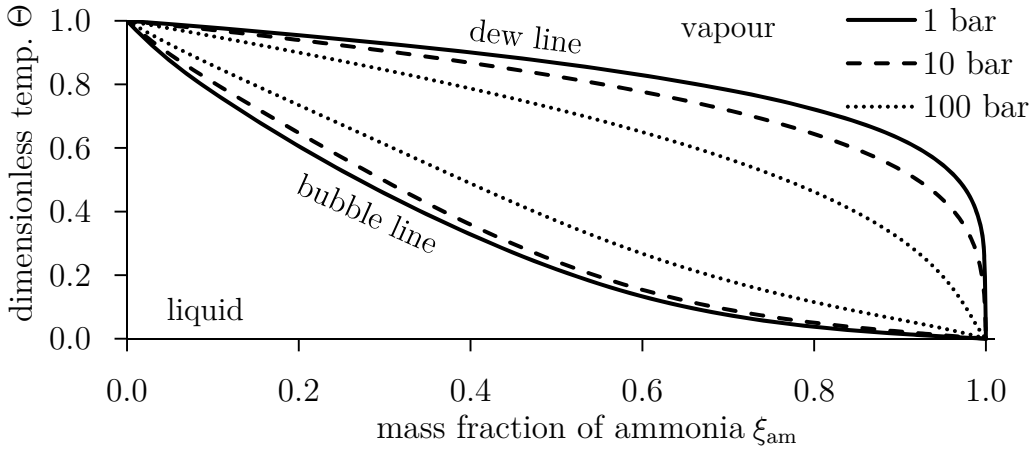

Figure 3.3.: Dew and bubble line of the mixture ammonia-water at p={1, 10, 100} bar in a Θ-ξ-diagram. The shape of the two-phase region is very similar for a wide range of pressures.

DAE system in the heat exchanger models presented in chapter 4, similar independent variables for the spline algorithms were selected. The absolute pressure p and the mass fraction ξ_1 of the first component are chosen as independent variables for the dew and bubble point algorithms. The absolute pressure p and the dimensionless temperature Θ are chosen as independent variables for the flash algorithm. The dew and bubble point can be calculated explicitly from the continuous time state variables $\{p, \xi\}$. The p-T-flash requires the independent variable temperature to identify the liquid and vapour state in thermal equilibrium. The iterative p-h-flash calls the p-T-flash.

Although it is useful to introduce a dimensionless temperature, other properties like density should not be described without dimension. In the critical region, dimensionless temperature requires a definition of the saturation temperature of the pure components even if the critical pressure is exceeded (see discussion in section 3.3.4). This is not possible for properties such as density.

3.3.1. Preparation of the Data Set

The presented spline-based flash algorithms are intended to reproduce the results that were obtained from the algorithms shown in section 3.2 as quickly as possible. They cannot replace VLE algorithms in general since VLE data still need to be generated from another algorithm or library.

In figure 3.4 the data generation algorithm is shown. To determine VLE, a bubble or dew point algorithm should preferably be applied, as they are more likely to find a

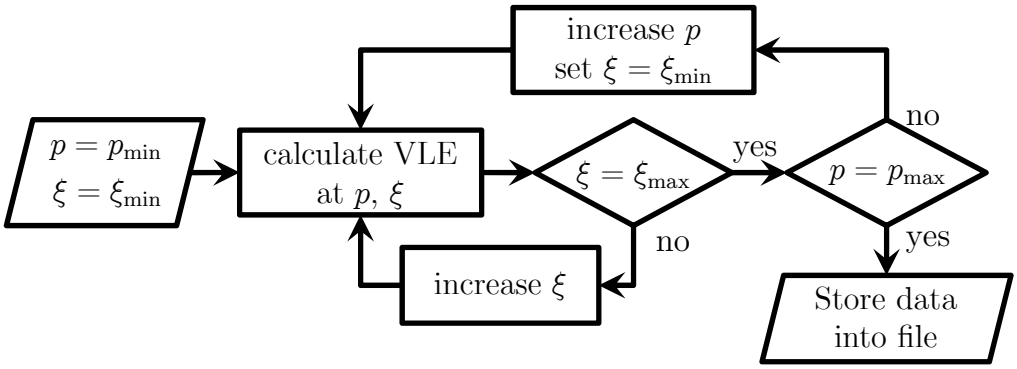

Figure 3.4.: VLE in Θ-ξ-diagram is stored at several pressure levels into one file

solution compared to a p-T-flash algorithm. In contrast to the dew and bubble point algorithms, the p-T-flash algorithm yields the composition in both phases - liquid and vapour.

The mass fractions and the dimensionless pressures are varied on a predefined grid and the properties at saturation are calculated and stored in a file. In the inner loop of the algorithm, the VLE data point must be removed if it cannot successfully be determined. The value of $\xi_{\max}$ can be adapted in the critical region.

3.3.2. Spline Interpolation Algorithms

In this section the explicit algorithms to calculate the dew and bubble point as well as an isobaric-isothermal flash are presented. Iterative algorithms for p-h- and p-s-flash are also presented. The basic concept of the explicit algorithms is a two-step procedure: first interpolate the properties at all pressures $p_{i=1..m}$ one-dimensionally and then interpolate in direction of p using the results of the first step. The routines are based on nested 1D interpolation.

The spline flash algorithm $f(p, T)$ is shown in figure 3.5. At m pressures $p_{1..m}$, the 1D Θ-splines (Θ is the independent variable) are created. They describe the saturation curves as illustrated in figure 3.3 for the relative temperature Θ. Θ-splines exist for the densities, mass fractions, specific enthalpies and specific entropies on the dew and bubble lines. After that the dimensionless temperature is calculated, and all Θ-splines are evaluated at Θ^*. A new set of splines - p-splines - is created with the results of the last step (p is the independent variable). They describe, for instance, the saturated liquid mass fraction ξ_{liq} as a function of pressure p at a given relative temperature Θ. Finally, the p-splines are evaluated at p^*. The vapour mass fraction can be calculated from liquid, vapour and total composition.

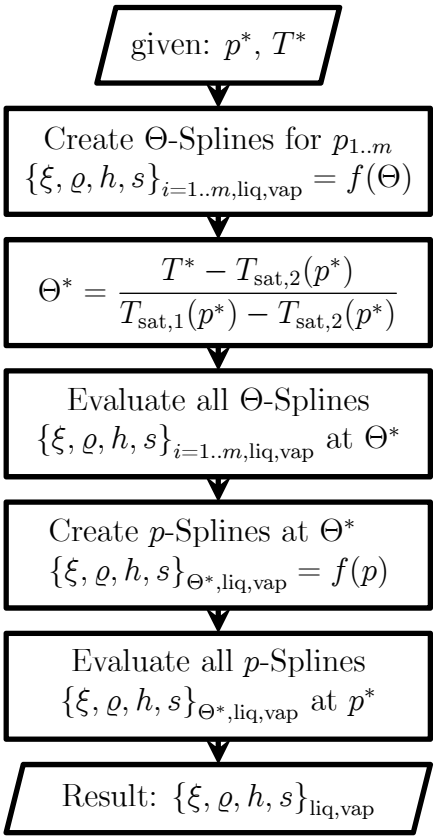

Figure 3.5.: Isobaric-isothermal flash algorithm based on splines explicitly calculates the VLE at a given pressure and temperature.

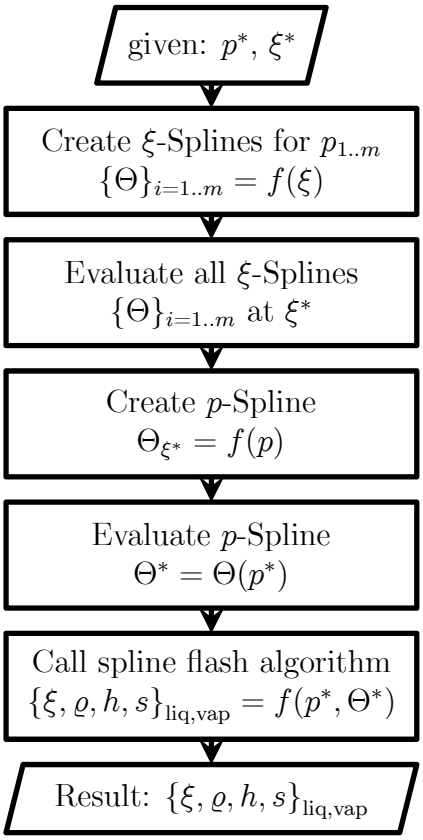

Figure 3.6.: Bubble point temperature algorithm based on splines explicitly calculates the VLE using the spline flash algorithm at a given pressure and mass fraction.

The spline bubble temperature algorithm $f(p, \xi)$ is shown in figure 3.6. At m pressures $p_{1..m}$ the 1D ξ_{liq}-splines are created. They describe the dimensionless bubble temperature as a function of the mass fraction ξ. The ξ-splines are evaluated at the liquid mass fraction ξ^*_{liq}. Then a new spline is created for the dimensionless bubble temperature as a function of the pressure p. The p-spline is evaluated at the pressure p^*, to get the actual dimensionless bubble temperature at p^* and ξ^*_{liq}. The bubble temperature algorithm can be interpreted as follows: first bubble temperature curves $T = f(p)$ at the given composition ξ^*_{liq} is created, then evaluated at p^*. The dew temperature can be calculated similarly to the bubble temperature.

Antoine's equation (Antoine, 1888) is a general equation for the vapour pressure of a pure fluid. It can be used as a boundary condition for the p-splines at both ends if it is locally fitted to the saturation point temperature. The other p- and Θ-splines are

natural splines, so the second derivative is set to 0.

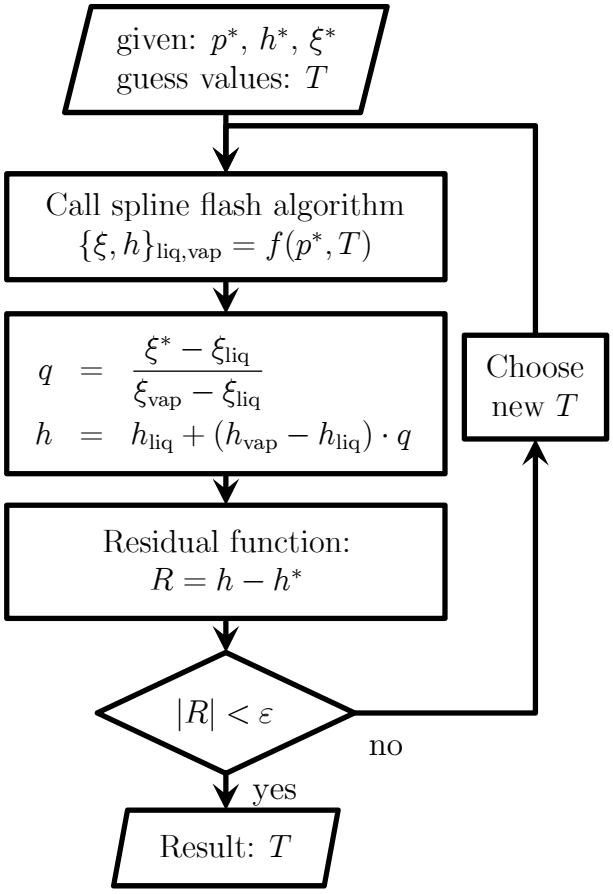

Figure 3.7.: Spline p-h-flash algorithm is an iterative procedure and requires a numerical root finding algorithm.

In figure 3.7 the spline p-h-flash algorithm is shown. It is an iterative procedure. First the p-T-flash algorithm is called to calculate the saturated compositions and specific enthalpies, after which the average specific enthalpy of the two-phases and the residual can be calculated. Newton's or Brent's (Brent, 1973, chapter 4) method can be applied to determine T. The non-linear connection between the surfaces $\xi_{\text{liq,vap}} = f(p, \Theta)$ and $h_{\text{liq,vap}} = f(p, \Theta)$ cannot efficiently be solved for Θ.

If Newton's method is used to solve the p-h-flash, then $\left(\frac{\partial h}{\partial \Theta}\right)_{p,\xi}$ (see appendix C) can be used to calculate the derivative of the residual function. A p-s-flash algorithm follows the same scheme as the p-h-flash.

3.3.3. Partial Derivatives of Density

The partial derivatives of density with respect to the continuous time state variables $\{p, h, \xi\}$ can be obtained from the spline surfaces as presented below. Specific volume v, specific enthalpy h and vapour quality q in the two-phase region are defined in equations (3.8)-(3.10).

$$q = \frac{\xi - \xi_{\mathrm{liq}}}{\xi_{\mathrm{vap}} - \xi_{\mathrm{liq}}} \tag{3.8}$$

$$v = v_{\mathrm{liq}} + (v_{\mathrm{vap}} - v_{\mathrm{liq}})q \tag{3.9}$$

$$h = h_{\mathrm{liq}} + (h_{\mathrm{vap}} - h_{\mathrm{liq}})q \tag{3.10}$$

The partial derivatives of these values with respect to the independent variables p, Θ and ξ are listed in appendix C on page 122. They enable the determination of the partial derivatives of density (3.11)-(3.13). These equations were derived from the definitions.

$$-\left(\frac{\partial \varrho}{\partial h}\right)_{p,\xi} v^2 = \left(\frac{\partial v}{\partial h}\right)_{p,\xi} = \frac{\left(\frac{\partial v}{\partial \Theta}\right)_{p,\xi}}{\left(\frac{\partial h}{\partial \Theta}\right)_{p,\xi}} \tag{3.11}$$

$$-\left(\frac{\partial \varrho}{\partial p}\right)_{h,\xi} v^2 = \left(\frac{\partial v}{\partial p}\right)_{h,\xi} = \left(\frac{\partial v}{\partial p}\right)_{\Theta,\xi} + \left(\frac{\partial v}{\partial \Theta}\right)_{p,\xi} \left(\frac{\partial \Theta}{\partial p}\right)_{h,\xi} \tag{3.12}$$

$$-\left(\frac{\partial \varrho}{\partial \xi}\right)_{p,h} v^2 = \left(\frac{\partial v}{\partial \xi}\right)_{p,h} = \left(\frac{\partial v}{\partial \Theta}\right)_{p,\xi} \left(\frac{\partial \Theta}{\partial \xi}\right)_{p,h} + \left(\frac{\partial v}{\partial \xi}\right)_{p,\Theta} \tag{3.13}$$

The dew and bubble algorithms are not fully consistent with the p-T-flash algorithm. The Θ-splines $\xi = f(\Theta)$ do not exactly describe the same curves as the ξ-splines $\Theta = f(\xi)$. An inversion of the Θ-splines at all pressure levels p_i is necessary to calculate the saturation states consistently. This method has not been chosen here because the calculation takes more time.

The specific volume v, specific entropy s and specific enthalpy h were stored on the dew and bubble surface to enable the calculation of the partial derivatives of density inside the two-phase region and to reduce the calculation effort. v, s and h could also be calculated from p^*, T^* and ξ using an EoS.

3.3.4. Critical Region

The algorithms presented are capable of describing the sub-critical region. The critical region requires a few adaptations (details further below):

- The saturated temperature curves $T_{\mathrm{sat}} = f(p)$ of the pure components have to be extrapolated beyond the critical point to supercritical region
- The evaluation of the Θ-splines is only necessary at subcritical pressure levels
- The critical properties have to be appended to the p-spline grid points to ensure that the critical liquid and vapour properties are equal
- The bubble temperature algorithm must occasionally output dew temperatures, because at some mass fractions, two dew temperatures exist (retrograde condensation)

The saturation temperature curves have to be extrapolated, since the definition of Θ requires a saturation temperature of both components even if the critical pressure of one component is exceeded. Assuming a logarithmic pressure dependency, equation (3.14) can be fitted to the properties at the critical point (see eq. (3.15) and (3.16)) and used to extrapolate the saturation temperature:

$$T_{\mathrm{sat}} = a + b \cdot \ln(p) \tag{3.14}$$

$$b = p_{\mathrm{crit}} \cdot \left(\frac{dT}{dp}\right)_{\mathrm{crit}} \tag{3.15}$$

$$a = T_{\mathrm{crit}} - b \cdot \ln(p_{\mathrm{crit}}) \tag{3.16}$$

The behaviour of the curve is not important as long as $T_{\mathrm{sat},1} \neq T_{\mathrm{sat},2}$ because Θ is not necessarily limited to the interval $[0, 1]$. The transition is not twice continuously differentiable, but if necessary the extrapolation equation can be replaced.

The maximal and minimal pressure of the interpolation region p_{min} and p_{max} depend on the total mass fraction ξ. If the two-phase region is to be described completely, then p_{max} (3.17) is the maximal and p_{min} (3.18) minimal pressure at which a two-phase region at the given mass fraction vector ξ occurs. p_{cc} here is the pressure of the isobar that is tangent to the two-phase region (cricondenbar).

$$p_{\mathrm{max}}(\xi) = p_{\mathrm{cc}}(\xi) \tag{3.17}$$

$$p_{\mathrm{min}}(\xi) = p_{\mathrm{triple}}(\xi) \tag{3.18}$$

To avoid an evaluation of the Θ-splines in a region that is not defined, the line of maximal pressure $p_{\mathrm{max}}(\xi)$ is used to cut off the p-spline and append the critical properties to the spline grid points. The same procedure is applied at the minimal pressure.

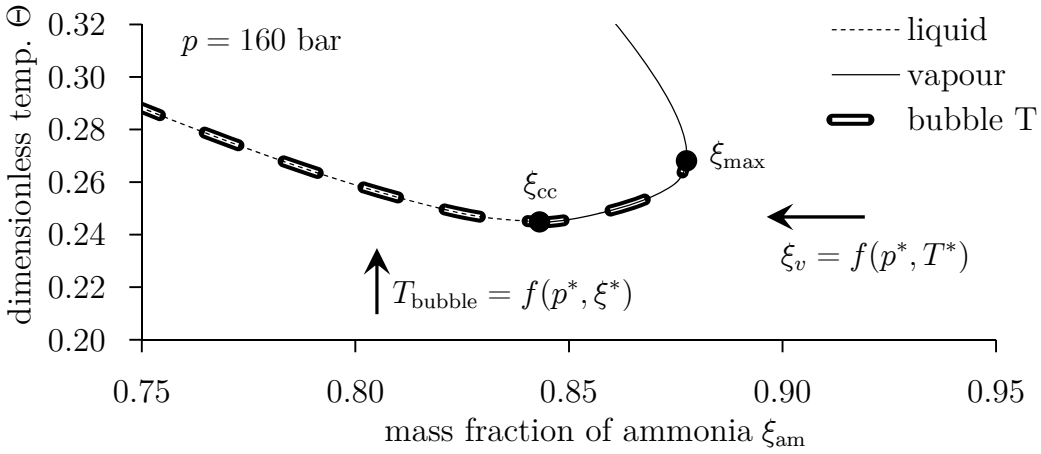

Figure 3.8.: Two-phase region of ammonia-water at 160 bar - area of retrograde condensation. There are two dew temperatures at $\xi_{\mathrm{am}} = 0.87$. The bubble temperature algorithm describes the liquid and vapour properties explicitly up to $\xi_{am} = \xi_{\mathrm{max}}$, the dew temperature algorithm describes the vapour explicitly up to $\xi_{am} = \xi_{\mathrm{max}}$.

Figure 3.8 illustrates one fundamental problem: there are two dew temperatures at $\xi_{\mathrm{am}} > \xi_{\mathrm{cc}}$, whereas ξ_{cc} is the point of maximal temperature (cricondentherm). To fully describe the two-phase region in explicit form, the bubble point algorithm occasionally has to output dew states. The surface between maximal temperature (cricondentherm) and maximal pressure (cricondenbar) must be calculated using the bubble temperature algorithm. The properties at saturation can be used to find out whether the state point is in the two-phase region or not.

3.4. Deviation of Spline Interpolation Algorithms from Iterative VLE Algorithms

In this section the precision of the spline p-T-flash algorithm and the bubble temperature algorithm are discussed. The number of grid points is set to a low value since the overall precision is mainly dependent on it. All deviation caused by the interpolation quality or inefficient spline boundary conditions can be reduced by increasing the number of grid points.

The saturation properties were calculated with REFPROP (Lemmon et al., 2010) using the IAPWS-1995 EoS for water (Wagner and Pruß, 2002), the EoS for ammonia from Tillner-Roth et al. (1993) and the mixture EoS from Tillner-Roth and Friend (1998).

The number of pressure levels m is set to 11, at each pressure level, 25 saturated liquid and 25 saturated vapour state points are saved. The pressure levels range from 1 bar to 100 bar. The saturation temperature of the pure components is described by splines with 100 grid points. The mass fractions ξ, densities ϱ, relative temperatures Θ, specific enthalpies h and specific entropies s of the liquid and vapour are saved in a file. The total amount of data is 29 KB if each value is saved with double precision (64 Bits per floating-point variable).

In figure 3.9 and 3.10 the deviation of the spline p-T-flash algorithm from the iterative p-T-flash (Wagner and Pruß, 2002; Tillner-Roth et al., 1993; Tillner-Roth and Friend, 1998) is plotted. In the first step of the p-T-flash, all Θ-splines are evaluated. The deviation of the Θ-splines from the iteratively calculated two-phase boundary plotted over Θ at a saved pressure level (10 bar) is shown in the upper diagrams. The spline boundary condition (second derivative equal to 0) is sufficient; the overall deviation is not dominated by the upper and lower bound. At $\Theta < 0.2$, the deviation increases. This effect is caused by the high slope of the bubble point properties over Θ (compare figure 3.3 on page 51). The slope $\left(\frac{\partial \xi_{\mathrm{liq}}}{\partial \Theta}\right)_p$ would go to infinity as approaching the azeotropic point; a polynomial cannot describe these shapes perfectly.

In the second step of the p-T-flash algorithm, the results of the Θ-splines are used to create a p-spline, which then is evaluated. The p-splines deviation from the iteratively calculated two-phase boundary at different Θ is shown in the diagrams below. In this case the overall deviation is high at both ends, so the boundary condition could be improved. In the centre the splines are able to reproduce the actual property curves highly accurately.

The deviation of the ξ- and p-splines of the bubble temperature algorithm are shown in figure 3.11. The overall deviation of the ξ-splines is dominated by the error caused by the boundary condition (second derivative equal to 0) at low ammonia mass fractions.

A locally fitted Antoine equation at different ξ_{am} was used as boundary constraint for the p-splines at the upper and lower limit. The parameters were calculated from the closest three grid points. At low and high ammonia mass fractions the derivative at both ends is described very well. At medium ammonia mass fractions Antoine's equation does not precisely describe the shape of the bubble temperature over the pressure at both ends.

The spline p-T-flash algorithm can be integrated into the fluid property calculation without discontinuities. The densities and mass fractions of the liquid and the vapour phase for a given pressure and temperature only define the location of the two-phase region. A deviation of these values causes a state of disequilibrium between vapour and liquid. As the temperature is defined and used as an independent variable of the

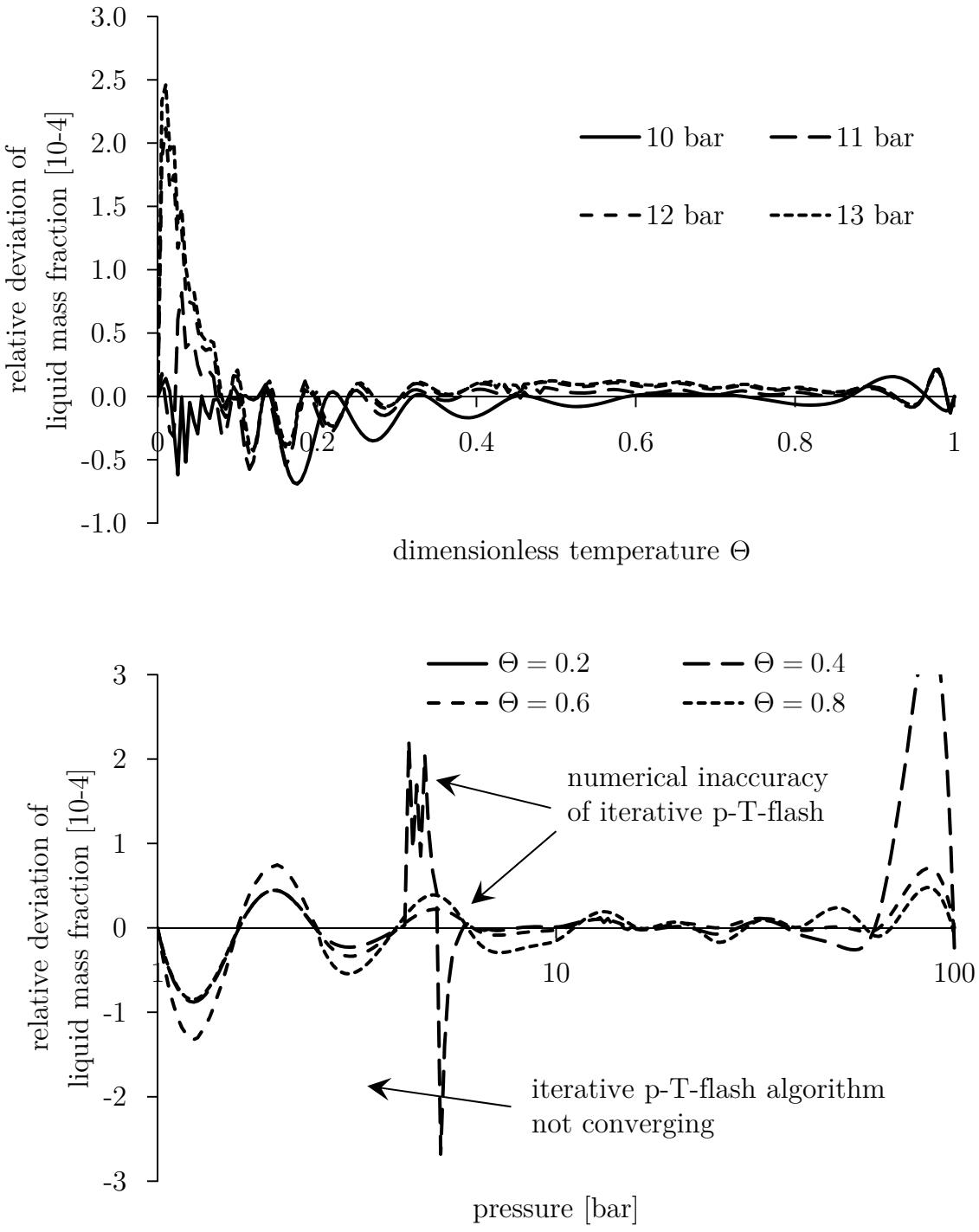

Figure 3.9.: Relative deviation of the Θ-splines (upper diagram) and the p-splines (lower diagram) of the liquid mass fraction ξ_{liq}. The p-T-flash algorithm uses only $m \cdot n = 11 \cdot 25$ grid points. The peaks around 5bar are caused by numerical inaccuracies in the iterative p-T-flash.

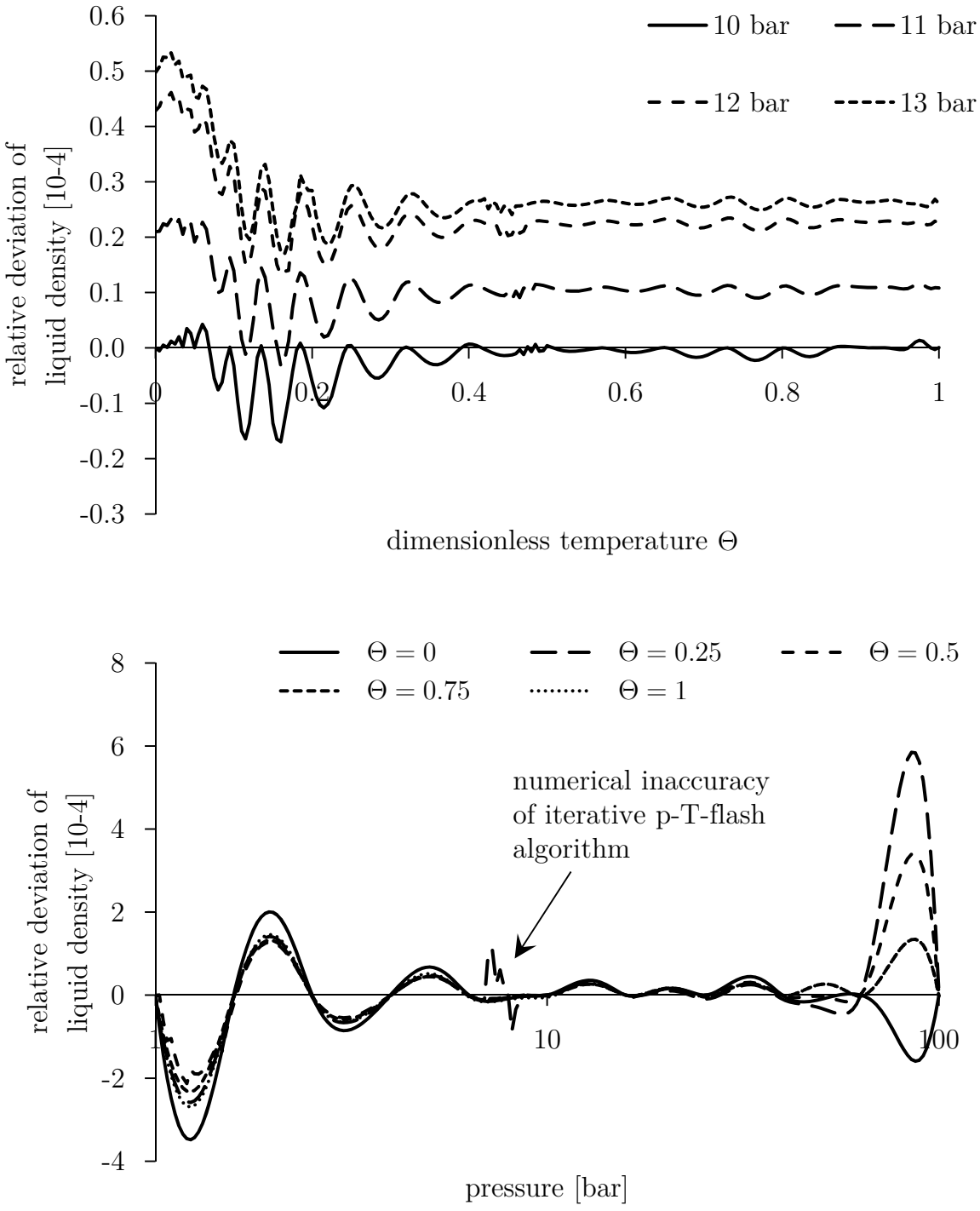

Figure 3.10.: Deviation of the Θ- (upper diagram) and p-splines (lower diagram) of the liquid density ϱ_{liq}. The deviation of the p-splines suggests another spline boundary condition.

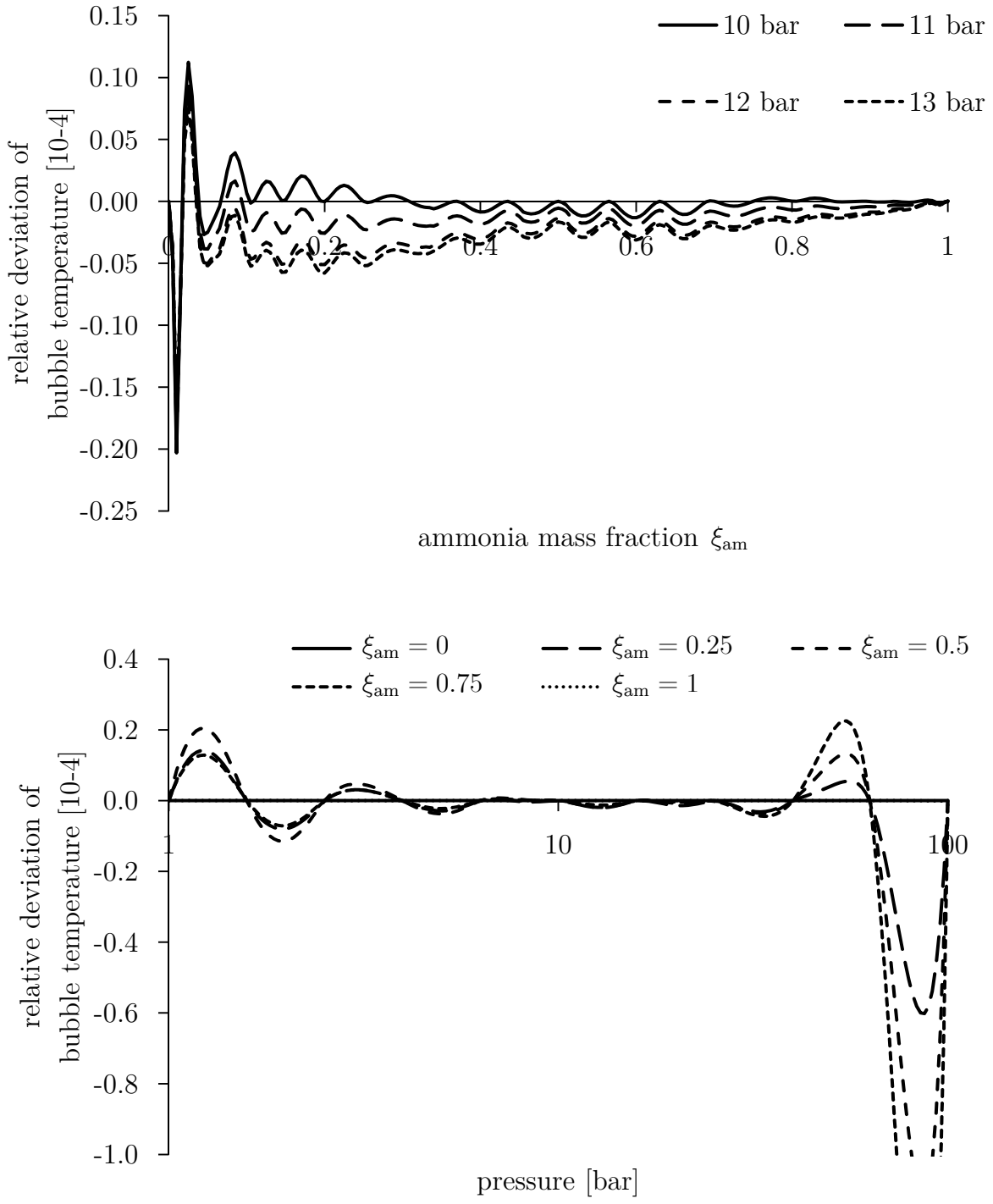

Figure 3.11.: Relative deviation of the bubble temperature T_{bubble} calculated with spline bubble temperature algorithm at medium ammonia mass fractions is dominated by the boundary condition

EoS, the thermal equilibrium will be fulfilled, but not the chemical and mechanical equilibrium condition ($p_{\mathrm{liq}} \neq p_{\mathrm{vap}}$ and $\mu_{\mathrm{vap}} \neq \mu_{\mathrm{liq}}$).

If the information about the specific enthalpy and specific entropy are used as well, then the two-phase region cannot be integrated into the one-phase region continuously without further effort. The equations for the partial derivatives of the density in section 3.3.2 must be adapted if the specific enthalpy surface is unknown, and the partial derivative of the EoS with respect to the mass fractions are also required.

The calculation speed of the p-h-flash and p-s-flash algorithms increases significantly if no evaluation of the EoS is necessary. The discontinuities of the specific enthalpy and specific entropy can be reduced to a minimum by increasing the number of grid points. The discontinuities at the edge of the two-phase region are an acceptable drawback.

3.5. Conclusion and Summary

In this chapter a new approach was presented to describe the two-phase region of a binary mixture. A p-T-flash, p-h-flash, p-s-flash, bubble temperature and dew temperature algorithm can be implemented based on the given descriptions.

The algorithms provide a deterministic, stable and precise description of the two-phase region. Additionally, the partial derivatives of the density with respect to pressure, specific enthalpy and mass fraction can be derived analytically, as required by the models presented in section 4.2.

The precision of the description can be adapted by the number of saved grid points. The deviation presented is only relevant for very low number of grid points.

The algorithms can be integrated continuously into the thermodynamics property description using a multiparameter EoS. If the specific enthalpy and specific entropy are described by splines as well, then the calculation speed will increase significantly, although this will cause a discontinuity at the edge of the two-phase region. Since the precision of the results can be adapted by the number of grid points, the discontinuity is an acceptable drawback.

Chapter 4.

Investigation of Singularities in a Simplified Finite Volume Method

In this chapter a fundamental solving problem of a simplified finite volume method is analysed and a new solution for this problem is presented.

A numerically efficient model for heat exchangers and tubes based on the finite volume method is presented. It is shown that models of this form cannot always be solved and a limiter approach is derived that enables the solving of these models. This approach applies to the finite volume method with dynamic energy and mass balance, neglected pressure drop, and ideally stirred volumes (upwind or upstream discretisation scheme).

4.1. Introduction

The finite volume method is based on three basic balance equations for each volume: mass balance, energy balance and momentum balance (Epple et al., 2009, section 3.3.1). A clever combination of simplifications and discretisation scheme enable a numerically efficient transient simulation of a thermodynamic cycle. The momentum balance in particular allows several simplifications since it usually does not affect the thermal system behaviour in technically relevant time scales.

The physical effects of interest can be modelled with a 1D discretisation of the heat exchanger or tube. The dynamic momentum balance specifies physical effects, such as shock waves in a tube. From a system modeller's point of view, these effects are not of interest and undesirable. To describe the sound distribution correctly, a far more detailed model of the heat exchanger geometry would be necessary.

If pressure is a continuous time state variable in each control volume, then the time constants of these variables in the DAE-system are usually small. A small pressure difference between two control volumes causes a comparably high mass flow rate, which equalises the difference. Small time constants limit the maximum possible DAE-solver step size.

One simple approach is to neglect the pressure drop in the heat exchanger. All control volumes (CV) share the same pressure. A similar approach is to assume the derivative $\frac{dp}{dt}$ is uniform in all CVs of a pressure level ($\frac{dp}{dt}$-approach, see Lemke, 2005). The second approach provides the correct pressure curve over a heat exchanger in steady state solution (see section 4.6.1).

Models employing pressure p as a continuous times state variable, allow an easy and visible implementation of these simplifications. The second chosen continuous time state variable is specific enthalpy h, which is a good choice for technical processes, as already discussed in the introduction 1.2. Temperature should not be chosen as state variable since the two-phase region cannot be described using pressure and temperature. Additionally, the independent mass fraction vector ξ (the vector length is the number of components minus 1) is used as an additional continuous time state variable for a mixture.

If an ideally stirred volume is assumed and the pressure drop is neglected or the $\frac{dp}{dt}$approach is applied, then the algebraic connection between the CVs via the pressure cannot always be solved. In this chapter the solving problems are discussed in detail and an approach to solve the problem under most circumstances is presented and discussed (cf. Schulze et al., 2011b, 2012).

4.2. Governing Equations of the investigated Model

In figure 4.1 the CV is shown. A heat exchanger or tube is discretised into a number of serially connected CVs. Fluid may enter or leave at both sides (A and B). A heat flow $\dot{Q}$ may enter or leave the CV. The mass flow rate and heat flow rate are defined as positive if they enter a CV. The connection to other CVs follows Kirchhoff's current law; a (negative) mass flow rate out of one CV is thus a (positive) mass flow rate into the neighbouring CV.

It is assumed that the fluid flow is homogeneous and that the volumes are ideally stirred, so that the fluid properties are uniform inside the CV. The general continuity equation can be used to derive the mass balance (4.1) (Patankar, 1980; Casella, 2006). The sum of the mass flow rates $\dot{m}_i$ is equal to the density change $\frac{d\varrho}{dt}$ multiplied by the volume V.

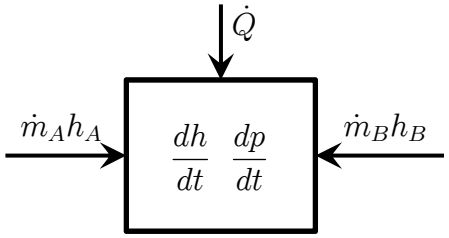

Figure 4.1.: Control volume having pressure and specific enthalpy as state variables, one heat flow $\dot{Q}$ and two mass flows $\dot{m}_A$ and $\dot{m}_B$.

The total derivative of $\frac{d\varrho}{dt}$ has already been inserted in (4.1):

$$V\frac{d\xi}{dt}\left(\frac{\partial\varrho}{\partial\xi}\right)_{p,h} + V\frac{dp}{dt}\left(\frac{\partial\varrho}{\partial p}\right)_{h,\xi} + V\frac{dh}{dt}\left(\frac{\partial\varrho}{\partial h}\right)_{p,\xi} = \dot{m}_A + \dot{m}_B \tag{4.1}$$

$$m\frac{d\xi}{dt} = \dot{m}_A(\xi_A - \xi) + \dot{m}_B(\xi_B - \xi) \tag{4.2}$$

For instance, a binary mixture requires a total mass balance, and a mass balance for the first mixture component (4.2). The length of the mass fraction vector ξ is equal to the number of mixture components minus 1. To simplify the further derivations, it is assumed that there is only one component. Hence, the mass balance for pure components can be simplified to (4.3).

$$V\frac{dp}{dt}\left(\frac{\partial\varrho}{\partial p}\right)_{h,\xi} + V\frac{dh}{dt}\left(\frac{\partial\varrho}{\partial h}\right)_{p,\xi} = \dot{m}_A + \dot{m}_B \tag{4.3}$$

In (4.3) the total derivative of the density is expressed by the two continuous time state variables pressure p and specific enthalpy h. As discussed previously, pressure and specific enthalpy are the preferred independent variables to describe technical processes. The energy balance is given in (4.4) Weigand et al. (2010). Again it is assumed that the fluid properties are uniform inside the CV:

$$m\frac{dh}{dt} = \dot{m}_A(h_A - h) + \dot{m}_B(h_B - h) + \dot{Q} + V\frac{dp}{dt} \tag{4.4}$$

The momentum balance is simplified to (4.5). The pressure drop is set to 0. Thus the differential equations that describe the pressure in the connected CVs have to be combined. An index reduction has to be performed (which is done automatically by Modelica-tools like Dymola or SimulationX, see e.g. Mattsson (1995)).

$$0 = p_B - p_A \tag{4.5}$$

4.3. Location of the Singularity

In this section the system of equations for a heat exchanger model is derived and a singularity is located.

A tube or heat exchanger is described by multiple CVs, as presented above. Since the pressure in connected CVs is equal, the algebraic relationship of the mass and energy balances has to be solved. This algebraic relationship is analysed below.

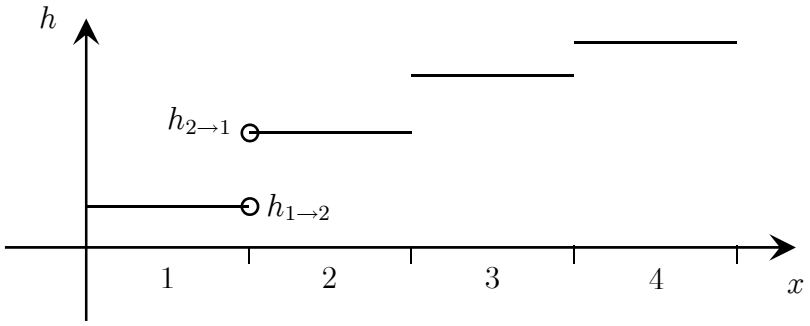

Figure 4.2.: Specific enthalpy curve over tube length. Specific enthalpy at the surface of the CV is dependent on the flow direction.

Figure 4.2 illustrates the basic assumptions: the fluid properties inside a CV are uniform (and so is the specific enthalpy), although the specific enthalpy may differ from one CV to another. If fluid flows from volume 1 to volume 2, this fluid has the specific enthalpy of volume 1. In case of a flow reversal, the specific enthalpy of the fluid flow is that of volume 2. Thus the specific enthalpy at the CV surface is dependent on the direction of the mass flow, but the specific enthalpy flowing out of a volume is always equal to the specific enthalpy inside that CV (see eq. (4.8) and (4.9)). This method is called UPSTREAM or UPWIND scheme (Patankar, 1980).

$$h_{i,A} = \begin{cases} h_{i,A,\text{outflow}} & \text{if } \dot{m}_{i,A} < 0 \\ h_{i-1,A,\text{outflow}} & \text{if } \dot{m}_{i,A} > 0 \end{cases} \tag{4.6}$$

$$h_{i,B} = \begin{cases} h_{i,B,\text{outflow}} & \text{if } \dot{m}_{i,A} < 0 \\ h_{i+1,B,\text{outflow}} & \text{if } \dot{m}_{i,A} > 0 \end{cases} \tag{4.7}$$

$$h_{i,A,\text{outflow}} = h_i \tag{4.8}$$

$$h_{i,B,\text{outflow}} = h_i \tag{4.9}$$

If the direction of the mass flow rates is known, the equation system defining the mass flow rates $\dot{m}_i$ and the derivative of the pressure $\frac{dp}{dt}$ is linear. Taking the flow dependency

into account, the system of equations can be interpreted as non-linear (if the mass flow rate is always evaluated to calculate h at the CV surface) or as a mixed discrete linear system. Both cases can be realised with the Modelica compiler Dymola (by generating an event at flow reversal or not), although the latter one is far more robust.

If the flow direction is known, the system of equations is linear and can be written as (4.10). Matrix A multiplied by the vector of unknowns x is equal to the right hand vector b. If the equation is solved for the unknowns x (4.11), it is necessary to calculate the inverse of matrix A.

$$A \cdot x = b \tag{4.10}$$

$$x = A^{-1} \cdot b = \frac{\mathrm{adj}(A)}{\det(A)} \cdot b \tag{4.11}$$

$$\dot{m}_{1,A} = -\dot{m}_{0,B} \tag{4.12}$$

$$h_{i,B} = h_{i+1,A} \tag{4.13}$$

The mass flow rate leaving one CV enters the next one, and due to Kirchhoff's current law the sign of the mass flow changes (4.12). The specific enthalpies at the CV surface must be equal (4.13). It is important to mention that the heat flow rate $\dot{Q}$ is assumed to be independent of the mass flow rate.

Equation (4.14) is derived from the mass balance (4.3) and the energy balance (4.4) of a single CV, eliminating $\frac{dh}{dt}$. It can be rearranged to (4.15), with ψ_i defined as (4.16) and γ_i defined as (4.17) - (4.18).

$$\begin{aligned} \dot{m}_{i,A} + \dot{m}_{i,B} = V_i \Bigg(& \frac{dp}{dt} \left(\left(\frac{\partial \varrho}{\partial p} \right)_{h,i} + \left(\frac{\partial \varrho}{\partial h} \right)_{p,i} \frac{1}{\varrho_i} \right) \\ & + \left(\frac{\partial \varrho}{\partial h} \right)_{p,i} \frac{1}{m_i} \left[\dot{m}_{i,A} \left(h_{i,A} - h_i \right) \right. \\ & \left. + \dot{m}_{i,B} \left(h_{i,B} - h_i \right) + \dot{Q}_i \right] \Bigg) \end{aligned} \tag{4.14}$$

$$\frac{dp}{dt} + \dot{m}_{i-1,B} \frac{\gamma_{i,A}}{\psi_i} - \dot{m}_{i,B} \frac{\gamma_{i,B}}{\psi_i} = -\frac{1}{\psi_i} \left(\frac{\partial \varrho}{\partial h} \right)_{p,i} \frac{1}{\varrho_i} \dot{Q}_i \tag{4.15}$$

$$\psi_i = \left(\left(\frac{\partial \varrho}{\partial p} \right)_{h,i} + \left(\frac{\partial \varrho}{\partial h} \right)_{p,i} \frac{1}{\varrho_i} \right) \tag{4.16}$$

$$\gamma_{i,A} = \left(1 - \left(\frac{\partial \varrho}{\partial h} \right)_{p,i} \frac{1}{\varrho_i} \left(h_{i,A} - h_i \right) \right) \tag{4.17}$$

$$\gamma_{i,B} = \left(1 - \left(\frac{\partial \varrho}{\partial h} \right)_{p,i} \frac{1}{\varrho_i} \left(h_{i,B} - h_i \right) \right) \tag{4.18}$$

If the mass flow rate at the inlet and outlet of a tube is given, the DAE-system can be used to calculate the behaviour of the pressure and specific enthalpy inside from the heat flow rates $\dot{Q}_i$. However, at each point in time the algebraic relationship between the CVs must be maintained. The derivative of the pressure $\frac{dp}{dt}$ must be calculated from all mass and energy balances at the same pressure, and therefore the mass flow rates between the CVs must be calculated. The unknown variables form the vector of unknowns x. The system of equations (4.19) describes n connected CVs.

$$\begin{pmatrix} \psi_1 & -\gamma_{1,B} & & \\ \psi_2 & \gamma_{2,A} & -\gamma_{2,B} & \\ \vdots & & \ddots & \ddots \\ \psi_n & & & \gamma_{n,A} \end{pmatrix} \begin{pmatrix} \frac{dp}{dt} \\ \dot{m}_{1,B} \\ \dot{m}_{2,B} \\ \vdots \\ \dot{m}_{n-1,B} \end{pmatrix} = \begin{pmatrix} -\dot{m}_{0,B}\gamma_{1,A} & -\frac{\partial \varrho}{\partial h}\frac{\dot{Q}_1}{\varrho_1} & \\ & -\frac{\partial \varrho}{\partial h}\frac{\dot{Q}_2}{\varrho_2} & \\ & \vdots & \\ & -\frac{\partial \varrho}{\partial h}\frac{\dot{Q}_n}{\varrho_n} & +\dot{m}_{n,B}\gamma_{n,B} \end{pmatrix} \tag{4.19}$$

The determinant $det(A)$ in (4.11) is defined in (4.20). In the case that determinant is zero, the system of equations is singular and cannot be solved. The physical consequence is that to fulfil the modelling assumptions, the mass flow rate must go to infinity when it approaches the singularity.

$$\det(A) \;=\; \sum_{i=1}^{n} \left[\psi_i \cdot \prod_{j=2}^{n} (\gamma_{j,A}) \cdot \prod_{k=1}^{i-1} (\gamma_{k,B}) \right] \tag{4.20}$$

The sign of the determinant is influenced by the ψ and γ terms only. If all terms are positive, the determinant is positive. The determinant is zero if the sum of the negative summands is equal to the sum of the positive summands (or if all summands are zero).

4.4. Elimination of the Singularity

In the following, the zero crossing of the determinant is prevented.

$$\psi \;=\; \left(\frac{\partial \varrho}{\partial p}\right)_s \tag{4.21}$$

ψ is dependent only on the thermodynamic properties of the fluid. Applying Bridgman's table (see appendix A), (4.16) can be rearranged as (4.21). The derivative of the density

with respect to pressure at constant specific entropy describes the change of the pressure during an isentropic compression of a closed system.

The ψ term can be interpreted physically, that is, based on the thermodynamic definition of the speed of sound (4.22) (Kabelac, 1998) and assuming that this definition is valid for the two-phase region, ψ can be calculated from the speed of sound w (4.23). If the speed of sound is positive, then ψ is positive. Therefore ψ always is positive in the one and two-phase regions.

$$w = \sqrt{\left(\frac{\partial p}{\partial \varrho}\right)_s} \tag{4.22}$$

$$\psi = \frac{1}{w^2} \tag{4.23}$$

By contrast, the γ terms may change the sign. The derivative of the density with respect to specific enthalpy $\left(\frac{\partial \varrho}{\partial h}\right)_p$ is always negative. γ_A can only be negative if the difference $(h_{i,A} - h_i)$ is less than zero, and γ_B can only be negative if the difference $(h_{i,B} - h_i)$ is less than zero.

In a normal system state all γ terms are positive, but if one or more of the γ terms are negative, the determinant may be equal to zero. A simple approach to prevent this is to prevent a zero crossing of the γ term. A zero crossing of a γ term is only possible if the specific enthalpy at the CV surface $h_{i,A}$ or $h_{i,B}$, is less than the specific enthalpy in the CV h_i. In other words, a zero crossing of a γ term can only occur when fluid with a lesser specific enthalpy enters a CV. Equations (4.24) and (4.25) are derived from (4.17) and (4.18); they limit the specific enthalpies leaving the neighbouring CV.

$$h_{i-1,B,\text{outflow}} > h_i + \frac{\varrho_i}{\left(\frac{\partial \varrho}{\partial h}\right)_{p,i}} \tag{4.24}$$

$$h_{i+1,A,\text{outflow}} > h_i + \frac{\varrho_i}{\left(\frac{\partial \varrho}{\partial h}\right)_{p,i}} \tag{4.25}$$

$$h_{\text{limit,i}} = h_i + y_{\text{limit}} \frac{\varrho_i}{\left(\frac{\partial \varrho}{\partial h}\right)_{p,i}} \tag{4.26}$$

$$h_{i-1,B,\text{modified,outflow}} = \max\left\{h_{i-1}, h_{i,\text{limit}}\right\} \tag{4.27}$$

$$h_{i+1,A,\text{modified,outflow}} = \max\left\{h_{i+1}, h_{i,\text{limit}}\right\} \tag{4.28}$$

The second summand on the right side is always negative, so by multiplying it with the factor $y_{\text{limit}} \in]0,1[$, a definition of the minimum specific enthalpy that may enter a CV is found (4.26). If h_{outflow} is equal to h_{limit} the inequations are fulfilled. The specific enthalpy that leaves a CV needs to be modified.

Figure 4.3 illustrates the specific enthalpy curve over a heat exchanger. CV 2 limits the specific enthalpy that may leave CV 1 in the direction of CV 2. If y_{limit} is in $]0,1[$

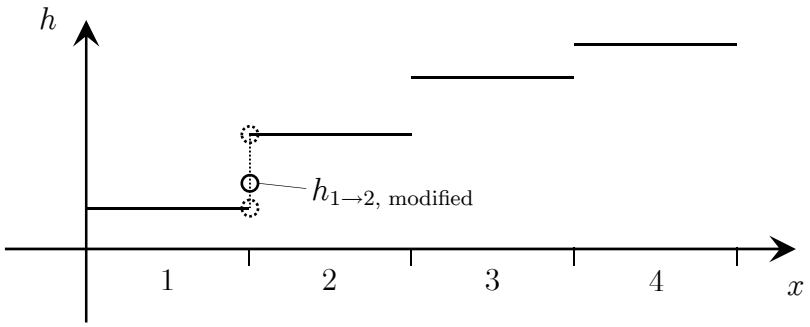

Figure 4.3.: Specific enthalpy curve over tube length. Modified specific enthalpy is always between the specific enthalpies of the connected CVs.

then the modified specific enthalpy is always between h_1 and h_2. Due to the $max()$ operator, it is only modified if the minimal specific enthalpy that is allowed to enter CV 2 is higher than the specific enthalpy of CV 1.

$\gamma < 0$ is a necessary condition, but it is not a sufficient condition for $det(A) <= 0$. One or more negative γ terms do not necessarily cause $det(A) <= 0$, so the system of equations is presumably solvable.

The assumption of ideal stirring is not the reason for the singularity. Neither are the possible flow reversal and switching of the specific enthalpy on the CV's surface. The singularity is caused by the assumption that the pressure is uniform along the tube. Without this assumption, the algebraic relation between the CV's mass and energy balances would not exist.

The local limitation of the specific enthalpy that may enter or leave a CV is useful for models that are used in varying contexts. It can easily be implemented in an object-oriented manner based on a model for the CV. This approach ab initio prevents the singularity. Since $\gamma \leq 0$ does not necessarily mean $det(A) \leq 0$, a more efficient global approach needs to be found. If a linear curve instead of uniform fluid properties along the longitudinal axis in the volume is assumed, then the density and its derivatives have to be calculated from the enthalpy curve (see Casella (2006) and Bonilla et al. (2010)). This "mean density" approach leads to a similar system of equations that turns out to be much more robust than the unmodified one that is created applying the presented balance equations.

The limiter presented in this section was implemented in the object-oriented modelling language Modelica. The implementation can be found in appendix D.

4.5. Discussion and Interpretation

4.5.1. Case study: Two connected control volumes

The singularity is demonstrated in this section using a tube discretised into two CVs with given mass flow rates at both ends. The system of equations is derived and singularity illustrated by residual plots.

$$\begin{pmatrix} \psi_1 & -\gamma_{1,B} \\ \psi_2 & \gamma_{2,A} \end{pmatrix} \begin{pmatrix} \frac{dp}{dt} \\ \dot{m}_{1,B} \end{pmatrix} = \begin{pmatrix} -\dot{m}_{0,B}\gamma_{1,A} & -\frac{\partial \varrho}{\partial h}\frac{\dot{Q}_1}{\varrho_1} \\ & -\frac{\partial \varrho}{\partial h}\frac{\dot{Q}_2}{\varrho_2} \quad +\dot{m}_{2,B}\gamma_{2,B} \end{pmatrix} \tag{4.29}$$

The system of equations (4.29) is derived from (4.19) with $n = 2$. The unknown variables are the mass flow rate between the two CVs and the derivative of the pressure $\frac{dp}{dt}$. As the sign of the mass flow rate between the CVs is unknown, the specific enthalpy at the CV surface can also not be determined. The whole system of equations is described by two linear systems: (4.30) if $\dot{m}_{1\to2} > 0$, and (4.31) if $\dot{m}_{1\to2} < 0$.

$$A_{\dot{m}_{1\to2}>0} = \begin{pmatrix} \frac{\partial \varrho}{\partial p}_1 + \frac{\partial \varrho}{\partial h}_1 \frac{1}{\varrho_1} & -1 \\ \frac{\partial \varrho}{\partial p}_2 + \frac{\partial \varrho}{\partial h}_2 \frac{1}{\varrho_2} & 1 - \frac{\partial \varrho}{\partial h}_2 \frac{h_{1,B,\text{outflow}} - h_2}{\varrho_2} \end{pmatrix} \tag{4.30}$$

$$A_{\dot{m}_{1\to2}<0} = \begin{pmatrix} \frac{\partial \varrho}{\partial p}_1 + \frac{\partial \varrho}{\partial h}_1 \frac{1}{\varrho_1} & -1 + \frac{\partial \varrho}{\partial h}_1 \frac{h_{2,A,\text{outflow}} - h_1}{\varrho_1} \\ \frac{\partial \varrho}{\partial p}_2 + \frac{\partial \varrho}{\partial h}_2 \frac{1}{\varrho_2} & 1 \end{pmatrix} \tag{4.31}$$

The determinant (4.32) is derived from the general form (4.20) with $n = 2$.

$$\begin{aligned} \det(A) &= \sum_{i=1}^{2} \left[\psi_i \cdot \prod_{j=2}^{2} (\gamma_{j,A}) \cdot \prod_{k=1}^{i-1} (\gamma_{k,B}) \right] \\ &= \psi_1\gamma_{2,A} + \psi_2\gamma_{1,B} \qquad (4.32) \\ &= \left(\left(\frac{\partial \varrho}{\partial p} \right)_{h,1} + \left(\frac{\partial \varrho}{\partial h} \right)_{p,1} \frac{1}{\varrho_1} \right) \left(1 - \left(\frac{\partial \varrho}{\partial h} \right)_{p,2} \frac{1}{\varrho_2} (h_{2,A} - h_2) \right) \\ &\quad + \left(\left(\frac{\partial \varrho}{\partial p} \right)_{h,2} + \left(\frac{\partial \varrho}{\partial h} \right)_{p,2} \frac{1}{\varrho_2} \right) \left(1 - \left(\frac{\partial \varrho}{\partial h} \right)_{p,1} \frac{1}{\varrho_1} (h_{1,B} - h_1) \right) \qquad (4.33) \end{aligned}$$

$$y_{\text{limit}} = 0.9 \tag{4.34}$$

$$h_{\text{limit},1} = h_1 + 0.9 \cdot \frac{\varrho_1}{\left(\frac{\partial \varrho}{\partial h}\right)_{p,1}} \tag{4.35}$$

$$h_{\text{limit},2} = h_2 + 0.9 \cdot \frac{\varrho_2}{\left(\frac{\partial \varrho}{\partial h}\right)_{p,2}} \tag{4.36}$$

$$h_{2,A,\text{modified,outflow}} = \max\left\{h_2, h_{1,\text{limit}}\right\} \tag{4.37}$$

$$h_{1,B,\text{modified,outflow}} = \max\left\{h_1, h_{2,\text{limit}}\right\} \tag{4.38}$$

y_{limit} is set to $0.9 \in]0,1[$ (4.34) and the minimal specific enthalpy that is allowed to enter h_{limit} of both CVs is given by (4.35) and (4.36). The specific enthalpy that leaves CV 2 in the direction of CV 1 (4.37) is limited using the max operator, and so is the specific enthalpy leaving CV 1 in the direction of CV 2 (4.38). If the modified "outflow" enthalpies replace the original ones in the A matrices, the algebraic system of equation can always be solved.

In the following a residual plot is discussed. If the system of equations is not interpreted as mixed discrete linear but rather as non-linear, the mass flow rate between the CVs can be selected as an iteration variable, and the residual can be defined by (4.40), the difference of the $\frac{dp}{dt}$ of the CVs.

$$\left(\frac{dp}{dt}\right)_i = -\dot{m}_{i-1,B}\frac{\gamma_{i,A}}{\psi_i} + \dot{m}_{i,B}\frac{\gamma_{i,B}}{\psi_i} - \frac{1}{\psi_i}\frac{\partial \varrho}{\partial h}\frac{1}{\varrho_i}\dot{Q}_i \tag{4.39}$$

$$\text{Residual} = f(\dot{m}_{1,B}) = \left(\frac{dp}{dt}\right)_2 - \left(\frac{dp}{dt}\right)_1 \tag{4.40}$$

In figure 4.4 the residual for three different system states is plotted over the mass flow rate. At zero mass flow rate the specific enthalpy on the CV surface (and therefore matrix A) is switched. The state a is most likely to occur in a simulation, the system of equations defining the mass flow rate and the derivative $\frac{dp}{dt}$ has only one solution. If the system of equations is singular, the residual cannot be influenced by the mass flow rate. The system in state b is singular at negative mass flow rates, but there is still a valid solution at positive mass flow rates. The system state c has two valid solutions, and both of them could be selected by the solving algorithm. In that case a positive and a negative mass flow rate fulfil the system of equations.

In figure 4.5 a system state is shown that cannot be solved. The residual cannot be reduced to zero, and as the algebraic relation of the variable in the DAE model cannot be solved, thus the simulation must terminate.

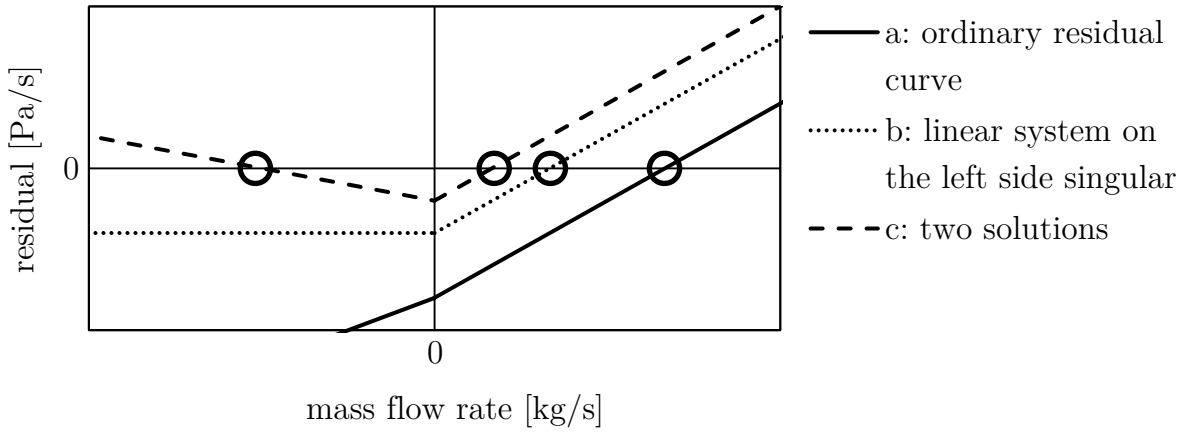

Figure 4.4.: Residual plot for three possible system states illustrating the switching of the matrix A from equation (4.30) to (4.31) at zero mass flow rate: An ordinary state (a) having one solution - A state (b) with valid solution but one of the linear systems is singular having a residual slope of 0 - A state (c) with two valid solutions.

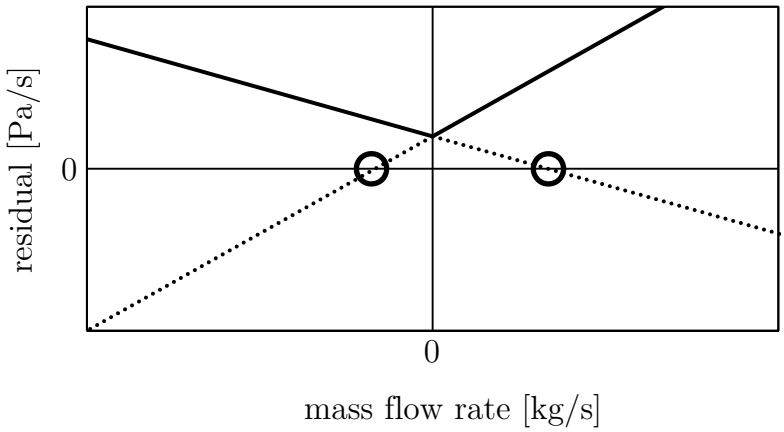

Figure 4.5.: Residual plot for a system state without a valid solution. Both linear systems have a solution but the result is not in a valid range.

4.5.2. Physical Interpretation

The solving problems based on the presented system of equations are rooted in the modelling assumptions. In this subsection a physical interpretation of the singularity is given.

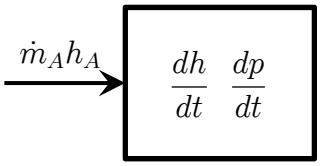

Figure 4.6.: Mass entering an adiabatic open CV may lead to a pressure decrease

An adiabatic open system described by only one CV illustrates the basic problem (see figure 4.6). The change of the pressure caused by mass entering the CV is analysed.

Generally there are two effects that influence the pressure in the system:

- an increase in mass in the system will lead to an increase in pressure, so $\left(\frac{\partial p}{\partial mass}\right)_{h,V} > 0$, $\left(\frac{\partial p}{\partial \varrho}\right)_h > 0$
- a decrease in specific enthalpy in the system will lead to a decrease in pressure, so $\left(\frac{\partial p}{\partial h}\right)_{\text{mass},V} > 0$, $\left(\frac{\partial p}{\partial h}\right)_{\varrho} > 0$

The pressure increase by the first effect can be reduced by the second effect, if the specific enthalpy h_A entering the system is less than the specific enthalpy in the system. In that case these effects counteract each other.

$$\frac{dp}{dt} - \dot{m}_A \frac{\gamma_A}{\psi} = 0 \tag{4.41}$$

Equation (4.41) is derived from (4.15). This equation reveals one interesting case: if γ_A is 0 then the pressure does not change over time, even if mass is put into the system. If γ_A has crossed zero, then an entering mass flow rate will lead to a pressure reduction. In other words, if the specific enthalpy of the entering mass is significantly less than that of the fluid in the system, it causes a pressure reduction instead of the expected pressure increase. The second effect overcompensates the first effect. This is very likely to happen if the fluid state in the CV is in of the two-phase region. The condensation of the vapour phase intensifies the influence of the second effect.

4.5.3. Drawbacks of the presented Local Limiter Approach

One basic issue of this limiter approach is that the specific enthalpy that leaves a CV may be modified to a higher value. Thus the temperature of the fluid leaving a CV may be higher than the temperature of the fluid inside the CV. This may cause a divergence of the transient simulation. If in steady state and the modification of the outflowing specific enthalpy extracts more energy from the CV than is compensated by a heat flow, the transient simulation diverges.

As mentioned previously, the singularity is caused by a fluid flow with a lesser specific enthalpy entering a CV. Assuming a steady state, this occurs only if heat is added to the fluid, for example in an evaporator.

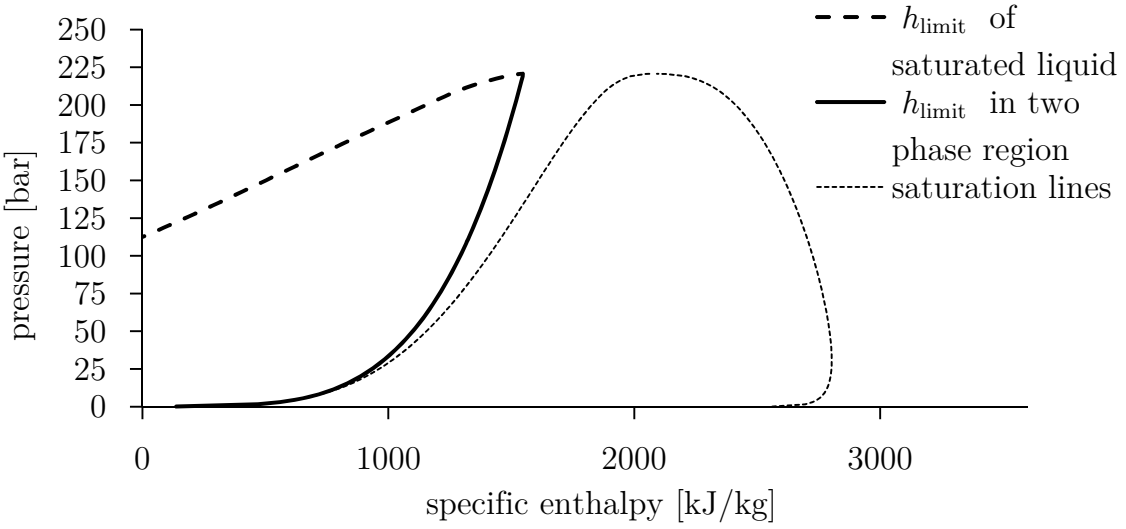

Figure 4.7.: Comparison between h_{limit} of saturated liquid and fluid in the two-phase region in a p-h-diagram of water. h_{limit} in the two-phase region is very close to the bubble line.

In figure 4.7 a p-h-diagram of water is shown. The solid line is the h_{limit} of a CV in the two-phase region. This value is not dependent on the vapour quality. In steady state, a CV in the liquid region must be located between the solid line and the bubble line; otherwise, the specific enthalpy of a fluid flowing towards a CV in the two-phase region is limited to the solid line. The dashed line is h_{limit} of a CV filled with saturated liquid.

The steady state results of an evaporator are not influenced by the limiter if the specific

enthalpy of the last CV with fluid in liquid state is between the solid line and the bubble line. Otherwise the steady state results are modified. In the one-phase region the limiter hardly influences the results. Problems arise from subcooled liquid entering a CV in the two-phase region.

The transient simulation of air conditioning systems is much more robust using the limiter approach. At high pressure, fluid is condensed, possibly subcooled, and throttled into the two-phase region. Finally the fluid is evaporated, superheated at low pressure and again compressed to high pressure. During this process, liquid fluid never is supposed to enter the evaporator. The inlet of the evaporator is in the two-phase region. For the transient simulation of an organic Rankine cycle the limiter has to be applied with caution. In a Rankine cycle starting from a liquid fluid, a pump increases the pressure. At high pressure the fluid is evaporated and superheated, expanded in a turbine and condensed again. Evaporation takes place at high pressure and liquid enters the evaporator. Particularly at pressures far less than the critical pressure, an evaporator is affected by the limiter.

To avoid such issues caused by the limiter, it can be deactivated locally by setting y_{limit} of a CV to a very high value $y_{\text{limit}} \gg 1 \notin]0, 1[$ causing h_{limit} to decrease. If the limiter is partially or fully deactivated, it cannot be guaranteed that the system of equations can be solved.

Another way to avoid issues is to partially abandon the assumption of uniform pressure. If, for example, the preheating zone is separated from the evaporator and a valve model as well as a receiver are placed between them, then the liquid part and the part in the two-phase region are cut off from each other. The mass flow rate at the valve is not part of the system of the equations. The preheating zone and the evaporation are described by two separate mixed discrete linear systems of equations.

Since the presented limiter is just one approach to modify the system of equations, others might be found that are not as restrictive as the one presented above. A global approach is possible that only intervenes if a singularity is about to cause the termination of the simulation.

Instead of the simplified finite volume method, other modelling approaches of similar complexity (for instance the moving boundary approach) can be applied to transient simulations of this kind of heat exchanger.

4.6. Extensions to the Presented Modelling Approach

4.6.1. Pressure Drop Correlations

The steady state results of heat exchanger models as presented above do not describe the temperature drop in the two-phase region that is caused by the pressure drop. This effect can be added to the models by assuming that the pressure derivative $\frac{dp}{dt}$ instead of the pressure is equal even if the pressure itself may differ (Lemke, 2005). Thus, all mass (4.42) and energy balances (4.43) refer to $\frac{dp}{dt}$ at a reference state. The pressure drop Δp_{state} is a "pseudo" continuous time state variable that follows the steady state pressure drop with delay.

$$V\frac{dp_{\text{reference}}}{dt}\frac{\partial \varrho_i}{\partial p_i} + V\frac{dh_i}{dt}\frac{\partial \varrho_i}{\partial h_i} = \dot{m}_{i,A} + \dot{m}_{i,B} \tag{4.42}$$

$$\begin{aligned} m_i\frac{dh_i}{dt} &= \dot{m}_{i,A}(h_{i,A} - h_i) + \\ &\quad \dot{m}_{i,B}(h_{i,B} - h_i) + \dot{Q}_i + V_i\frac{dp_{\text{reference}}}{dt} \end{aligned} \tag{4.43}$$

$$\frac{d\Delta p_{\text{state}}}{dt} = \frac{1}{\tau_{\text{state}}}\left(\Delta p_{\text{correlation}} - \Delta p_{\text{state}}\right) \tag{4.44}$$

Replacing the derivative of the pressure in all mass and energy balances is an approximation and leads to a small mass defect during transient simulation. The mass in all CVs can be calculated using (4.45). If the pressure in a CV is calculated relative to the reference pressure (4.46), then (4.47) describes the mass in the CVs. Thus, if all CVs refer to $\frac{dp_{\text{reference}}}{dt}$, then (4.48) describes the error in mass calculation during the simulation.

$$m = m_0 + \int_{t_0}^{t_1} \sum^{n} V_i \left[\left(\frac{\partial \varrho}{\partial p}\right)_h \frac{dp}{dt} + \left(\frac{\partial \varrho}{\partial h}\right)_p \frac{dh}{dt}\right]_i dt \tag{4.45}$$

$$p_i = p_{\text{reference}} + \sum_{j=1}^{i-1} \Delta p_i \tag{4.46}$$

$$m = m_0 + \int_{t_0}^{t_1} \sum^{n} V_i \left[\left(\frac{\partial \varrho}{\partial p}\right)_{h,i} \frac{d\left(p_{\text{reference}} + \sum_{j=1}^{i-1} \Delta p_i\right)}{dt} + \left(\frac{\partial \varrho}{\partial h}\right)_{p,i} \frac{dh_i}{dt}\right] dt \tag{4.47}$$

$$\Delta m = \int_{t_0}^{t_1} \sum^{n} V_i \left[\left(\frac{\partial \varrho}{\partial p}\right)_{h,i} \frac{d\left(\sum_{j=1}^{i-1} \Delta p\right)}{dt}\right] dt \tag{4.48}$$

A mass defect only occurs if the sum of the pressure drops $\sum \Delta p_i$ changes over time. To reduce the mass defect, the reference pressure should be placed close to the CV with the highest $V_i \cdot \left(\frac{\partial \varrho}{\partial p}\right)_{h,i}$.

This approach inverts the temporal behaviour of the system. In physical systems, mass needs to be accelerated by a pressure difference before the mass flow rate increases, or the mass flow rate is a result of a local pressure difference. In contrast, here an increased mass flow rate causes a pressure drop with a certain delay.

4.6.2. Complex Heat Transfer Correlations

In the preceding sections the heat flow rate $\dot{Q}$ was assumed to be independent of the mass flow rate. The motivation for this assumption has to explained as it is physically unusual, but crucial for the presented approach. In this section the γ terms are derived for a heat flow rate that is linearly dependent on the mass flow rate. Additionally, a method is presented to integrate non-linear heat transfer correlations.

$$\dot{Q} = \alpha A \left(T_A - T_B\right) \tag{4.49}$$

$$Re = \frac{v \cdot d}{\nu} \tag{4.50}$$

Equation (4.49) describes the heat flow rate $\dot{Q}$ (Fourier's law). The heat transfer is proportional to the negative gradient of the temperature and to the area across which the heat is flowing.

Numerous heat transfer correlations describing the heat transfer coefficient α for one or two-phase heat transfer have been published in recent decades. Most of them are non-linearly dependent on the Reynolds Number Re (for example the correlation by Gnielinksi or Dittus-Boelter, Incropera and DeWitt, 2007) which is dependent on the kinematic viscosity ν, a characteristic length d and the speed v orthogonal to the heat transfer.

If $\dot{Q}$ depends on the mass flow rate, the system of equations looks different and most likely is non-linear. In case the momentum balance was simplified to $p_\mathrm{A} = p_\mathrm{B}$, solving the algebraic system of equations is much more complex if the heat transfer is non-linear. The number of valid solutions for the mass flow rates between the CVs is dependent on the heat transfer correlation. If $\dot{Q}$ is linearly dependent on the mass flow rate $\dot{m}_{i,A}$ (4.51), then (4.15) can be transformed to (4.53). The linearly dependent summand of the heat flow rate is added to $\gamma_{i,A}$ and forms the new term $\gamma_{i,A,Q}$ (4.53).

$$\dot{Q}_i = q_{i,0} + \dot{m}_{i-1,B} \cdot q_{i,1} \tag{4.51}$$

$$\frac{dp}{dt}\psi_i + \dot{m}_{i-1,B}\left(\gamma_{i,A} + \frac{\partial \varrho}{\partial h}\frac{1}{\varrho_i}\cdot q_{i,1}\right) \qquad (4.52)$$
$$-\dot{m}_{i,B}\gamma_{i,B} = -\frac{\partial \varrho}{\partial h}\frac{1}{\varrho_i}q_{i,0}$$

$$\gamma_{i,A,Q} = \gamma_{i,A} + \frac{\partial \varrho}{\partial h}\frac{1}{\varrho_i}\cdot q_{i,1} \qquad (4.53)$$

$$\begin{pmatrix} \psi_1 & -\gamma_{1,B} & & \\ \psi_2 & \gamma_{2,A,Q} & -\gamma_{2,B} & \\ \vdots & & \ddots & \ddots \\ \psi_n & & & \gamma_{n,A,Q} \end{pmatrix} \begin{pmatrix} \frac{dp}{dt} \\ \dot{m}_{1,B} \\ \dot{m}_{2,B} \\ \vdots \\ \dot{m}_{n-1,B} \end{pmatrix} = \begin{pmatrix} -\dot{m}_{0,B}\gamma_{1,A,Q} & -\frac{\partial \varrho}{\partial h}\frac{q_{1,1}}{\varrho_1} \\ & -\frac{\partial \varrho}{\partial h}\frac{q_{2,1}}{\varrho_2} \\ & \vdots \\ & -\frac{\partial \varrho}{\partial h}\frac{q_{n,1}}{\varrho_n} \quad +\dot{m}_{n,B}\gamma_{n,B} \end{pmatrix} \qquad (4.54)$$

$$\det(A) = \sum_{i=1}^{n}\left[\psi_i \cdot \prod_{j=2}^{n}\left(\gamma_{j,A,Q}\right)\cdot \prod_{k=1}^{i-1}\left(\gamma_{k,B}\right)\right] \qquad (4.55)$$

The system of equations (4.54) is still mixed discrete linear. The determinant of A now contains $\gamma_{i,A,Q}$ instead of $\gamma_{i,A}$, so the zero crossing of the determinant moves if $q_{i,1} \neq 0$. In case of a linear dependency of $\dot{Q}$ on the mass flow rate, a zero crossing of $\gamma_{i,A,Q}$ has to be avoided.

The heat transfer correlations usually describe the steady state heat transfer. The transient behaviour, especially for two-phase heat transfer correlations, is usually not taken into account. The direct relation between the mass flow rate between two CVs and a heat transfer coefficient in a distant CV is non-physical. The reason for this relation is the assumption that the heat transfer correlation is always valid, even in transient state.

To simplify the solving procedure and to remove this non-physical algebraic dependency, a pseudo continuous time state variable α_{state} is implemented (4.56). The heat transfer coefficient that is used to calculate the heat flow rate $\dot{Q}$ is delayed.

$$\frac{d\alpha_{\text{state}}}{dt} = \frac{1}{\tau_{\text{state}}}\left(\alpha_{\text{correlation}} - \alpha_{\text{state}}\right) \qquad (4.56)$$
$$\dot{Q} = \alpha_{\text{state}} A (T_A - T_B) \qquad (4.57)$$

4.7. Conclusion and Summary

The simplified finite volume method is a good choice for the transient system simulation of thermodynamic cycles, although the models fail under certain circumstances. This method is easy to understand, robust and easy to initialise.

Simulation of thermodynamic cycles based on a simplified finite volume method has one drawback: the pressure-level-wide algebraic relationship cannot always be solved. The solution was analysed, the singularity that may occur was exemplified using simple cases. The singularity is caused by the simplification of the momentum balance of an ideally stirred control volume and is not necessarily caused by flow reversal.

A limiter was presented that prevents the singularity by modifying the specific enthalpy flowing out of a control volume. The limiter should be used with caution if the models are used to describe liquid fluid that is evaporated. Thus it should preferably be used for transient simulation of air conditioning systems rather than Rankine cycles.

It was shown how complex heat transfer and pressure drop correlations can be integrated into these models enabling a numerically efficient description of the steady state results.

Chapter 5.

Investigation of Alternative Air Conditioning Systems for a City Bus

In this chapter the possibilities that the methods presented in the previous chapters afford is demonstrated on two alternative air conditioning systems for a city bus.

A conventional R-134a air conditioning (AC) system in a city bus is presented. The system is used as a reference for evaluating the alternative AC systems. For all simulations, the heat exchanger and tube models are based on the equations described in chapter 4.

The two alternative AC systems are a conventional AC system with the blend R-445A as drop-in refrigerant (based on chapter 2), and an absorption system with the working pair ammonia-water (based on chapter 3.1). The thermophysical properties of R-445A are described using the bicubic spline interpolation of each property (sections 2.3.2 and 2.5). A system model for the absorption system and a simple control strategy are presented. The thermophysical properties are calculated employing the models presented in chapter 3.

5.1. Description of a Conventional City Bus Air Conditioning System

The bus examined in this chapter is a two-axle city bus with a length of twelve meters. The conventional R-134a AC system is shown in figure 5.1 and 5.2. It is composed of three evaporators in the front box and on the left and right side of the roof compact unit and a condenser placed in the centre of the roof compact unit. The compressor is driven mechanically and located in the back of the bus, close to the engine. The refrigerant is expanded in thermostatic expansion valves.

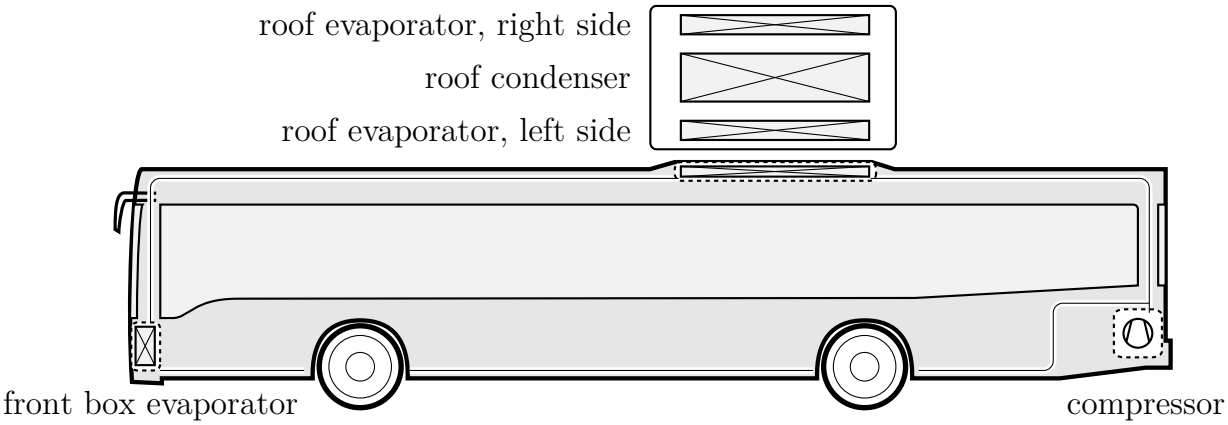

Figure 5.1.: Placement of the air conditioning system components on a city bus with two-axle. One evaporator in the front, two evaporators on the roof, condenser on the roof, and the compressor in the back. (taken from Schulze et al., 2011b)

The thermostatic expansion valves have a variable effective flow area, utilising a PI-controller to maintain the superheating behind the evaporators at approximately 14 °C. The efficiency of the steady state compressor model is obtained from a map. The compressor is used to control the system cooling capacity with an On-Off-strategy. When the average cabin temperature falls below 21 °C, the compressor is switched off. When it rises above 24 °C, the compressor is reactivated.

The heat transfer area of a roof box evaporator is about twice as large as the heat transfer area of the front box evaporator. While the front box evaporator is supplied with fresh air, the roof box evaporators can operate with fresh or recirculated air. The three evaporators and the condenser were implemented as ideal counterflow heat exchangers.

In figure 5.2 the model of the AC system is shown. The system model is implemented in Modelica using the TIL library and was published in Schulze et al. (2011b). See also Kaiser et al. (2012b). The model includes the four heat exchangers visible in figure 5.1. Tubing is partially included in the model to account for volume and time delay.

Fresh outside and recirculated air move through the three evaporators into the passenger compartment. Diffusive and direct solar radiation as well as the influence of passengers on temperature and moisture based on VDI Guideline 2078 (VDI, 1996) are considered in the multi-zone bus compartment model.

The simulation results of this system are compared in section 5.4 to the drop-in scenario with R-445A and an absorption AC system.

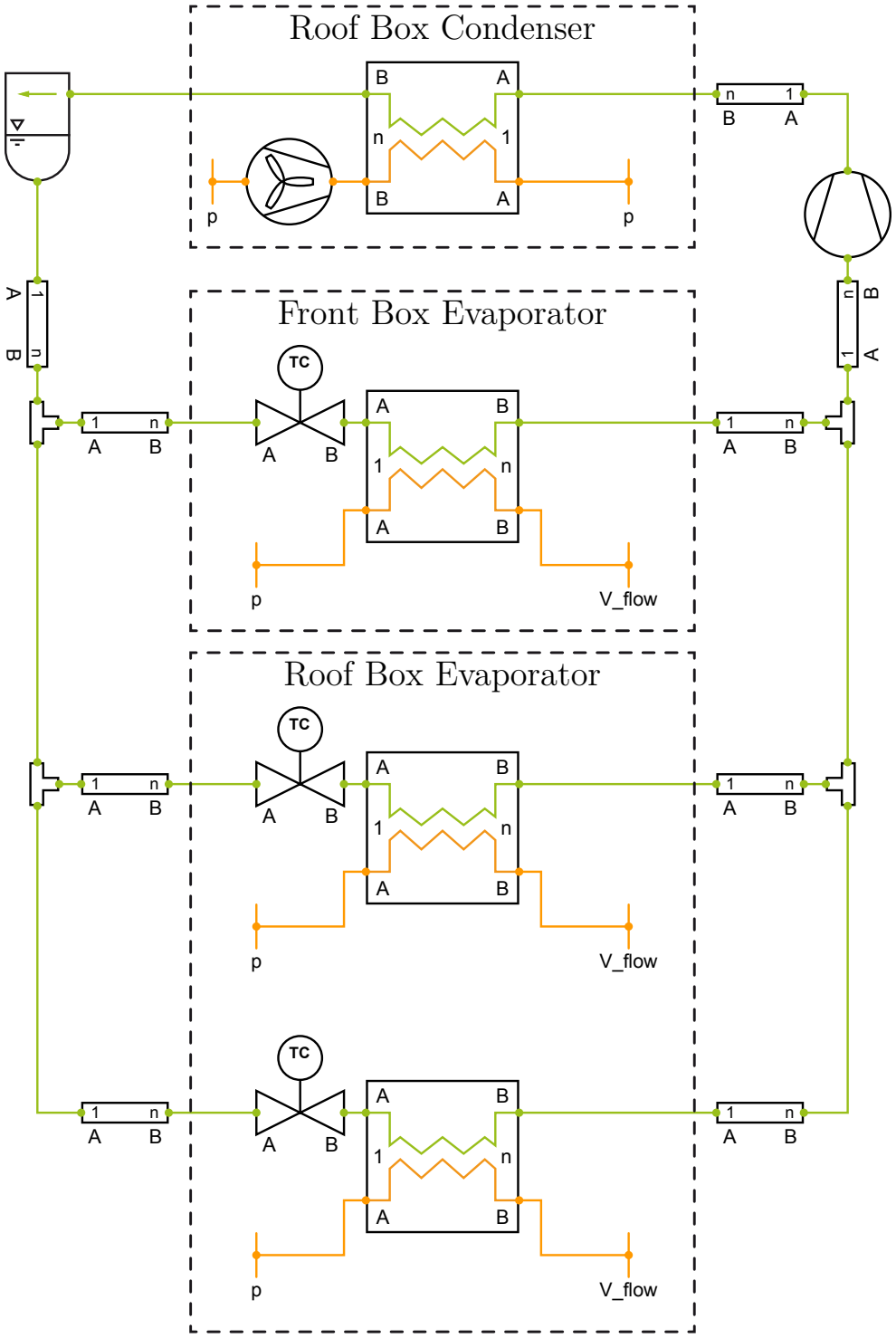

Figure 5.2.: Air conditioning system model with condenser and front box evaporator, thermostatic expansion valves, and roof box evaporators. The compressor is switched off depending on the cabin temperature.

5.2. Alternative Air Conditioning System with the Blend R-445A

The European Union (EU) has specified a global warming potential (GWP) limit of 150 for refrigerants used in mobile air conditioning (MAC) systems. One of the possible replacements for the widespread R-134a, which has a GWP of about 1400, is the refrigerant blend R-445A. The GWP for this blend is about 135, that is less than the regulatory limit set by the European Union (EU). It is considered non-flammable (Transport & handling - MSDS), non-toxic, affordable and available (L'Huillier and Peral, 2011; Peral-Antunez, 2012).

R-445A is a ternary mixture composed of (% by mass):

- 85% R-1234ze(E),
- 9% R-134a,
- 6% R-744/CO_2.

REFPROP version 9 (Lemmon et al., 2010) was used to calculate the thermophysical properties, but the binary interaction parameters were altered. Multiparameter EoS for the Helmholtz potential are available for all pure substances (McLinden et al., 2010; Tillner-Roth and Baehr, 1994; Span and Wagner, 1996). The binary interaction parameter for the subsystem CO_2 - R-1234ze(E) was fitted by Eric Lemmon (NIST) and is based on molecular simulation (Raabe, 2013) using a new force field for fluoropropenes by Raabe (2012). The interaction parameter for the pair CO_2 - R-134a was fitted by Eric Lemmon based on experimental data (Duran-Valencia et al., 2002). The interaction parameters for the pair R-134a - R-1234ze(E) were estimated by REFPROP (Lemmon et al., 2010).

The refrigerant blend has a wide temperature glide, which affects the temperature distribution over the heat exchanger length, and the COP of an AC system. Due to the temperature glide, a counterflow heat exchanger is better from a thermodynamic point of view because the temperature difference between air and refrigerant is more uniform (see figure 5.3). The average pressure levels in a thermodynamic cycle are slightly higher than in an R-134a cycle.

Based on the extension to the bicubic spline interpolation algorithm in section 2.5, the blend can be evaluated at a constant composition more conveniently and it can be used for transient system simulation.

In figure 5.3 the temperature distribution of R-134a and R-445A over the front box evaporator length is depicted in a steady state of the system. The AC system model

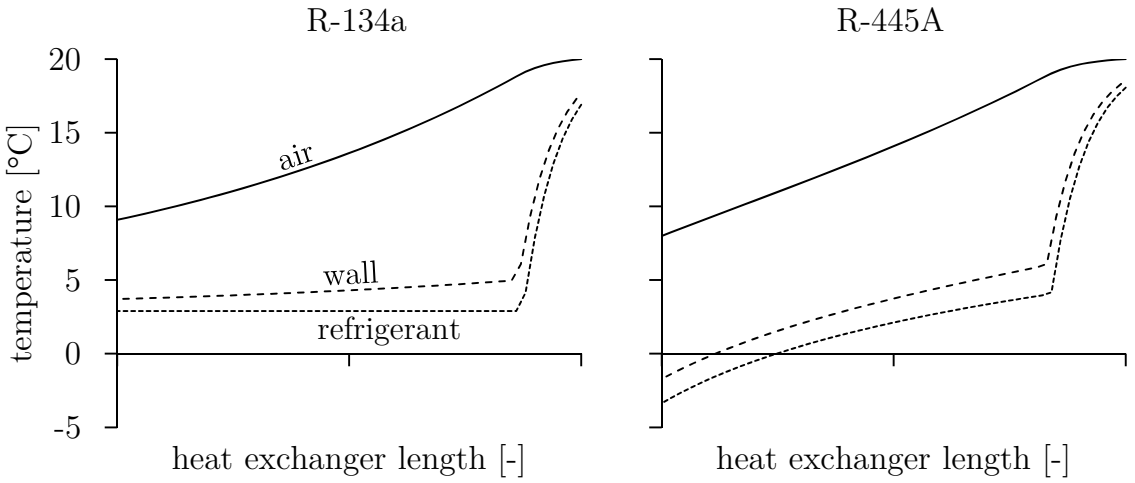

Figure 5.3.: Steady state temperature distribution over the front box evaporator length at the same cooling capacity. The average temperature difference from the refrigerant to the air is equal, but due to the temperature glide the inlet temperature of R-445A is significantly lower.

presented above was used with an increased number of control volumes in the front box evaporator. The distributions are plotted for the same front box evaporator cooling capacity and the superheating, so the average temperature difference to the air is the same (assuming the same heat transfer coefficient). Due to the temperature glide in the two-phase region, the inlet temperature of R-445A is below 0 °C. Depending on the pressure levels, system state and cooling capacity, this may cause ice formation. A pressure drop in the evaporator causes a reduction of the temperature difference from the inlet to the outlet, as mentioned by L'Huillier and Peral (2011). In fact, it is possible to increase the pressure drop on purpose, so that the evaporation temperature of the blend is constant.

In figure 5.4 a typical system state for the R-134a AC system and the R-445A AC system are shown in a p-h-diagram for the same cooling capacity. In many system states the high pressure level of the R-445A system increases by about 2 bar compared to the reference R-134a system. The low pressure increases slightly. The compressor outlet temperature, which is relevant for the compressor lifetime, usually increases by 5-10°C.

The conventional city bus R-134a AC system model mentioned above is used for transient evaluation of the R-445A drop-in scenario on a driving cycle by Dreyer (1975). The same models, compressor efficiencies and heat transfer coefficients are used. Only the thermophysical property model was replaced. Additionally, the influence of selective leakage on the AC system performance is discussed. The simulation results are compared in section 5.4.

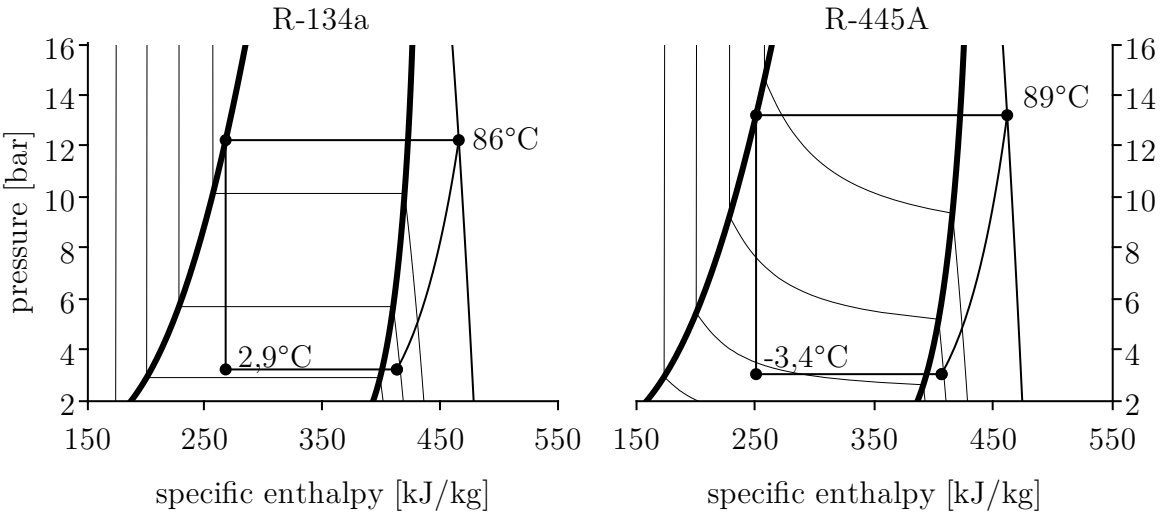

Figure 5.4.: Typical state of a R-445A system compared to a R-134a system.

5.3. Alternative Air Conditioning System based on Absorption Refrigeration

The concept of absorption refrigeration for mobile applications with ammonia-water mixture as refrigerant has been examined and prototyped repeatedly in recent decades. Fernández-Seara et al. (1998) examined an absorption refrigeration plant in trawler chiller fishing vessels. The high amount of available exhaust heat at constant temperature level is an ideal field of application. Manzela et al. (2010) and Horuz (1998) carried out experimental studies on exhaust heat recovery systems for automotive application. Both agree that exhaust heat is a potential power source. Horuz (1998) suggests more detailed studies on the fluctuations in cooling capacity due to variations in vehicle speed. Köhler et al. (1997) designed, built and tested a prototype of an absorption refrigeration system for trucks. The prototype has not been examined under transient system states.

The absorption system investigated in this section operates under highly dynamic boundary conditions as would occur in typical usage scenarios of a city bus. The working pair is ammonia-water with ammonia as refrigerant. The goal is to examine the basic behaviour of the system under dynamic boundary conditions and to illustrate what type of simulation is enabled by the fluid property calculation methods described in chapter 3.

In figure 5.5 the model of the absorption refrigeration system is shown. It is based on a system model developed for the conference contribution Somdalen et al. (2012) (although only part of the oral presentation) on the refrigeration system described by

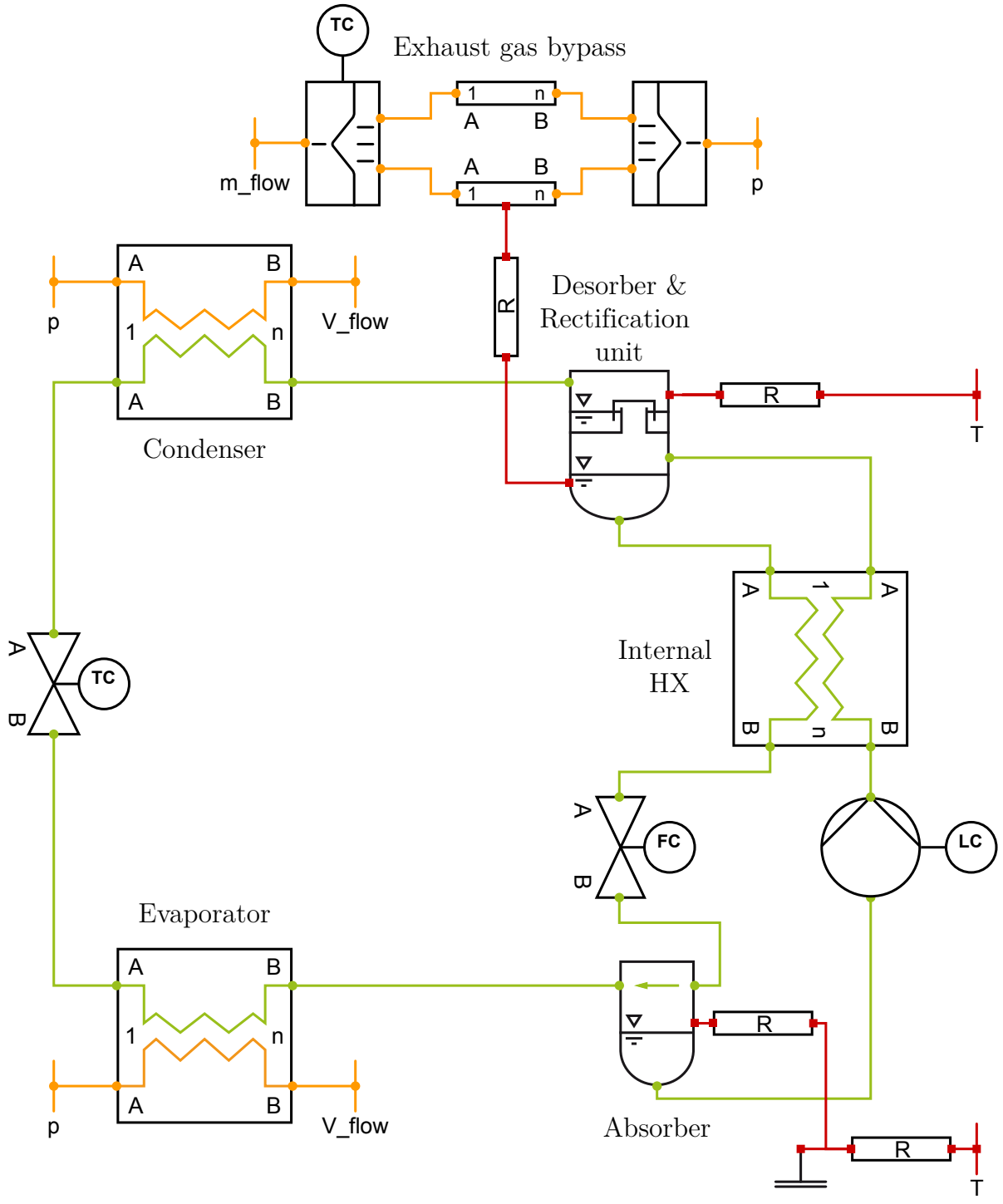

Figure 5.5.: TIL model representing an absorption system: condenser and evaporator on the left, solution cycle on the right. Subcooling at the condenser is controlled by the refrigerant expansion valve opening, the mass flow ratio controlled by the solution expansion valve opening, the filling level controlled by the solution pump mass flow rate. The compartment temperature controlled by the system performance using an exhaust gas bypass. The compartment model is connected to the evaporator.

Köhler et al. (1997). A few adaptations had to be made to the system to be used for air conditioning:

- the temperature level of the cabin is higher than the cold room temperature of a truck
- the exhaust gas temperature is significantly reduced since the average momentum and engine speed of the city bus is lower
- the internal heat exchangers were reconfigured to a simple one-stage cycle (Ziegler, 1999, page 192)
- the evaporator and condenser models of the R-134a system are used
- increased ammonia mass fraction

The absorber is modelled as a single control volume on the fluid side with a volume of 10 litres. It is cooled with air and a thermodynamic equilibrium is assumed. It is a separator model that could be used in an AC system to represent a receiver with ideal separation of liquid and vapour phase. Thus, the solution at the absorber outlet is saturated. The thermal capacity of the component is modelled as a thermal capacitor with 22 kg of steel. The heat transfer coefficient of the absorber is set to 7500 WK^{-1} on the air side and to 12000 WK^{-1} on the refrigerant side, which is a marginally higher heat transfer on the air side compared to the evaporator used.

The exhaust gas heat exchanger is placed behind the turbo compressor of the engine. The exhaust gas temperature and mass flow rate are obtained from a map with experimental data (appendix E on page 126). With the independent variable engine speed rpm and engine momentum M, the map describes the gas temperature T and mass flow rate $\dot{m}$ using nested spline interpolation. A bypass is used to limit the exhaust gas power provided to the absorption system.

The desorber and rectification-unit are represented by two separator models, thus one ideally stirred control volume for each of them. One corresponds to the desorber, which is heated with exhaust gas and has a volume of 10 litres. The other corresponds to the rectification unit, which is cooled with ambient air and has a volume of 1 litre. Both control volumes are based on a separator model with ideal phase separation. The rectification unit feeds back condensed liquid to the desorber in order to keep a constant filling level.

The heat transfer coefficient on the refrigerant side of the desorber is 12000 WK^{-1} and 7500 WK^{-1} on air side. The component weight is 30 kg. The heat transfer coefficient from the rectification unit to the ambient air is 20 WK^{-1}.

The absorption system has only one evaporator. This evaporator is twice as large as

one of the roof evaporators of the reference R-134a AC system. The condenser is the same as applied in the reference R-134a system. The front box evaporator is missing in the absorption system, so the air side evaporation heat transfer area is smaller.

To realise a transient system model, the following control strategy was developed:

- the expansion valve between condenser and evaporator is used to control the subcooling of the condenser
- the solution expansion valve is used to control the mass flow rate ratio leaving the desorber/rectification unit model
- the solution pump is used to control the filling level in the absorber
- the exhaust gas bypass flap is used to control the output cooling capacity

The basic idea is to control the cooling capacity in partial load using the heat source power. The exhaust gas temperature has a direct influence on the available heat that drives the absorption system. The maximum power against the backdrop of transient operation is the point of interest. The COP could be optimised according to Albers et al. (2008).

The model suggests that the real system reacts very quickly if the gain of condenser subcooling controller is high. If the exhaust gas temperature and power decreases, the subcooling at the condenser decreases at the same time. Thus, often the condenser expansion valve is closed completely by a controller with high gain in order to keep constant subcooling. Since zero mass flow rate leads to a cooling capacity of 0 W, these system states should be avoided. If the subcooling controller gain is increased, the system reacts more slowly and the cooling capacity is smoothed.

The evaporator turned out to be storing refrigerant at low exhaust gas powers. If the exhaust gas power is increased with a “filled” evaporator, the refrigerant evaporates and causes a high peak in the cooling capacity. This effect should be validated and further examined by measurement.

The system model is an optimistic scenario. The geometries and heat transfer coefficients of absorber and desorber were approximated by the conventional bus evaporators, as they have not yet been designed. In reality, the mass transfer in the absorber and desorber will not reach thermodynamic equilibrium. To describe the mass transfer in more detail, the two phases could be balanced separately using a two-fluid model (Städtke, 2006, chapter 3 or Epple et al., 2009, page 119).

5.4. Evaluation of the Alternative Air Conditioning Systems

In this section, transient simulation results of the alternative AC systems presented above are compared to the performance of the conventional R-134a AC system.

The ambient temperature and humidity was set to 25 °C and 55%. This decision was made based on Strupp et al. (2009) where climatic conditions (like temperature, humidity and solar radiation) mapped over space and time were related to an average automotive usage profile. If a similar usage profile for buses is assumed, the selected ambient conditions represent a highly relevant scenario.

The roof box evaporators operate with a constant 40:60 mixture of fresh and recirculated air. The direct solar heat flux is set to 360 Wm^{-2} and the diffusive solar heat flux to 240 Wm^{-2}. The number of passengers is set at 28.

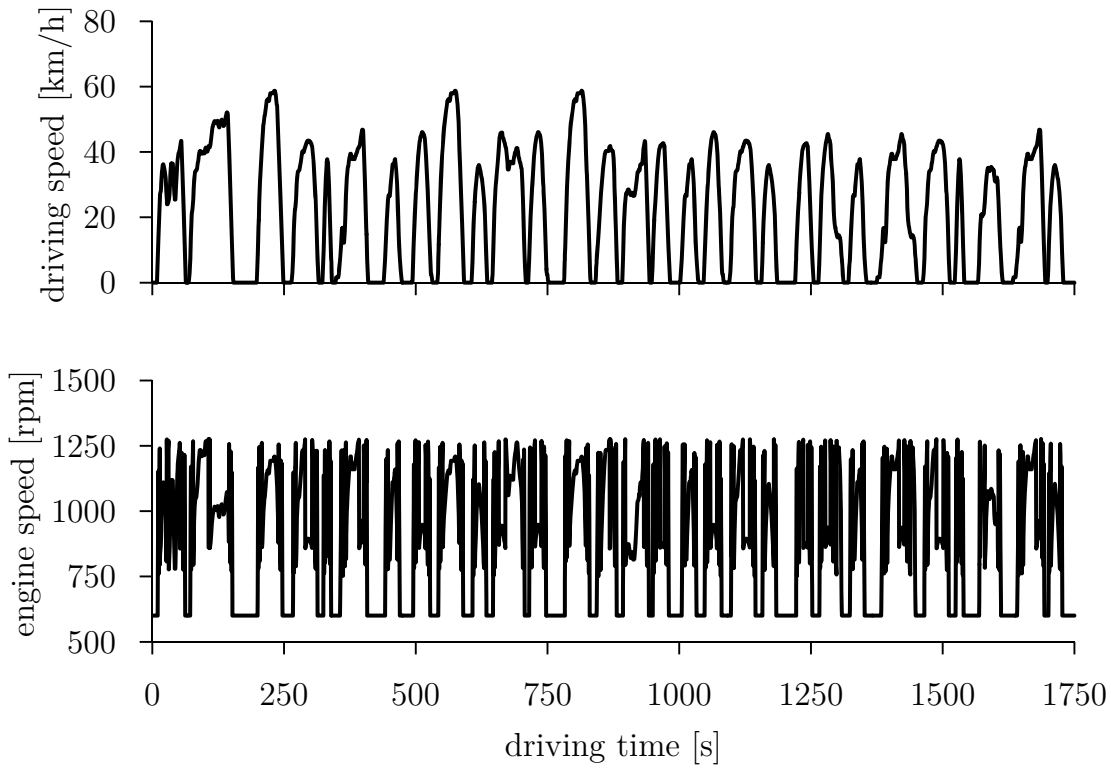

Figure 5.6.: Assumed driving cycle from Dreyer (1975), and engine speed calculated from Kossel et al. (2008), which are applied to the system models.

The AC system is evaluated on a driving cycle for a city bus published in Dreyer (1975) as illustrated in figure 5.6. The driving cycle is based on a survey of transport companies on the number of bus-stops, distances between them, travel speeds and intermediate stops caused by traffic. The engine speed was calculated based on the driving speed according to Kossel et al. (2008). Due to the dense acceleration and deceleration phases and the involved shifting of gears, the engine speed is more aggressive than the driving speed.

Alternative R-445A AC system compared to conventional R-134a AC system

In figure 5.7 the average cabin temperature (upper diagram) and the cooling capacity (lower diagram) are depicted. The average cabin temperature of both the R-134a system and the R-445A system remains within the ambient temperature and the lower compressor shut down temperature. Each time the cabin temperature falls below 21 °C, the compressor is turned off until the cabin temperature rises above 24 °C. Both systems operate at part load, and have a maximum cooling capacity of ca. 30 kW. The cooling capacity of both systems is sufficient and in the same order of magnitude.

The frequency of compressor shut down for the R-445A system is less than that for the R-134a system. The cooling capacity of the R-445A system is lower, which means it takes more time to cool to 21 °C. Here the compressor was only shut down twice.

The results reveal one possible problem for a drop-in solution of a refrigerant with high temperature glide: the thermostatic expansion valves provide for constant superheating behind the evaporators and hence the temperature glide causes lower evaporator inlet temperatures. Here the refrigerant temperature at the evaporator inlet is below 0 °C, resulting in a high risk of ice formation in the heat exchangers.

In figure 5.8 the inlet refrigerant temperature for the front box evaporator is plotted. The inlet temperature in a normal operating state is below 0 °C. In figure 5.3 an exemplary temperature distribution in the evaporator in steady state is shown. A possible counter measure to avoid ice formation could be to increase the pressure drop in the evaporators and decrease the pressure drop in the thermostatic expansion valve. An intermediate expansion in the evaporator is also a possible solution.

The average COP (cumulated evaporator heat flow rates divided by cumulated compressor power) of the R-445A AC system (drop-in solution) is about 92% of the R-134a AC system COP.

Figure 5.9 shows the simulation speed on an Intel Core i7-2620M @ 2.7GHz (real time plotted over simulated time). The multi-zone bus compartment model and the multi

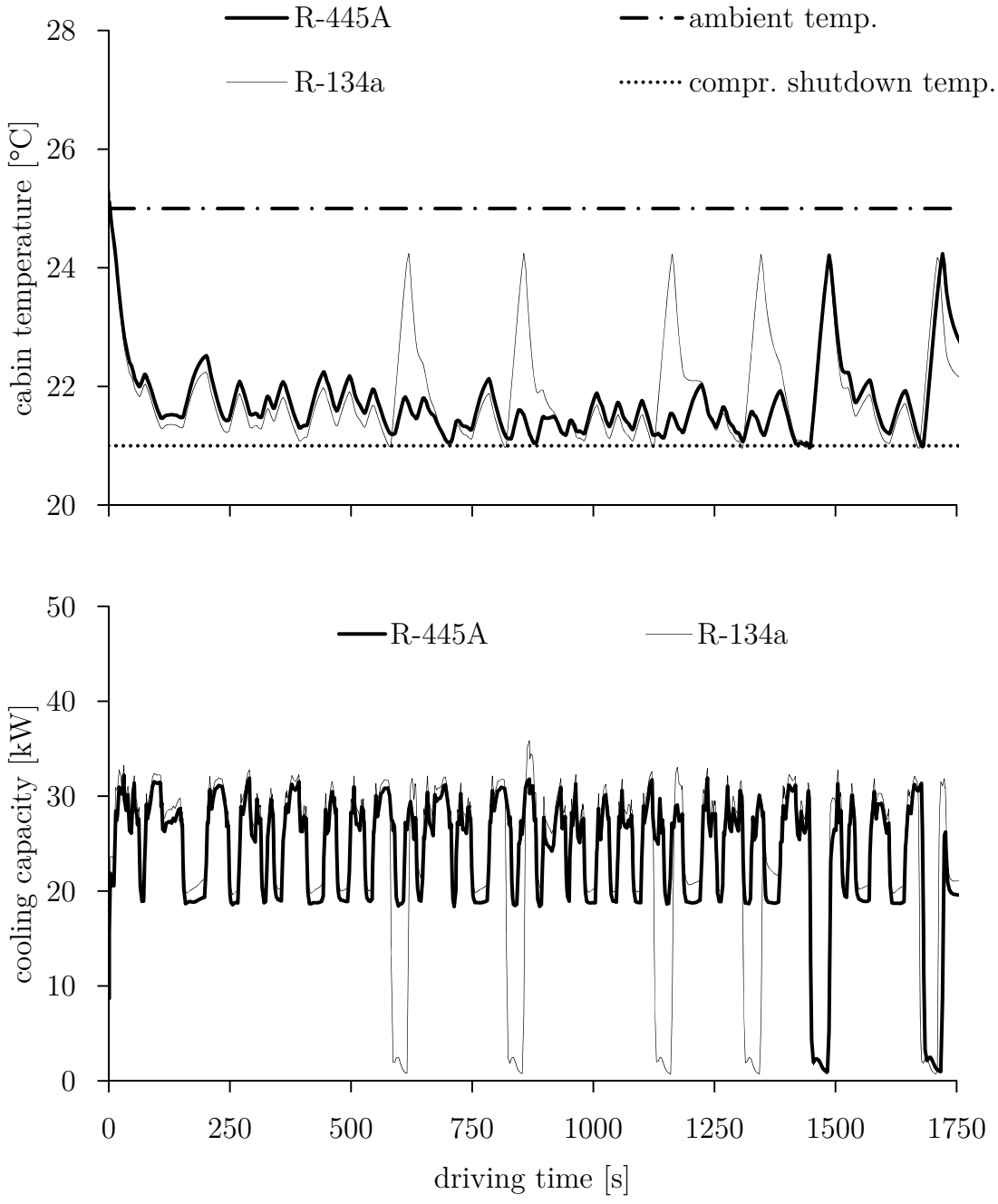

Figure 5.7.: Cooling capacities and average cabin temperature of R-445A drop-in compared to reference R-134a AC system. Cooling capacity of the reference AC system is slightly higher.

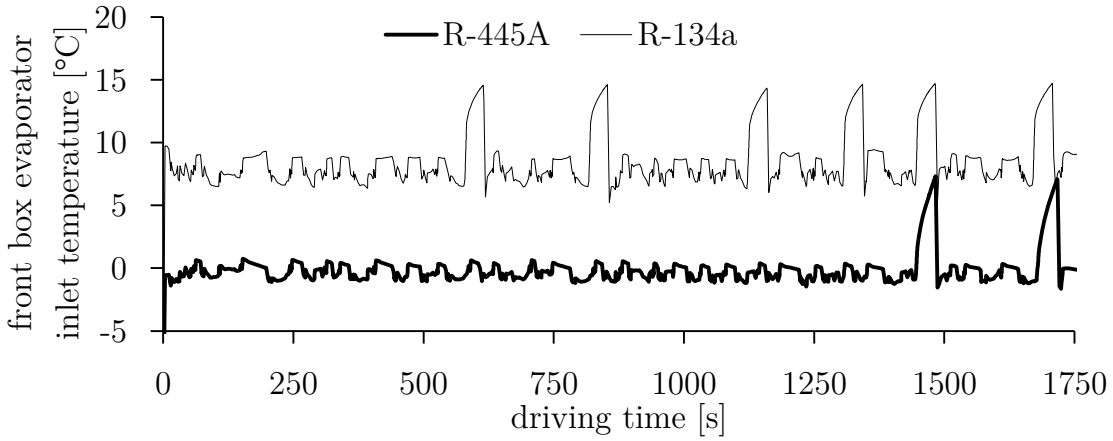

Figure 5.8.: Front box evaporator inlet temperature of R-445A compared to R-134a. The temperature glide causes lower temperatures at the inlet of the evaporators and might cause ice formation in this setup.

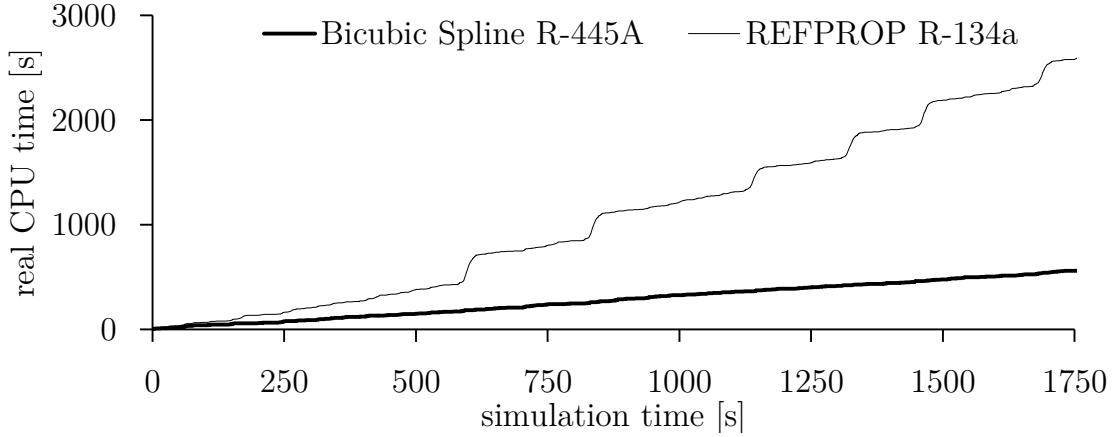

Figure 5.9.: Real time plotted over simulated time for the conventional R-134a system using thermodynamic properties of REFPROP, and the R-445A system using bicubic spline interpolation for property calculation. When the compressor is turned off, the step size of the DAE-solver is reduced due to numerical inaccuracies of REFPROP R-134a.

evaporator AC system model are simulated in one model. The simulations were performed with Dymola (2013), the relative and absolute tolerance of the DAE-solver DASSL was set to 10^{-4}. The DAE-system of the AC system is described by 193 continuous time state variables, only two of which are pressures. The simulation speed is about 3 times faster than real time. The solver step size is reduced each time the compressor is turned off in the conventional R-134a AC system. This is caused by minor numerical inaccuracies in REFPROP. The simulation based on bicubic spline interpolation is not hampered by similar effects.

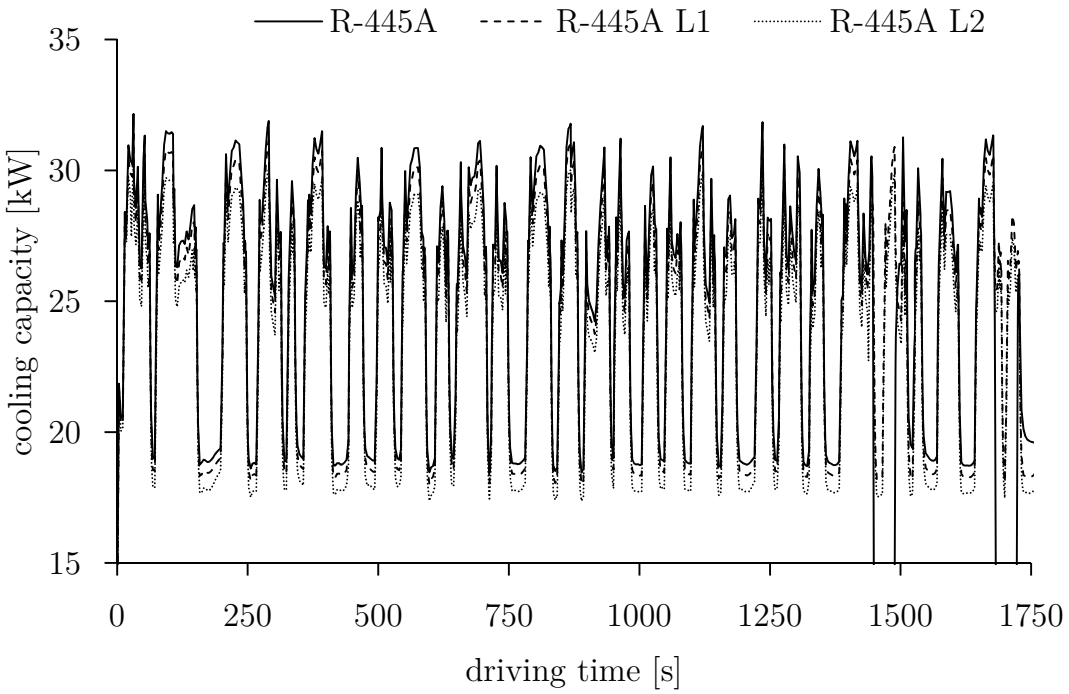

Figure 5.10.: Cooling capacity simulated for three different R-445A mixture compositions. Selective leakage causes a cooling capacity reduction of approximately 6% from the initial composition of R-445A to R-445A L2 with only 2% R-744 in the AC system.

Selective leakage of R-445A is discussed in Peral-Antunez (2012), where a figure with temperature dependent leakage rates of the mixture components is presented. The leakage rate of R-744 is about twice as high as the leakage rate of R-1234ze(E); R-134a leaks slightly slower than R-1234ze(E). Based on the leakage rate ratio in this presentation, two possible mixture compositions were estimated, one with 4% (R-445A L1) and one with 2% (R-445A L2) of R-744 left in the mixture (see table 5.1). The city bus AC system was simulated with these three mixture compositions; the results are

Table 5.1.: Compositions by mass at different stages of selective leakage.

Name	R-1234ze(E)	R-134a	R-744
R-445A	0.85	0.09	0.06
R-445A L1	0.8736	0.0864	0.04
R-445A L2	0.8973	0.0827	0.02

depicted in figure 5.10. The cooling capacity is reduced by approximately 5.5% from R-445A to R-445A L2, the COP is increased by 12%. The influence of CO_2 on the blend's properties is high.

Absorption AC System compared to conventional R-134a AC system

In figure 5.11 the average cabin temperature of the absorption system is compared to the reference R-134a AC system. The cooling capacity of the absorption AC system is only available if the engine speed is high enough. About 15 kW cooling capacity is available in many intermediate states. At engine idling speed often no cooling capacity can be provided.

The absorption AC system is capable of keeping the average cabin temperature close to the ambient temperature of 25 °C, but the cooling capacity is at its maximum. The exhaust gas bypass is not used.

In figure 5.12 the exhaust gas temperature is shown. The temperature is below 100 °C and therefore possibly below the acid dew point. The desorber temperature could be increased to avoid corrosion.

The average COP (cumulated evaporator heat flow rate divided by cumulated exhaust gas heat flow rate) is at 0.68. Often the exhaust gas heat flow rate is lower than the cooling capacity of the reference R-134a AC system. This applies in particular at engine idling speed. To provide a similar level of comfort, a significantly higher COP of the absorption system or a higher exhaust gas heat flow rate would be required.

5.5. Conclusion and Summary

In this chapter, models and simulation results were shown applying the techniques presented in the preceding chapters.

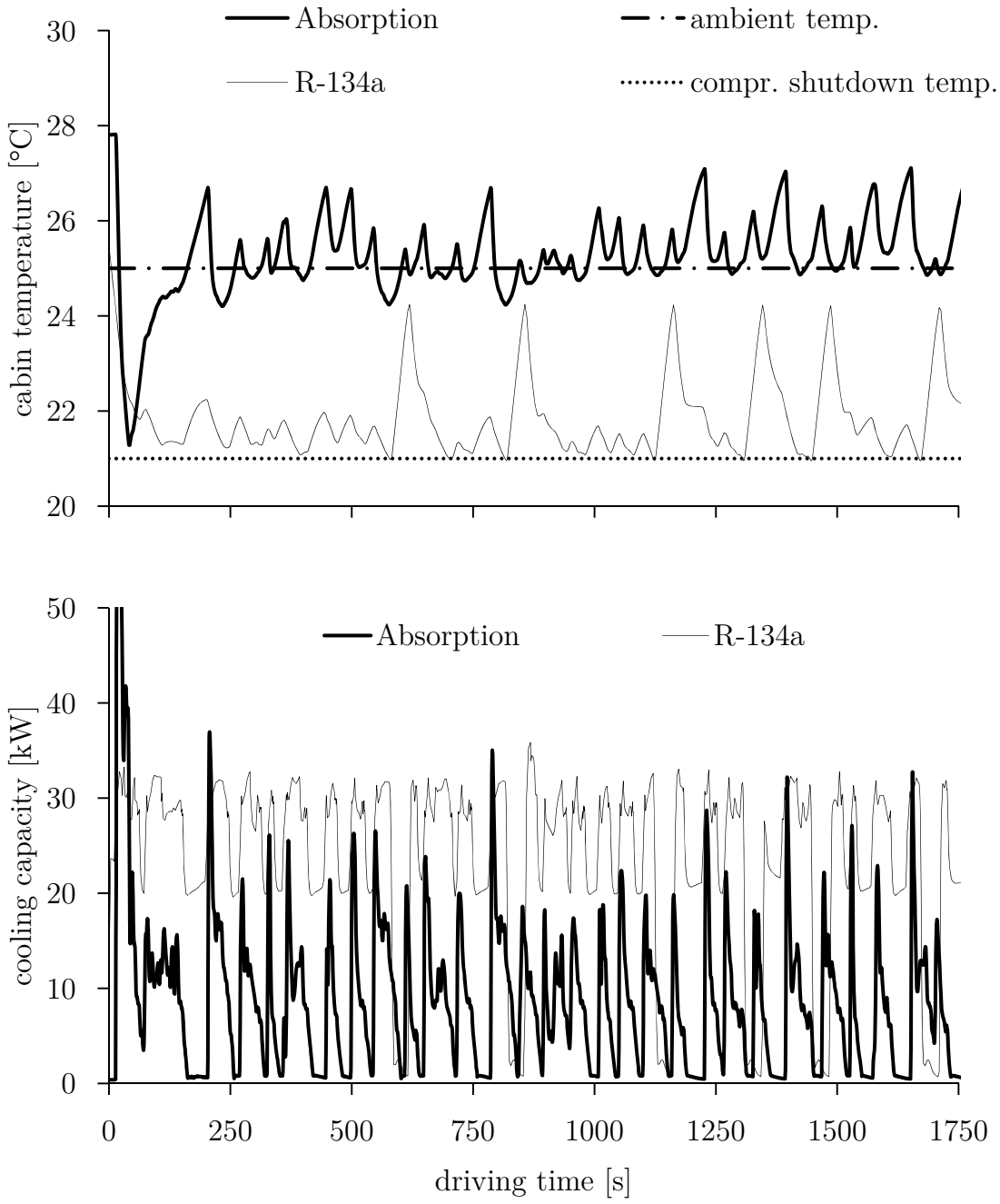

Figure 5.11.: Cooling capacities and average cabin temperature of ammonia-water absorption AC system compared to reference R-134a AC system. Cooling capacity of the reference AC system is significantly higher, even at engine idling speed.

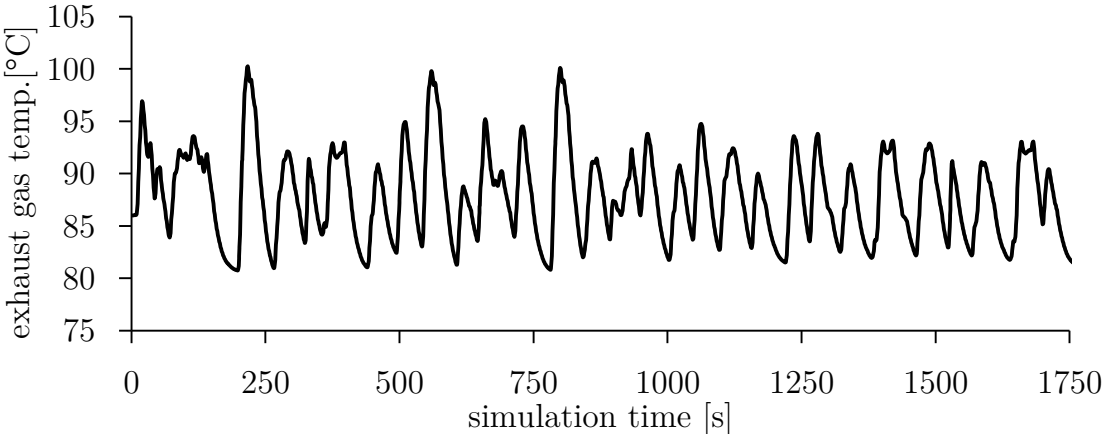

Figure 5.12.: Exhaust gas temperature behind absorption AC system. The temperature is below 100 °C and therefore corrosion must be further assessed.

The table-based calculation methods discussed in chapter 2 (bicubic spline interpolation section 2.3.2) are used to calculate the properties of the zeotropic blend R-445A and enable an evaluation of a drop-in solution in an R-134a AC system for a technically relevant scenario. The COP of the R-445A system is slightly lower, but in the same order of magnitude. Possible issues with the drop-in solution are evaporator inlet temperature $\leq 0\,°C$ and an increase in the pressure levels.

The absorption system applied the calculation algorithms presented in chapter 3. The two-phase region of the mixture ammonia-water was calculated, saved in a data table and interpolated using splines. The strategy to control the cooling capacity of the system using the exhaust gas (Albers et al., 2008) necessarily links cooling capacity to engine speed and momentum. The average COP of the absorption system model is higher than the measured data by Köhler et al. (1997), but the overall system is undersized. It cannot provide the same level of comfort as the R-134a AC system.

All models are based on the equations derived in chapter 4. The compressor speed varies proportionately to the engine speed and occasionally turned off to control the cooling capacity. The limiter effectively prevents the occurrences of the derived singularity and enables robust simulation of multi evaporator AC systems under highly transient boundary conditions.

Chapter 6.

Conclusion and Outlook

6.1. Conclusion

The main goal of this thesis was to contribute to the field of numerical efficient modelling of thermodynamic systems. Some fields of application such as HIL, RCP or NPMC, require a fast and precise calculation of thermophysical properties and numerically efficient system models. Transient simulations in general also benefit from efficient property calculation since more results can be obtained in the same amount of time.

In this thesis, four table-based calculation methods for the thermophysical properties of pure fluids were presented, implemented and compared. A new general method for the description of the two-phase region of a binary mixture was also presented. A singularity in a simplified finite volume method was located and eliminated. Finally the methods and models were applied to evaluate alternative air conditioning systems for a city bus.

It was shown by means of profiling of transient simulations that the calculation of thermophysical properties contributes significantly to the total calculation effort of a transient simulation. Not only is calculation speed of the fluid properties important but also the smoothness of the fluid property surfaces, which influences the DAE-solver of the system model. An overview of published interpolation techniques for the thermophysical properties of pure fluids was provided. Many different methods have been developed in recent decades to provide thermophysical properties in a more convenient and more efficient way. To the best knowledge of the author, this thesis is the first comparison of thermophysical property calculation methods accounting for all relevant aspects in terms of transient simulation of thermodynamic cycles. Four interpolation algorithms were discussed in detail, implemented, and compared: linear interpolation, bicubic spline interpolation, bicubic interpolation of an equation of state and sets of curves. The new approach of a piecewise-defined fundamental equation of state $s(p, h)$

using bicubic interpolation is capable of providing thermopyhsical properties for transient simulation, but it should be used only in the one-phase region. Linear interpolation is fast, but requires significantly more data than the others and hampers the DAE-solving procedure. The new set of curves interpolation algorithm is an appropriate method for real-time simulation, but it requires a manual fitting procedure, so it is not as flexible as the others. In contrast, the bicubic spline interpolation of each property fulfils all requirements. It performs well with a comparably small amount of data, automatic table generation for several fluids is possible, it is fast and does not affect the DAE-solving procedure.

The vapour-liquid equilibrium calculation of a mixture is often calculated with an iterative algorithm. The solving the vapour-liquid equilibrium of multiparameter equations of state is particularly complicated due to the non-physical behaviour of these equations in the two-phase region. Success of the iterative algorithms cannot be guaranteed. Simple fit equations for selected saturated properties and selected mixtures can be found in the literature. Their range of validity and precision is limited. Additionally, they apply only a particular equation of state. To overcome the drawbacks of simple fit equations or iterative vapour-liquid equilibrium algorithms, a general method is presented in this thesis to describe the two-phase region of a binary mixture. This method is based on cubic spline interpolation and does not require any fitting procedure. Data tables can be generated automatically. This new method enables a fail-safe and fast provision of vapour-liquid equilibria data for binary mixtures that have a shape of the two-phase region similar to that of ammonia-water.

The transient system simulation of thermodynamic cycles requires the fast and robust modelling of heat exchangers and tubes. In this thesis a simplified finite volume method with ideally stirred volumes and simplified momentum balance was analysed in detail. A singularity in the algebraic relationship between control volumes, which to the best knowledge of the author has not yet been discussed in the literature, was identified and located. Additionally, a new method to prevent the singularity was presented that can be implemented in an object-oriented manner. The presented simplified finite volume method should ideally be used for the simulation of vapour compression cycles since the method to avoid the derived singularity is more likely to affect the results of power cycles. The presented models enable a numerically efficient simulation of the thermal behaviour of vapour compression cycles and the new approach to prevent the singularity avoids a simulation failure.

Finally, the presented methods and models were applied in an investigation of alternative air conditioning systems for a city bus. The reference system operated with the refrigerant R-134a. The first investigated alternative was an R-445A drop-in scenario. The thermophysical properties of the zeotropic ternary mixture R-445A were obtained from recently published mixing parameters implemented in REFPROP. The properties were described by bicubic spline interpolation of each property. The air conditioning

system was evaluated on the basis of a highly transient random driving cycle and compared to the R-134a reference air conditioning system. A slight increase in pressure levels and a slight decrease in COP and maximum cooling capacity were predicted. Additionally, partial frosting of the evaporators was identified as a possible issue for the drop-in scenario. The second investigated alternative was a mobile one-stage absorption air conditioning system. The thermodynamic properties were calculated from the mixture multiparameter equation of state by Tillner-Roth and Friend (1998). To enable the transient system evaluation on the same random driving cycle, the three-dimensional two-phase region from 1 to 100 bar was described by cubic spline interpolation. The simulation showed that available exhaust gas power is not high enough to provide the same level of comfort as the one-stage absorption system. The subcooling control at the condenser has an impact on transient behaviour. If necessary, the cooling capacity of an absorption system can be controlled to react quickly to the available exhaust heat. However, here a uniform cooling capacity is desired and therefore the proportional and integral gain of the PI-controller is set to a low value.

6.2. Outlook

The newly presented piecewise definition of the fundamental equation of state $s(p,h)$ with bicubic interpolation requires a further assessment of the interpolation methods. Two aspects that are worth investigating are the extrapolation into the two-phase region and the order of spline interpolation. The first increases the accuracy around the two-phase region, the latter increases the quality of the partial derivatives of the equation of state. The spline-based calculation of the two-phase region of mixtures has to date been limited to binary mixtures. Since this approach is based on nested 1D-spline interpolation, it can be extended to ternary mixtures by adding an additional layer of interpolation.

The local approach to prevent the singularity in the simplified finite volume method should be extended to enable the robust simulation of power cycles. A local approach should be found that can be implemented in an object-oriented manner and does not interfere as often as the one presented above. Perhaps even a new and more robust simplification of the finite volume method based on the mean density approach by Casella (2006) can be found.

The R-445A AC system could be adapted to the specific requirements of R-445A to enable a comparison between two optimised AC systems. The efficiency of the absorption system has not yet been optimised. New control parameters or a redesign of the cycle could increase the COP.

Nomenclature

Acronyms

ANFIS	Adaptive Neuro-Fuzzy Interference System
ANN	Artificial Neural Network
BDF	Backward Differentiation Formula
CCS	Carbon Capture and Storage
CFD	Computational Fluid Dynamics
COP	Coefficient Of Performance [-]
CV	Control Volume
DAE	Differential Algebraic Equation
DASSL	Differential Algebraic System Solver
EoS	Equation of State
EU	European Union
GWP	Global Warming Potential
HIL	Hardware-in-the-Loop
IAPWS	International Association for the Properties of Water and Steam
IF-97	Industrial Formulation 1997
IfT	Institut für Thermodynamik
MAC	Mobile Air Conditioning
MPC	Model Predictive Control
NIST	National Institute of Standards and Technology

NMPC	Non-linear Model Predictive Control
ODE	Ordinary Differential Equation
RCP	Rapid-Control-Prototyping
SAFT	Statistical Associating Fluid Theory
TIL	TLK-IfT-Library
TLK	Tegethoff Lemke Köhler
TTSE	Tabular Taylor Series Expansion
VLE	Vapour-Liquid Equilibrium
VLEFluid	Real fluid with a Vapour-Liquid Equilibrium

General Symbols

$\dot{m}$	Mass flow rate [$\mathrm{kg\,s^{-1}}$]
$\dot{Q}$	Heat flow rate [W]
A	Algebraic relation matrix [-]
A	Surface area [$\mathrm{m^2}$]
b	Right hand side vector of the algebraic relation [-]
c_p	Isobaric specific heat capacity [$\mathrm{J\,(kgK)^{-1}}$]
c_v	Isochoric specific heat capacity [$\mathrm{J\,(kgK)^{-1}}$]
c_{ij}	Coefficient of a polynomial [-]
f	Specific Helmholtz energy [$\mathrm{J\,kg^{-1}}$]
g	Specific Gibbs energy [$\mathrm{J\,kg^{-1}}$]
h	Specific enthalpy [$\mathrm{J\,(kg)^{-1}}$]
M	Engine momentum [Nm]
m	Mass [kg]
m	Number of steps in direction of x_1 [-]
n	Number of steps in direction of x_2 [-]
p	Pressure [Pa]

q	Vapour quality (mass basis)
q_0	Heat flow rate offset [W]
q_1	Heat flow rate per mass flow rate [$\mathrm{Ws\,kg^{-1}}$]
Re	Reynolds number [-]
rpm	Rotations per minute [$\mathrm{min^{-1}}$]
S	Objective function [-]
s	Specific entropy [$\mathrm{J\,(kgK)^{-1}}$]
T	Temperature [K]
u	Specific internal energy [$\mathrm{J\,kg^{-1}}$]
V	Volume [$\mathrm{m^{-1}}$]
v	Specific volume [$\mathrm{m^3\,kg^{-1}}$]
w	Speed of sound [$\mathrm{m\,s^{-3}}$]
x	Mole fraction vector of liquid [-]
x	Vector of unknowns [-]
y	Mole fraction vector of vapour [-]
z	Mole fraction vector [-]

Greek Symbols

α	Heat transfer coefficient [$\mathrm{W\,K^{-1}m^{-2}}$]
β	Isobaric thermal expansion coefficient [$\mathrm{K^{-1}}$]
β	Vapour quality (mole basis) [-]
η	Dynamic viscosity [Pa s]
γ	Term that may cause singularity [-]
κ	Isothermal compressibility [$\mathrm{Pa^{-1}}$]
λ	Thermal conductivity [$\mathrm{W\,(Km)^{-1}}$]
μ	Chemical potential [$\mathrm{J\,kg^{-1}}$]
ν	Kinematic viscosity [$\mathrm{m^2\,s^{-1}}$]

ψ	Secondary term in limiter derivation [-]
Θ	Dimensionless temperature [-]
φ	Fugacity factor [-]
ϱ	Density [$\mathrm{kg\,m^{-3}}$]
ξ	Mass fraction vector [-]

Subscripts

bub	Bubble point
dew	Dew point
inverse	Inverse function
limit	Minimal property, that is allowed to enter a control volume
liq	Liquid
lower	Closest lower grid point
max	Maximum
min	Minimum
modified	Modified property (limiter approach)
outflow	Property of a fluid if it flows out of a control volume
Q	Related to the linear heat transfer model
reference	Reference state for $\frac{dp}{dt}$-approach
state	Pseudo state variable
upper	Closest higher grid point
vap	Vapour

References

Albers, J., Kuhn, A., Petersen, S., and Ziegler, F. (2008). Control of absorption chillers by insight: the characteristic equation. *Czasopismo Techniczne. Mechanika*, 105(5-M):3–12.

Andresen, T. (2009). *Mathematical Modeling of CO2 Based Heat Pumping Systems: New Developments for Simulation Tools to Aid the Design of Systems for Non-residential Buildings*. Doktoravhandlinger ved NTNU. Norwegian University of Science and Technology, Faculty of Engineering Science and Technology, Department of Energy and Process Engineering.

Antoine, C. (1888). Tensions des vapeurs: nouvelle relation entre les tensions et les temperatures. *Comptes Rendus des Séances de l'Académie des Sciences. Paris.*, 101:681–684, 778–780, 836–837.

ASPEN Plus (2013). ASPEN Plus Manual - About Physical Property Methods and Models. Aspen Technology, Inc., Burlington, Massachusetts 01803 USA.

Baehr, H. (1998). Thermodynamische fundamentalgleichungen und charakteristische funtionen. *Forschung im Ingenieurwesen*, 64(1-2):35–43.

Baehr, H. D. (1971). Kanonische Zustandsgleichungen und ihre Bedeutung für die technischen Anwendungen der Thermodynamik. *Kältetechnik-Klimatisierung*, 3(23):78–81.

Bejan, A. (2006). *Advanced Engineering Thermodynamics*. Wiley, New York, third edition.

Bender, E. (1970). Eine Zustandsgleichung für dissoziierte Luft mit Entropie, Enthalpie und Druck als Variablen. *Zeitschrift für Flugwissenschaften*, 18(1):1–7.

Bonilla, J., Yebra, L., and Dormido, S. (2012). Chattering in dynamic mathematical two-phase flow models. *Applied Mathematical Modelling*, 36(5):2067 – 2081.

Bonilla, J., Yebra, L. J., and Dormido, S. (2010). Mean Densities in Dynamic Mathematical Two-phase Flow Model. *CMES*, 67(1):13–37.

Brent, R. P. (1973). *Algorithms for minimization without derivatives*. Dover books on mathematics. Dover Publications, Incorporated.

Bronštejn, I. N., Semendjaev, K. A., Grosche, G., and Zeidler, E. (2003). *Teubner-Taschenbuch der Mathematik. [1]*. Number Bd. 1 in Teubner-Taschenbuch der Mathematik. Teubner.

Brunnemann, J., Gottelt, F., Wellner, K., Renz, A., Thüring, A., Roeder, V., Hasenbein, C., Schulze, C., Schmitz, G., and Eiden, J. (2012). Status of ClaRaCCS: Modelling and Simulation of Coal-Fired Power Plants with CO2 Capture. In *Proceedings of the 9th International Modelica Conference*, München.

Casella, F. (2006). Object-Oriented Modelling of Two-Phase Fluid Flows by the Finite Volume Method. In *Proceedings 5th MATHMOD Vienna*.

Casella, F. and Leva, A. (2006). Modelling of thermo-hydraulic power generation processes using Modelica. *Mathematical and Computer Modelling of Dynamical Systems*, 12(1):19–33.

Cellier, F. (1991). *Continuous System Modeling*. Springer.

Cellier, F. and Kofman, E. (2006). *Continuous System Simulation*. Springer.

Chapman, W. G., Gubbins, K. E., Jackson, G., and Radosz, M. (1990). New reference equation of state for associating liquids. *Industrial and Engineering Chemistry Research*, 29(8):1709–1721.

Clauss, C., Elmqvist, H., Mattsson, S., Otter, M., and Schwarz, P. (2004). Mixed-Domain Modeling in Modelica. In Villar, E. and Mermet, J., editors, *System Specification and Design Languages*, pages 29–40. Springer US.

Conde-Petit, M. R. (2006). Thermophysical Properties of {NH3+H2O} Mixtures for the Industrial Design of Absorption Refrigeration Equipment. M. Conde Engineering.

Corberán, J., Gonzálvez, J., and Fuentes, D. (2005). Calculation of refrigerant properties by linear interpolation of bidimensional meshes. In *IIR International Conference on Commercial Refrigeration/ Thermophysical Properties and Transfer Processes of Refrigerants*, italy.

de Boor, C. (1962). Bicubic spline interpolation. *Journal of Mathematics and Physics*, 41(3):212–218.

de Boor, C. (2001). *A Practical Guide to Splines*. Number Bd. 27 in Applied Mathematical Sciences. Springer.

Dehli, M. (1975). *Über kanonische Zustandsgleichungen und ihre Anwendungsmöglichkeiten in der Technik*, volume 570 of *VDI-Forschungsheft*. VDI Verlag.

Ding, G., Han, W., Zhao, D., and Wu, Z. (2009). Extension of the implicit curve-fitting method for fast calculation of thermodynamic properties of subcooled refrigerants. *HVAC&R Research*, 15(5):875–888.

Dohrn, R. (1994). *Berechnung von Phasengleichgewichten*. Fundamentals and Advances in the Engineering Sciences.

Dreyer, W. (1975). *Stochastischer Fahrzyklus für Stadt-Linienomnibusse*. Braunschweig.

Duran-Valencia, C., Pointurier, G., Valtz, A., Guilbot, P., and Richon, D. (2002). Vapor-Liquid Equilibrium (VLE) Data for the Carbon Dioxide (CO2) + 1,1,1,2-Tetrafluoroethane (R134a) System at Temperatures from 252.95 K to 292.95 K and Pressures up to 2 MPa. *Journal of Chemical and Engineering Data*, 47(1):59–61.

Dymola (2013). Dymola 2013 FD01. Dassault Systemes, Lund, Sweden (Dynasim).

Elmqvist, H., Tummescheit, H., and Otter, M. (2003). Object-oriented modeling of thermo-fluid systems. In *Proceedings of the 3rd International Modelica Conference*, pages 269–286.

Şencan Şahin, A., İsmail İlke Köse, and Selbaş, R. (2012). Comparative analysis of neural network and neuro-fuzzy system for thermodynamic properties of refrigerants. *Applied Artificial Intelligence*, 26:662–672.

Epple, B., Leithner, R., Linzer, W., and Walter, H. (2009). *Simulation von Kraftwerken und wärmetechnischen Anlagen*. Springer Wien.

Fernández-Seara, J., Vales, A., and Vázquez, M. (1998). Heat recovery system to power an onboard nh3-h2o absorption refrigeration plant in trawler chiller fishing vessels. *Applied Thermal Engineering*, 18(12):1189 – 1205.

Franke, R., Casella, F., Otter, M., Sielemann, M., Elmqvist, H., Mattson, S. E., and Olsson, H. (2008). Stream connectors - an extension of modelica for device-oriented

modeling of convective transport phenomena. In *Proceedings 7th Modelica Conference*, Como, Italy.

Fritzson, P. (2011). *Introduction to Modeling and Simulation of Technical and Physical Systems with Modelica*. Wiley.

Ganesh, N. S. and Srinivas, T. (2010). Thermodynamic properties of binary mixture for power generation systems. *International Journal of Refrigeration*, 5(10):11–25.

Gmehling, J., Kolbe, B., Kleiber, M., and Rarey, J. (2012). *Chemical Thermodynamics for Process Simulation*. Wiley.

Gräber, M., Kosowski, K., Richter, C., and Tegethoff, W. (2010). Modelling of heat pumps with an object-oriented model library for thermodynamic systems. *Mathematical and Computer Modelling of Dynamical Systems*, 16(3):195–209.

Gräber, M., Kirches, C., Schlöder, J., and Tegethoff, W. (2012). Nonlinear Model Predictive Control of a Vapor Compression Cycle Based on First Principle Models. In *7th Vienna International Conference on Mathematical Modelling MATHMOD*, Wien.

Hall, C. A. and Mutafelija, B. A. (1975). Transfinite interpolation of steam tables. *Journal of Computational Physics*, 18(1):79 – 91.

Helrich, C. (2009). *Modern Thermodynamics with Statistical Mechanics*. Springer.

Herbst, G. (1976). *Zustandsgleichungen des Druckwassers für technische Anwendungen : Die Freie Enthalpie g(T,p) in der nach h(s,p) umformbaren Darstellung durch eine Spline-Funktion*. PhD thesis, Technische Universität Hannover, Fakultät für Maschinenwesen, Hannover.

Horuz, I. (1998). An alternative Road Transport Refrigeration, 1997. *Turkish Journal of Engineering and Environmental*, 22:211,222.

Incropera, F. P. and DeWitt, D. P. (2007). *Fundamentals of Heat and Mass Transfer*. Wiley, Hoboken.

Johnson, R. (1998). *The Handbook of Fluid Dynamics*. Mechanical engineering. C R C Press LLC.

Kabelac, S. (1998). Die Schallgeschwindigkeit als thermodynamische Zustandsgröße. *Forschung im Ingenieurwesen*, 64:47–54. 10.1007/PL00010851.

Kaiser, C., Försterling, S., Strupp, C., Lemke, N., Sonnekalb, M., and Köhler, J. (2012a). *Simulation zur verbrauchsorientierten Bewertung von Omnibus-Klimatisierungskonzepten*. Steinberg, P., Expert Verlag.

Kaiser, C., Tegethoff, W., Köhler, J., and Sonnekalb, M. (2012b). Verbrauchseffiziente Regelungs- und Verschaltungskonzepte für Omnibusklimaanlagen. In *DKV-Tagungsbericht*, Würzburg.

Köhler, J., Tegethoff, W. J., Westphalen, D., and Sonnekalb, M. (1997). Absorption refrigeration system for mobile applications utilizing exhaust gases. *Heat and Mass Transfer*, 32(5):333–340.

Klaus, R. L. and Ness, H. C. V. (1967). An extension of the spline fit technique and applications to thermodynamic data. *AIChE Journal*, 13(6):1132–1136.

Kobza, J. (1995). Computing local parameters of biquartic interpolatory splines. *J. Comput. Appl. Math.*, 63(1-2):229–236.

Kossel, R. (2011). *Hybride Simulation thermischer Systeme am Beispiel eines Reisebusses*. PhD thesis, Technische Universität Carolo-Wilhelmina zu Braunschweig. Institut für Thermodynamik.

Kossel, R., Försterling, S., and Tegethoff, W. (2008). *Einsatz hybrider Simulationstechnik für die Bewertung mobiler Heiz- und Kühlkonzepte*. Expert-Verlag, Berlin.

Kretzschmar, H. J. (2012). personal communication.

Kunick, M., Kretzschmar, H.-J., and Gampe, U. (2008). Fast Calculation of Thermodynamic Properties of Water and Steam in Process Modelling using Spline Interpolation. In *15th Conference on the Properties of Water and Steam*, Berlin.

Laughman, C. R., Zhao, Y., and Nikovski, D. (2012). Fast Refrigerant Property Calculations Using Interpolation-BasedMethods. In *International Refrigeration and Air Conditioning Conference at Purdue*, Purdue.

Lemke, N. C. (2005). *Untersuchung zweistufiger Flüssigkeitskühler mit dem Kältemittel CO_2*. PhD thesis, Technische Universität Carolo-Wilhelmina zu Braunschweig, Stuttgart. Forschungsberichte des Deutschen Kälte- und Klimatechnischen Vereins Nr. 73.

Lemmon, E. (2003). Pseudo-Pure Fluid Equations of State for the Refrigerant Blends R-410A, R-404A, R-507A, and R-407C. *International Journal of Thermophysics*, 24:991–1006.

Lemmon, E. W., Huber, M. L., and McLinden, M. O. (2010). *NIST Standard Reference Database 23: Reference Fluid Thermodynamic and Transport Properties - REFPROP 9.0*. National Institute of Standards and Technology, Standard Reference Data Program, Gaithersburg.

Levenberg, K. (1944). A method for the solution of certain problems in least squares. *Quart. Applied Math.*, 2:164–168.

L'Huillier, J. and Peral, E. (2011). Renault experiences with zeotropic blend for MAC. In *SAE Alternative Refrigerant and System Efficiency Symposium*, Scottsdale (Phoenix), Arizona USA.

Lucas, C., Rusche, H., Schröder, A., and Köhler, J. (2013). Experimental and numerical investigation of a two-phase CO2 Ejector at zero suction flow operating conditions. *International Journal of Thermal Sciences*, in submission process.

Lyness, J. N. and Moler, C. B. (1966). Van der Monde systems and numerical differentiation. *j-NUM-MATH*, 8(5):458–464.

Ma, Q., Wang, R., Luo, L., Xia, Z., and Lin, P. (2009). Transportation of low-grade thermal energy over long distance by ammonia-water absorption. *Chinese Science Bulletin*, 54(6):948–957.

Manzela, A. A., Hanriot, S. M., Cabezas-Gómez, L., and Sodré, J. R. (2010). Using engine exhaust gas as energy source for an absorption refrigeration system. *Applied Energy*, 87(4):1141 – 1148.

Mattsson, S. E. (1995). Simulation of object-oriented continuous time models. *Mathematics and Computers in Simulation*, 39(5-6):513 – 518.

McLinden, M. J. O., Thol, M., and Lemmon, E. W. (2010). Thermodynamic Properties of trans-1,3,3,3-tetrafluoropropene [R1234ze(E)]: Measurements of Density and Vapor Pressure and a Comprehensive Equation of State. *Purdue e-Pubs*.

Möhlenkamp, A., Lemke, N., and Köhler, J. (2012). Experimentelle Untersuchungen einer zweistufigen Transportkälteanlage mit R744. In *DKV-Tagungsbericht*, Würzburg.

Michelsen, M. L. and Mollerup, J. M. (2007). *Thermodynamic Models: Fundamentals and Computational Aspects*. Tie-Line Publications.

Miyagawa, K. and Hill, P. (2001). Rapid and accurate calculation of water and steam

properties using the tabular Taylor series expansion method. *Journal of engineering for gas turbines and power*, 123(3):707–712.

Müller, W. C. (1994). Fast and accurate water and steam properties programs for two-phase flow calculations. *Nuclear Engineering and Design*, 149(1-3):449 – 458.

Orbey, H. and Sandler, S. (1998). *Modeling Vapor Liquid Equilibria: Cubic Equations of State and Their Mixing Rules*. Cambridge Series in Chemical Engineering Series. Cambridge University Press.

Otten, R., Li, B., and Alleyne, A. (2010). Hardware-in-the-loop load emulation for air-conditioning and refrigeration systems. In *International Refrigeration and Air Conditioning Conference at Purdue*, purdue.

Patankar, S. V. (1980). *Numerical Heat Transfer and Fluid Flow*. Hemisphere Pub. Corp., Washington and New York.

Patek and Klomfar (1995). Simple functions for fast calculations of selected thermodynamic properties of the ammonia-water system. *International Journal of Refrigeration*, 18(4):228–234.

Peral-Antunez, E. (2012). MAC Refrigerant Blend Cooperative Research Program Update. In *SAE Thermal Management Systems Symposium*, Scottsdale (Phoenix), Arizona USA.

Petzold, L. R. (1983). A description of DASSL: a differential/algebraic system solver. In *Scientific computing (Montreal, Quebec, 1982)*, pages 65–68. IMACS, New Brunswick, NJ.

Poling, B. E., Prausnitz, J. M., and O'Connell, J. P. (2001). *The properties of gases and liquids*. McGraw Hill professional. McGraw-Hill Professional Publishing.

Popovici, K. and Mosterman, P. (2013). *Real-time Simulation Technologies: Principles, Methodologies, and Applications*. Computational Analysis, Synthesis, and Design of Dynamic Systems Series. CRC Press.

Pratihar, A., Kaushik, S., and Agarwal, R. (2010). Simulation of an ammonia-water compression-absorption refrigeration system for water chilling application. *International Journal of Refrigeration*, 33(7):1386 – 1394.

Press, W. H., Teukolsky, S. A., Vetterling, W. T., and Flannery, B. P. (2007). *Numerical Recipes Source Code CD-ROM 3rd Edition: The Art of Scientific Computing*. Cambridge University Press, New York, NY, USA, 3 edition.

Raabe, G. (2012). Molecular Modeling of Fluoropropene Refrigerants. *The Journal of Physical Chemistry B*, 116(19):5744–5751.

Raabe, G. (2013). Molecular Simulation Studies on the Vapor–Liquid Phase Equilibria of Binary Mixtures of R-1234yf and R-1234ze(E) with R-32 and CO2. *Journal of Chemical and Engineering Data*, 58(6):1867–1873. ASAP.

Rasmussen, B. P. (2012). Dynamic modeling for vapor compression systems - part i: Literature review. *HVAC&R Research*, 18(5):934–955.

Richter, C. C. (2008). *Proposal of New Object-Oriented Equation-Based Model Libraries for Thermodynamic Systems*. PhD thesis, Technische Universität Carolo-Wilhelmina zu Braunschweig.

Rohani, A. A., Pazuki, G., Najafabadi, H. A., Seyfi, S., and Vossoughi, M. (2011). Comparison between the artificial neural network system and SAFT equation in obtaining vapor pressure and liquid density of pure alcohols. *Expert Systems With Applications*, 38:1738–1747.

Sadhukhan, K., Chowdhuri, A., and Mandal, B. (2012). Computer Based Thermodynamic Properties of Ammonia-Water Mixture for the Analysis of Power and Refrigeration Cycles. *International Journal of Thermodynamics*, 15(3).

Schiavo, F. and Casella, F. (2007). Object-oriented modelling and simulation of heat exchangers with finite element methods. *Mathematical and Computer Modelling of Dynamical Systems*, 13(3):211–235.

Schiebener, P. (1989). *Schnelle Berechnungsverfahren fur Zustandeseigenschaften am Beispiel Wasser*. PhD thesis, Technische Universität München - Lehrstuhl A für Thermodynamik, Munchen.

Schot, J. (1968). *A Spline-function Method for Generating the Thermodynamic Properties of Water Substance*. Defense Technical Information Center, Naval Ship Research and Development Center Washington D.C. Applied Mathematics Lab.

Schuler, H. (2008). *Prozeßsimulation*. Wiley.

Schulze, C., Gräber, M., and Tegethoff, W. (2012). A Limiter for Preventing Singularity in Simplified Finite Volume Methods. In *7th Vienna International Conference on Mathematical Modelling MATHMOD*, Wien.

Schulze, C., Gräber, M., Huhn, M., and Grätz, U. (2011a). Real-Time Simulation

of Vapour Compression Cycles. In *Proceedings of the 8th International Modelica Conference*, Dresden. Modelica.

Schulze, C., Kaiser, C., Tegethoff, W., and Köhler, J. (2011b). Numerisch effiziente Simulation von Mehrverdampfer-Klimaanlagen unter hochdynamischen Randbedingungen. In *DKV-Tagungsbericht*, Aachen. AA II.2.07.

Schulze, C. and Köhler, J. (2013). Spline based interpolation of the two phase region of binary mixtures using multiparameter equations of state. In *4th IIR Conference on Thermophysical Properties and Transfer Processes of Refrigerants*, Delft. status: accepted.

Schulze, C., Tegethoff, W., Huhn, M., and Köhler, J. (2010). Numerisch effiziente Berechnungsmethoden für die Stoffeigenschaften von Fluiden für die Systemsimulation. In *DKV-Tagungsbericht*, Magdeburg.

Shearer, J. M. and Wolfe, M. A. (1985). ALGLIB, a simple symbol-manipulation package. *Commun. ACM*, 28(8):820–825.

Sieres, J., Varas, F., and Martínez-Suárez, J. A. (2012). A hybrid formulation for fast explicit calculation of thermodynamic properties of refrigerants. *International Journal of Refrigeration*, 35(4):1021 – 1034.

Somdalen, R. (2011). Dynamic simulation of a kalina cycle using real mixture uid properties. Diplomarbeit.

Somdalen, R., Schulze, C., and Köhler, J. (2012). An Alternative Calculation Procedure for Real Mixture Fluid Properties Demonstrated With a Kalina Cycle. In *10th Gustav Lorenzen Conference on Natural Refrigerants*, Delft.

Span, R. (2000). *Multiparameter Equations of State: An Accurate Source of Thermodynamic Property Data*. Engineering online library. Springer.

Span, R. and Wagner, W. (1996). A New Equation of State for Carbon Dioxide Covering the Fluid Region from the Triple-Point Temperature to 1100 K at Pressures up to 800 MPa. *Journal of Physical and Chemical Reference Data*, 25(6):1509–1596.

Span, R. and Wagner, W. (2003). Equations of State for Technical Applications. I. Simultaneously Optimized Functional Forms for Nonpolar and Polar Fluids. *International Journal of Thermophysics*, 24:1–39.

Späth, H. (1995a). *One Dimensional Spline Interpolation Algorithms*. A K Peters.

Späth, H. (1995b). *Two Dimensional Spline Interpolation Algorithms*. A K Peters.

Spurk, H., Spurk, J., and Aksel, N. (2008). *Fluid mechanics*. Springer London, Limited.

Städtke, H. (2006). *Gasdynamic Aspects of Two-Phase Flow: Hyperbolicity, Wave Propagation Phenomena, and Related Numerical Methods*. John Wiley and Sons.

Strupp, N. C., Lemke, N., Kling, M., Köhler, J., and Böttcher, C. (2009). Average mobile A/C customer usage model: for design, simulation and testing purposes. In *VDA Alternative Refrigerant winter meeting*, Saalfelden.

Sun, D. (1997). Thermodynamic design data and optimum design maps for absorption refrigeration systems. *Applied Thermal Engineering*, 17(3):211 – 221.

Swesty, F. (1996). Thermodynamically consistent interpolation for equation of state tables. *Journal of Computational Physics*, 127(1):118 – 127.

Sözen, A., Arcaklioglu, E., Menlik, T., and Özalp, M. (2009). Determination of thermodynamic properties of an alternative refrigerant (R407c) using artificial neural network. *Expert Systems With Applications*, 36:4346–4356.

Tegethoff, W., Schulze, C., Gräber, M., Huhn, M., Stulgies, N., Kaiser, C., and Loeffler, M. (2011). TEMO - Thermische Echtzeitfähige Modelle-Abschlussbericht zu einem vom BMBF geförderten Verbundvorhaben mit dem Förderkennzeichen 01IS08013A, 01IS08013B, 01IS08013C. Technical report, TLK-Thermo GmbH.

Thorade, M. (2010a). Eine Fundamentalgleichung mit den Variablen Entropie, Druck und Enthalpie für technische Anwendungen. In *VDI Thermodynamik-Kolloquium*.

Thorade, M. (2010b). Eine Fundamentalgleichung mit den Variablen Entropie, Druck und Enthalpie fuer technische Anwendungen. In *GeoEn International Meeting*, Potsdam. http://edoc.gfz-potsdam.de/gfz/15444.

Thorin, E. (2001). Thermophysical Properties of Ammonia-Water Mixtures for Prediction of Heat Transfer Areas in Power Cycles. *International Journal of Thermophysics*, 22(1):201–214.

Thürmer, H. (1969). *Empirische Gleichungen für die Enthalpie des Wassers mit der Entropie und dem Druck als unabhängigen Variablen*. PhD thesis, Technische Universität Carolo-Wilhelmina zu Braunschweig.

Tillner-Roth, R. (1998). *Fundamental equations of state*. Shaker-Verlag, Aachen.

Tillner-Roth, R. and Baehr, H. D. (1994). An International Standard Formulation for the Thermodynamic Properties of 1,1,1,2-Tetrafluoroethane (HFC-134a) for Temperatures from 170 K to 455 K and Pressures up to 70 MPa. *Journal of Physical and Chemical Reference Data*, 23(5):657–729.

Tillner-Roth, R. and Friend, D. G. (1998). A Helmholtz Free Energy Formulation of the Thermodynamic Properties of the Mixture {Water + Ammonia}. *Journal of Physical and Chemical Reference Data*, 27(1):63–96.

Tillner-Roth, R., Harms-Watzenberg, F., and Baehr, H. D. (1993). Eine neue Fundamentalgleichung für Ammoniak. *DKV Tagungsbericht*, 20:167–180.

Togashi, E., Tanabe, S., and Ataku, T. (2007). Development of fast calculation method for ammonia refrigeration cycle and parameter adjustment with genetic algorithm. In *Proceedings of Building Simulation 2007*.

Tummescheit, H., Eborn, J., and Prölss, K. (2005). Airconditioning–a Modelica library for dynamic simulation of AC systems. In *Paper presented at the 4th International Modelica Conference*.

Valderrama, J. O. (2003). The state of the cubic equations of state. *Industrial and Engineering Chemistry Research*, 42(8):1603–1618.

VDI (1996). VDI 2078 - Berechnung der Kühllast klimatisierter Räume (VDI-Kühllastregeln).

Wagner, W., Cooper, J. R., Dittmann, A., Kijima, J., Kretzschmar, H. J., Kruse, A., Mareš, R., Oguchi, K., Sato, H., Stöcker, I., Šifner, O., Takaishi, Y., Tanishita, I., Trübenbach, J., and Willkommen, T. (2000). The IAPWS Industrial Formulation 1997 for the Thermodynamic Properties of Water and Steam. *Journal of Engineering for Gas Turbines and Power*, 122(1):150–184.

Wagner, W. and Pruß, A. (2002). The IAPWS Formulation 1995 for the Thermodynamic Properties of Ordinary Water Substance for General and Scientific Use. *Journal of Physical and Chemical Reference Data*, 31(2):387–535.

Wang, X., An, B., Duan, Y., Wang, Z., and Lee, D. (2012). Efficient and accurate computation scheme of p-t thermodynamic properties of water and steam. *Journal of the Taiwan Institute of Chemical Engineers*, 43(6):845 – 851.

Weigand, B., Köhler, J., and von Wolfersdorf, J. (2010). *Thermodynamik Kompakt*. Springer-Lehrbuch. Springer.

White, R. (1964). *COMPLEX: A least squares method for fitting quadratically interpolated tables to a two-dimensional data array.* Lawrence Radiation Laboratory.

Ziegler, B. and Trepp, C. (1984). Equation of state for ammonia-water mixtures. *International Journal of Refrigeration*, 7(2):101 – 106.

Ziegler, F. (1999). Recent developments and future prospects of sorption heat pump systems. *International Journal of Thermal Sciences*, 38(3):191 – 208.

Appendix A.

Bridgeman's Table

This table is was taken from Bejan (2006, Bridgeman's Table, page 182). Variable transformations and derivations of equations in this thesis are based on this table.

$$
\begin{aligned}
(\partial T)_p = -(\partial p)_T &= 1 \\
(\partial v)_p = -(\partial p)_v &= \beta v \\
(\partial s)_p = -(\partial p)_s &= \frac{c_p}{T} \\
(\partial u)_p = -(\partial p)_u &= c_p - \beta p v \\
(\partial h)_p = -(\partial p)_h &= c_p \\
(\partial f)_p = -(\partial p)_f &= -s - \beta p v \\
(\partial g)_p = -(\partial p)_g &= -s
\end{aligned}
$$

$$
\begin{aligned}
(\partial v)_T = -(\partial T)_v &= \kappa v \\
(\partial s)_T = -(\partial T)_s &= \beta v \\
(\partial u)_T = -(\partial T)_u &= \beta T v - \kappa T v \\
(\partial h)_T = -(\partial T)_h &= -v + \beta T v \\
(\partial f)_T = -(\partial T)_f &= -\kappa p v \\
(\partial g)_T = -(\partial T)_g &= -v
\end{aligned}
$$

$$
\begin{aligned}
(\partial s)_v = -(\partial v)_s &= \beta^2 v^2 - \frac{\kappa v c_p}{T} \\
(\partial u)_v = -(\partial v)_u &= T\beta^2 v^2 - \kappa v c_p \\
(\partial h)_v = -(\partial v)_h &= T\beta^2 v^2 - \beta v^2 - \kappa v c_p \\
(\partial f)_v = -(\partial v)_f &= \kappa v s \\
(\partial g)_v = -(\partial v)_g &= \kappa v s - \beta v^2
\end{aligned}
$$

$$
\begin{aligned}
(\partial u)_s = -(\partial s)_u &= \beta^2 v^2 p - \frac{\kappa v c_p p}{T} \\
(\partial h)_s = -(\partial s)_h &= -\frac{v c_p}{T} \\
(\partial f)_s = -(\partial s)_f &= \beta v s + \beta^2 v^2 p - \frac{\kappa v c_p p}{T} \\
(\partial g)_s = -(\partial s)_g &= \beta v s - \frac{v c_p}{T}
\end{aligned}
$$

$$
\begin{aligned}
(\partial h)_u = -(\partial u)_h &= p\beta v^2 + \kappa v c_p p - v c_p - pT\beta^2 v^2 \\
(\partial f)_u = -(\partial u)_f &= sT\beta v - \kappa v c_p p - \kappa v s p + pT\beta^2 v^2 \\
(\partial g)_u = -(\partial u)_g &= \beta v^2 p + \beta v s T - v c_p - \kappa v s p
\end{aligned}
$$

$$
\begin{aligned}
(\partial f)_h = -(\partial h)_f &= (s - v\beta p)(v - v\beta T) - \kappa v c_p p \\
(\partial g)_h = -(\partial h)_g &= \beta v s T - v(s + c_p)
\end{aligned}
$$

$$
(\partial f)_g = -(\partial g)_f = \kappa v s p - v s - \beta v^2 p
$$

Appendix B.

Derivatives of the Density in the Two-Phase Region of a Pure Fluid

The density and the specific volume in the two-phase region are defined as follows:

$$\varrho = \frac{1}{v_{\mathrm{liq}} + (v_{\mathrm{vap}} - v_{\mathrm{liq}}) \cdot q} \tag{B.1}$$

$$v = v_{\mathrm{liq}} + (v_{\mathrm{vap}} - v_{\mathrm{liq}}) \cdot q \tag{B.2}$$

Consequently the partial derivatives of the density are:

$$\left(\frac{\partial \varrho}{\partial p}\right)_h = -\frac{1}{v^2}\left(\frac{\partial v}{\partial p}\right)_h \tag{B.3}$$

$$\begin{aligned}\left(\frac{\partial v}{\partial p}\right)_h = {} & \left(\frac{\partial v_{\mathrm{liq}}}{\partial p}\right)_{\mathrm{sat}} + \left(\left(\frac{\partial v_{\mathrm{vap}}}{\partial p}\right)_{\mathrm{sat}} - \left(\frac{\partial v_{\mathrm{liq}}}{\partial p}\right)_{\mathrm{sat}}\right) \cdot q \\ & + (v_{\mathrm{vap}} - v_{\mathrm{liq}}) \cdot \left(\frac{\partial q}{\partial p}\right)_h\end{aligned} \tag{B.4}$$

$$\left(\frac{\partial \varrho}{\partial h}\right)_p = -\frac{1}{v^2}\left(\frac{\partial v}{\partial h}\right)_p \tag{B.5}$$

$$\left(\frac{\partial v}{\partial h}\right)_p = \frac{v_{\mathrm{vap}} - v_{\mathrm{liq}}}{h_{\mathrm{vap}} - h_{\mathrm{liq}}} \tag{B.6}$$

The total derivative of the specific volume of the liquid can be rearranged using the definition of the isothermal compressibility κ and the linear isobaric thermal expansion

coefficient β to calculate the derivatives of the saturated specific volume:

$$dv_{\mathrm{liq}} = \left(\frac{\partial v_{\mathrm{liq}}}{\partial p}\right)_T \cdot dp + \left(\frac{\partial v_{\mathrm{liq}}}{\partial T}\right)_p \cdot dT \tag{B.7}$$

$$\kappa = -\frac{1}{v}\left(\frac{\partial v}{\partial p}\right)_T \tag{B.8}$$

$$\beta = \frac{1}{v}\left(\frac{\partial v}{\partial T}\right)_p \tag{B.9}$$

$$\left(\frac{\partial v_{\mathrm{liq}}}{\partial p}\right)_{\mathrm{liq}} = \beta_{\mathrm{liq}} v_{\mathrm{liq}} \left(\frac{\partial T}{\partial p}\right)_{\mathrm{liq}} - \kappa_{\mathrm{liq}} v_{\mathrm{liq}} \tag{B.10}$$

The equations for the vapour follow the same pattern:

$$\left(\frac{\partial v_{\mathrm{vap}}}{\partial p}\right)_{\mathrm{vap}} = \beta_{\mathrm{vap}} v_{\mathrm{vap}} \left(\frac{\partial T}{\partial p}\right)_{\mathrm{vap}} - \kappa_{\mathrm{vap}} v_{\mathrm{vap}} \tag{B.11}$$

The steam mass fraction q and its derivative can be calculated from the specific enthalpies:

$$q = \frac{h - h_{\mathrm{liq}}}{h_{\mathrm{vap}} - h_{\mathrm{liq}}} \tag{B.12}$$

$$\left(\frac{\partial q}{\partial p}\right)_h = \frac{-\left(\frac{\partial h_{\mathrm{liq}}}{\partial p}\right)_{\mathrm{liq}}}{h_{\mathrm{vap}} - h_{\mathrm{liq}}} - \frac{h - h_{\mathrm{liq}}}{(h_{\mathrm{vap}} - h_{\mathrm{liq}})^2} \cdot \left(\left(\frac{\partial h_{\mathrm{vap}}}{\partial p}\right)_{\mathrm{vap}} - \left(\frac{\partial h_{\mathrm{liq}}}{\partial p}\right)_{\mathrm{liq}}\right) \tag{B.13}$$

The total derivative of the specific enthalpy can be used to calculate the derivatives of the saturated specific enthalpies using the definition of the specific heat capacity c_p and the isobaric thermal expansion coefficient β:

$$dh = \left(\frac{\partial h}{\partial p}\right)_T dp + \left(\frac{\partial h}{\partial T}\right)_p dT \tag{B.14}$$

$$\left(\frac{\partial h_{\mathrm{liq}}}{\partial p}\right)_{\mathrm{sat}} = v_{\mathrm{liq}}\left(1 - \beta_{\mathrm{liq}} T\right) + c_{\mathrm{p,liq}} \left(\frac{\partial T}{\partial p}\right)_{\mathrm{liq}} \tag{B.15}$$

$$\left(\frac{\partial h_{\mathrm{vap}}}{\partial p}\right)_{\mathrm{sat}} = v_{\mathrm{vap}}\left(1 - \beta_{\mathrm{vap}} T\right) + c_{\mathrm{p,vap}} \left(\frac{\partial T}{\partial p}\right)_{\mathrm{vap}} \tag{B.16}$$

The derivative of the saturation temperature can be calculated based on Clausius Clapeyron's equation:

$$\left(\frac{\partial T}{\partial p}\right)_{\mathrm{liq}} = \left(\frac{\partial T}{\partial p}\right)_{\mathrm{vap}} = \left(\frac{\partial T}{\partial p}\right)_{\mathrm{sat}} \tag{B.17}$$

$$\left(\frac{\partial T}{\partial p}\right)_{\mathrm{sat}} = T\frac{v_{\mathrm{vap}} - v_{\mathrm{liq}}}{h_{\mathrm{vap}} - h_{\mathrm{liq}}} \tag{B.18}$$

Summary:

$$\left(\frac{\partial \varrho}{\partial h}\right)_p = -\frac{1}{v^2}\frac{v_{\mathrm{vap}} - v_{\mathrm{liq}}}{h_{\mathrm{vap}} - h_{\mathrm{liq}}} \tag{B.19}$$

$$\left(\frac{\partial T}{\partial p}\right)_{\mathrm{sat}} = T\frac{v_{\mathrm{vap}} - v_{\mathrm{liq}}}{h_{\mathrm{vap}} - h_{\mathrm{liq}}} \tag{B.20}$$

$$\left(\frac{\partial h_{\mathrm{liq}}}{\partial p}\right)_{\mathrm{sat}} = v_{\mathrm{liq}}\left(1 - \beta_{\mathrm{liq}}T\right) + c_{\mathrm{p,liq}}\left(\frac{\partial T}{\partial p}\right)_{\mathrm{sat}} \tag{B.21}$$

$$\left(\frac{\partial h_{\mathrm{vap}}}{\partial p}\right)_{\mathrm{sat}} = v_{\mathrm{vap}}\left(1 - \beta_{\mathrm{vap}}T\right) + c_{\mathrm{p,vap}}\left(\frac{\partial T}{\partial p}\right)_{\mathrm{sat}} \tag{B.22}$$

$$\left(\frac{\partial v_{\mathrm{liq}}}{\partial p}\right)_{\mathrm{sat}} = \beta_{\mathrm{liq}}v_{\mathrm{liq}}\left(\frac{\partial T}{\partial p}\right)_{\mathrm{sat}} - \kappa_{\mathrm{liq}}v_{\mathrm{liq}} \tag{B.23}$$

$$\left(\frac{\partial v_{\mathrm{vap}}}{\partial p}\right)_{\mathrm{sat}} = \beta_{\mathrm{vap}}v_{\mathrm{vap}}\left(\frac{\partial T}{\partial p}\right)_{\mathrm{sat}} - \kappa_{\mathrm{vap}}v_{\mathrm{vap}} \tag{B.24}$$

$$\left(\frac{\partial q}{\partial p}\right)_h = \frac{-\left(\frac{\partial h_{\mathrm{liq}}}{\partial p}\right)_{\mathrm{sat}}}{h_{\mathrm{vap}} - h_{\mathrm{liq}}} - \frac{h - h_{\mathrm{liq}}}{(h_{\mathrm{vap}} - h_{\mathrm{liq}})^2} \cdot \left(\left(\frac{\partial h_{\mathrm{vap}}}{\partial p}\right)_{\mathrm{sat}} - \left(\frac{\partial h_{\mathrm{liq}}}{\partial p}\right)_{\mathrm{sat}}\right) \tag{B.25}$$

$$\begin{aligned}\left(\frac{\partial v}{\partial p}\right)_h = {} & \left(\frac{\partial v_{\mathrm{liq}}}{\partial p}\right)_{\mathrm{sat}} + \left(\left(\frac{\partial v_{\mathrm{vap}}}{\partial p}\right)_{\mathrm{sat}} - \left(\frac{\partial v_{\mathrm{liq}}}{\partial p}\right)_{\mathrm{sat}}\right) \cdot q \\ & (v_{\mathrm{vap}} - v_{\mathrm{liq}}) \cdot \left(\frac{\partial q}{\partial p}\right)_h\end{aligned} \tag{B.26}$$

$$\left(\frac{\partial \varrho}{\partial p}\right)_h = -\frac{1}{v^2}\left(\frac{\partial v}{\partial p}\right)_h \tag{B.27}$$

Appendix C.

Derivatives of the Density in the Two-Phase Region of a Binary Mixture

The steam mass fraction q can be calculated from the liquid and vapour composition:

$$q = \frac{\xi - \xi_{\mathrm{liq}}}{\xi_{\mathrm{vap}} - \xi_{\mathrm{liq}}} \tag{C.1}$$

Consequently, the partial derivatives of the steam mass fraction with respect to the independent variables Θ, p and ξ can be derived from the ξ_{liq} and ξ_{vap} surfaces:

$$\left(\frac{\partial q}{\partial \Theta}\right)_{p,\xi} = \frac{-\left(\frac{\partial x}{\partial \Theta}\right)_p}{\xi_{\mathrm{vap}} - \xi_{\mathrm{liq}}} - \frac{\xi - \xi_{\mathrm{liq}}}{(\xi_{\mathrm{vap}} - \xi_{\mathrm{liq}})^2}\left(\left(\frac{\partial \xi_{\mathrm{vap}}}{\partial \Theta}\right)_p - \left(\frac{\partial \xi_{\mathrm{liq}}}{\partial \Theta}\right)_p\right) \tag{C.2}$$

$$\left(\frac{\partial q}{\partial p}\right)_{\Theta,\xi} = \frac{-\left(\frac{\partial x}{\partial p}\right)_\Theta}{\xi_{\mathrm{vap}} - \xi_{\mathrm{liq}}} - \frac{\xi - \xi_{\mathrm{liq}}}{(\xi_{\mathrm{vap}} - \xi_{\mathrm{liq}})^2}\left(\left(\frac{\partial \xi_{\mathrm{vap}}}{\partial p}\right)_\Theta - \left(\frac{\partial \xi_{\mathrm{liq}}}{\partial p}\right)_\Theta\right) \tag{C.3}$$

$$\left(\frac{\partial q}{\partial \xi}\right)_{p,\Theta} = \frac{1}{\xi_{\mathrm{vap}} - \xi_{\mathrm{liq}}} \tag{C.4}$$

The specific volume in the two-phase region is calculated from the steam mass fraction, specific volume of liquid and vapour:

$$v = v_{\mathrm{liq}} + (v_{\mathrm{vap}} - v_{\mathrm{liq}})q \tag{C.5}$$

The partial derivatives of the specific volume with respect to the independent variables are obtained from the specific volume of liquid and vapour as well as the steam mass

fraction:

$$\left(\frac{\partial v}{\partial \Theta}\right)_{p,\xi} = \left(\frac{\partial v_{\mathrm{liq}}}{\partial \Theta}\right)_{p} + \left(\left(\frac{\partial v_{\mathrm{vap}}}{\partial \Theta}\right)_{p} - \left(\frac{\partial v_{\mathrm{liq}}}{\partial \Theta}\right)_{p}\right) q + (v_{\mathrm{vap}} - v_{\mathrm{liq}}) \left(\frac{\partial q}{\partial \Theta}\right)_{p,\xi} \quad \text{(C.6)}$$

$$\left(\frac{\partial v}{\partial p}\right)_{\Theta,\xi} = \left(\frac{\partial v_{\mathrm{liq}}}{\partial p}\right)_{\Theta} + \left(\left(\frac{\partial v_{\mathrm{vap}}}{\partial p}\right)_{\Theta} - \left(\frac{\partial v_{\mathrm{liq}}}{\partial p}\right)_{\Theta}\right) q + (v_{\mathrm{vap}} - v_{\mathrm{liq}}) \left(\frac{\partial q}{\partial p}\right)_{\Theta,\xi} \quad \text{(C.7)}$$

$$\left(\frac{\partial v}{\partial \xi}\right)_{p,\Theta} = (v_{\mathrm{vap}} - v_{\mathrm{liq}}) \left(\frac{\partial q}{\partial \xi}\right)_{p,\Theta} \quad \text{(C.8)}$$

The specific enthalpy in the two-phase region is also calculated from the liquid and vapour properties:

$$h = h_{\mathrm{liq}} + (h_{\mathrm{vap}} - h_{\mathrm{liq}}) q \quad \text{(C.9)}$$

Its derivatives are derived from the liquid and vapour property surfaces:

$$\left(\frac{\partial h}{\partial \Theta}\right)_{p,\xi} = \left(\frac{\partial h_{\mathrm{liq}}}{\partial \Theta}\right)_{p} + \left(\left(\frac{\partial h_{\mathrm{vap}}}{\partial \Theta}\right)_{p} - \left(\frac{\partial h_{\mathrm{liq}}}{\partial \Theta}\right)_{p}\right) q + (h_{\mathrm{vap}} - h_{\mathrm{liq}}) \left(\frac{\partial q}{\partial \Theta}\right)_{p,\xi} \quad \text{(C.10)}$$

$$\left(\frac{\partial h}{\partial p}\right)_{\Theta,\xi} = \left(\frac{\partial h_{\mathrm{liq}}}{\partial p}\right)_{\Theta} + \left(\left(\frac{\partial h_{h}}{\partial p}\right)_{\Theta} - \left(\frac{\partial h_{\mathrm{liq}}}{\partial p}\right)_{\Theta}\right) q + (h_{h} - h_{\mathrm{liq}}) \left(\frac{\partial q}{\partial p}\right)_{\Theta,\xi} \quad \text{(C.11)}$$

$$\left(\frac{\partial h}{\partial \xi}\right)_{p,\Theta} = (h_{\mathrm{vap}} - h_{\mathrm{liq}}) \left(\frac{\partial q}{\partial \xi}\right)_{p,\Theta} \quad \text{(C.12)}$$

The following relations can be obtained from the total derivative of the specific enthalpy:

$$\left(\frac{\partial \Theta}{\partial p}\right)_{h,\xi} = -\frac{\left(\frac{\partial h}{\partial p}\right)_{\Theta,\xi}}{\left(\frac{\partial h}{\partial \Theta}\right)_{p,\xi}} \quad \text{(C.13)}$$

$$\left(\frac{\partial \Theta}{\partial \xi}\right)_{p,h} = -\frac{\left(\frac{\partial h}{\partial \xi}\right)_{p,\Theta}}{\left(\frac{\partial h}{\partial \Theta}\right)_{p,\xi}} \quad \text{(C.14)}$$

Finally, an equation for the partial derivatives of the specific volume with respect to the independent variables of the thermodynamic system model $\{p,\, h,\, \xi\}$ can be found:

$$\left(\frac{\partial v}{\partial h}\right)_{p,\xi} = \frac{\left(\frac{\partial v}{\partial \Theta}\right)_{p,\xi}}{\left(\frac{\partial h}{\partial \Theta}\right)_{p,\xi}} \quad \text{(C.15)}$$

$$\left(\frac{\partial v}{\partial p}\right)_{h,\xi} = \left(\frac{\partial v}{\partial p}\right)_{\Theta,\xi} + \left(\frac{\partial v}{\partial \Theta}\right)_{p,\xi} \left(\frac{\partial \Theta}{\partial p}\right)_{h,\xi} \quad \text{(C.16)}$$

$$\left(\frac{\partial v}{\partial \xi}\right)_{p,h} = \left(\frac{\partial v}{\partial \Theta}\right)_{p,\xi} \left(\frac{\partial \Theta}{\partial \xi}\right)_{p,h} + \left(\frac{\partial v}{\partial \xi}\right)_{p,\Theta} \quad \text{(C.17)}$$

Appendix D.

Implementation of the Limiter presented in Chapter 4 in Modelica

Signal-oriented languages and tools like Matlab/Simulink can be used to develop physical models, but due to the strong interconnection and variability of these models, implementation of physical models in these languages are rarely easy to read or maintain. A new generation of physical modelling languages like Modelica (Clauss et al., 2004) enable an easier implementation, model maintenance and more efficient simulation (Fritzson, 2011, section 2.7). The models and the limiter presented in this chapter are implemented in the object-oriented modelling language Modelica and used in the TIL library (Gräber et al., 2010; Richter, 2008; Schulze et al., 2011a). The implementation is shown in this section.

To enable a system wide usage of the limiter approach, connectors (Fritzson, 2011, section 2.8) can be applied to propagate h_{limit}. A connector is a Modelica class that is used to define an interface from one model to the connected ones.

The stream connector discussed by Franke et al. (2008) is an appropriate method to implement the interfaces between CVs. This type of connector eases the implementation of tube or heat exchanger models that are based on separate models for a CV. In figure D.1 the communication of connected CVs is depicted. The *inStream()* operator can be used here to obtain h_{limit} of the neighbouring CV. h_{limit} can then be used, to limit the potentially outflowing specific enthalpy of the neighbouring CV towards that first CV.

Compared to the connector proposed in Franke et al. (2008), only a stream variable h_{limit} has to be added. A possible implementation of the connector for a pure fluid may be:

```
connector FluidPort "Fluid port"
  import SI = Modelica.SIunits;
```

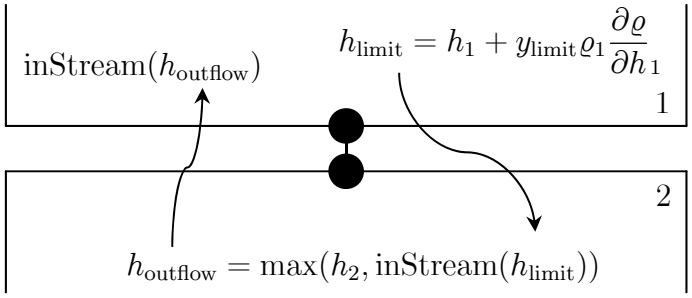

Figure D.1.: Propagation of h_{limit} using the stream connector concept. CV 1 limits the specific enthalpy that leaves CV 2 in the direction of CV 1.

```
        SI.AbsolutePressure p;
  flow  SI.MassFlowRate     m_flow;
  stream SI.SpecificEnthalpy h_outflow;
  stream SI.SpecificEnthalpy h_limit;
end FluidPort;
```

The specific enthalpy in the case that fluid leaves the volume at port A h_{outflow} is modified using the max-operator. The minimal specific enthalpy that is allowed to enter the considered CV (4.26) is calculated and propagated using h_{limit}:

```
portA.h_limit = h + yLimit*density/drhodh;
portB.h_limit = h + yLimit*density/drhodh;

portA.h_outflow = noEvent(max(h,
                  inStream(portA.h_limit)));
portB.h_outflow = noEvent(max(h,
                  inStream(portB.h_limit)));

der(h) = 1/mass*(
  portA.m_flow*(actualStream(portA.h_outflow)-h)
 +portB.m_flow*(actualStream(portB.h_outflow)-h)
 +heatPort.Q_flow + volume*der(p));
```

The *actualStream()* operator is used in the energy balance, so that the system of equations is interpreted as mixed discrete linear. The Modelica compiler Dymola triggers an event if the specific enthalpy at the CV surface is switched.

Appendix E.

Bus Engine Map

The bus engine maps are based on experimental data.

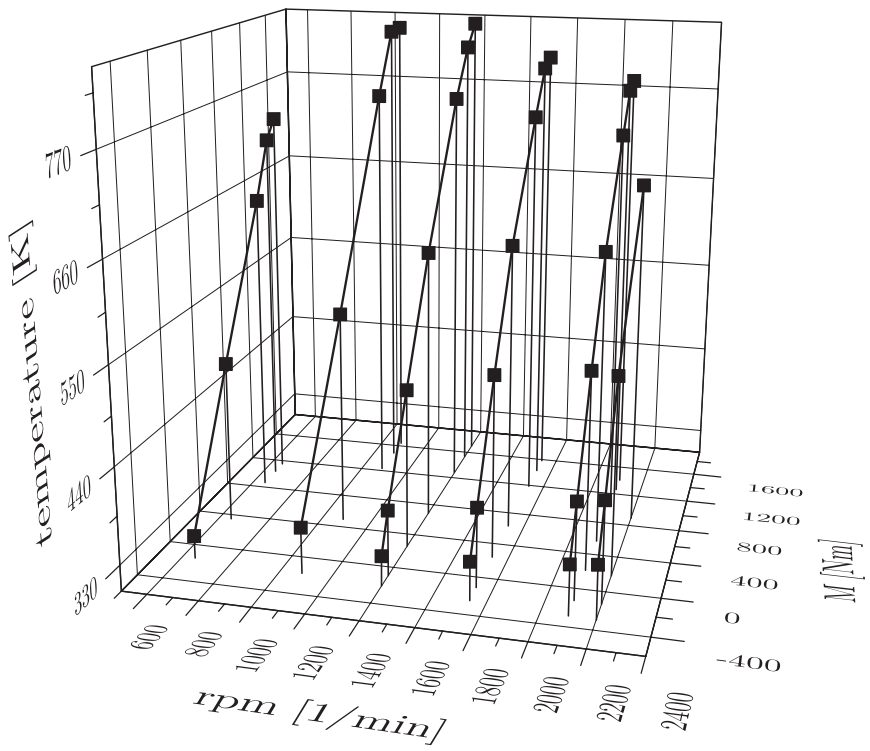

Figure E.1.: Exhaust gas temperature behind turbo compressor

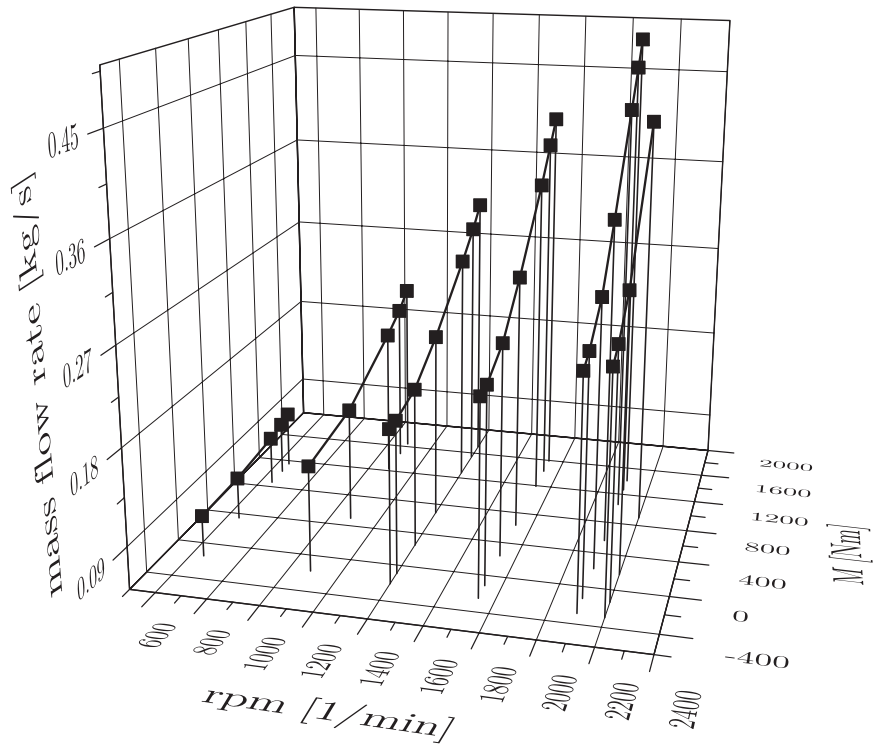

Figure E.2.: Exhaust gas mass flow rate